New Target Tracking and Monitoring Guidance Laws for UAV

Niki Regina [1]

March 3, 2011

[1]Dipartimento di Elettronica, Informatica e Sistemistica Viale Risorgimento 2, 40136 Bologna, Italia. email:niki.regina2@unibo.it

To my mentor, every day source of new ideas.
To my family, for the support.
To Irene.

Abstract

A pursuer UAV tracking and loitering around a target is the problem analyzed in this thesis. The UAV is assumed to be a fixed-wing vehicle and constant airspeed together with bounded lateral accelerations are the main constraints of the problem. Three different guidance laws are designed for ensuring a continuos overfly on the target. Different proofs are presented to demonstrate the stability properties of the laws. All the algorithms are tested on a 6DoF Pioneer software simulator. Classic control design methods have been adopted to develop autopilots for implementig the simulation platform used for testing the guidance laws.

This page is intentionally left blank.

Contents

This page is intentionally left blank.

List of Figures

List of Tables

This page is intentionally left blank.

Chapter 1

Introduction

1.1 Scope of the Thesis

The design of guidance laws for the UAVs (Unmanned Air Vehicle) is one of the main problems for the researchers in the field of aerospace applications.

Since the last ten years, it has been occurred an exponentially growth of different kind of solutions for the UAV guidance laws based on the scientific works which have been developed in robot applications. In fact, as it will be explained in the next sections, the mathematical model of the dynamic system describing the mass-point kinematics, called unycicle, is used for a fixed-wing UAVs in the same ways it has been exploited in robotics, but with differences due to some important constraints.

In particular, the main constraints which have to be considered for UAVs respect to the unycicle model can be summarized as:

- the speed of the UAVs is considered constant in order to ensure the lift force to sustain the vehicle

- the lateral acceleration must be limited by the flight envelope (usually the lateral acceleration is also considered as normal acceleration)

While a lot of solutions designed for the unicycle model exist for tracking a desired path or loitering around a point, and consequently there are different

kinds of guidance laws, for the UAVs the creation of guidance laws which fulfills the requirement above stated is still a current research activity.

The aim of this work is to give a large overview of the most important techniques used for the automatic guidance of fixed-wing UAVs. All the techniques which will be presented have been used for the creation of different suitable guidance laws in order to oversee a fixed target. In some of them the guidance laws are used also to follow a moving target and a comparison with some others guidance law is done.

The thesis is organized as follows. The first chapter is concluded with the sections 1.2 and 1.3 which defines the state of the art and the mathematical model used in all the approaches. The second chapter is dedicated to the analysis of the most important guidance laws: *Pursuit Navigation* (**PN**) and *Proportional Navigation Guidance* (**PNG**). They are explained to facilitate the reader to understand the problem of tracking a fixed or moving target. Chapter 3 shows the design of a feedback non linear guidance law and proof its stability through a Lyapunov function. In Chapter 4 the technique of the guidance vector field is explained and a particular solution is presented to overflight a target.

Assumption

- the actual position of the target is known together with its velocity
- future position of the target are not known

1.2 State of the Art

The problem of finding UAV guidance laws for the UAV can be divided in these three principal categories:

1. loitering around a fixed point;
2. following a moving target;
3. tracking of a fixed path created with specific techniques.

For the first category the most innovative approach is based on the *Lyapunov Vector Field* [20], [26]. The works presented in these two papers are based on the concept of path following through the construction of a vector field surrounding the path to be followed. General speaking, in this technique the vector fields provide the course command to guide the UAV towards the desired path. Usually the method is not used for tracking a target but it can be used also to switch between different predefined way points in order to create a more complicated trajectory.

The desired path created with this technique has the problem that it does not guarantee a continue overflight on the fixed point because the chosen fields are of circular Lyapunov.

The second category includes a lot of techniques. A particular introduction must be done for the **PN** and the **PNG** [21]. In the pursuit navigation the follower aims directly at the target throughout the encounter, like a dog chasing a cat. As it will explained in chapter 2 the angle between the longitudinal axis of the UAV or its velocity vector and the line of sight (**LOS**) to the target is driven to zero or some constant value. The proportional navigation guidance is one in which the follower heading rate is made proportional to the UAV-target **LOS** rate. The purpose of such a course is to counter the tendency for the **LOS** to rotate and, hence, to approximate a constant-bearing course. Recently a new approach has been proposed in [28]. The guidance method discussed in this paper adapts the method of the **PN** to create the lateral acceleration commands for controlling a UAVs. A reference point on the desired path is designed and the normal acceleration command is generated according to the direction of the reference point, relative to the vehicle velocity. The reference point on the desired path is considered at a constant distance L forward to the vehicle. This nonlinear guidance law method demonstrates a number of benefits over the *Lyapunov Vector Field* approaches:

1. Naturally it follows any circular path of radius greater than a specific limit imposed by the dynamics of the vehicle;

2. Has an element of anticipation of the desired flight path;

3. Incorporates instantaneous vehicle speed adding an adaptive feature with respect to changes in vehicle ground speed caused by external disturbances such as wind;

4. Is asymptotically stable;

5. It is very simple and straightforward to apply in actual flight.

Although this guidance law shows a lot of benefits respect to the *Lyapunov Vector Field*, it is created for tracking circular paths. As before this law it is not adapt to overflight a fixed point.

In [12] a guidance logic that overcomes some of these problems is presented. As the method just cited it involves a reference point moving on the desired path. The motion of this reference point is coupled to the motion of the real vehicle by a factious mechanical link. In [28] there is a fixed length distance requirement while in [12] approach is a springlike and supplemented by a factious drag.

This paper is focused on the development of a 3d guidance law suitable for different paths. However in this paper a lot examples are shown and some of them can be related to the problem of monitoring a target.

The third category is more related to problems of operation research than to automatic control. A lot of different algorithms can be used in order to find the shortest paths, or the minimum energy path, or minimum fuel consumption path, between various prestabilized way points. Once a suitable path is stabilized it is usually followed through any guidance laws or, better, a control law for tracking a reference signal. One of the most important technique used to construct a path is the Dubins Theorem [8]. In [25] the problem of constructing minimum time trajectory for a Dubins vehicle in the presence of a time-varying wind vector field is considered. The results proposed in this paper extend the conclusion of the well-known Dubins theorem.

1.3 Kinematic Equations

Kinematic Modeling of the UAV

In this section an introduction to controllability and observability of the main system used in all the subsequent chapters is given. The work is based on the chapter 9 and chapter 11 of [34]. As it is discussed in 1, this thesis has the aim to investigate and give some solutions to the problem of tracking a ground target. The position of the target is assumed to be known by the by the UAV guidance system. In the next chapter a brief introduction to sensors of a guidance system is given.

The system model can descripted by the subsequent relations:

$$\begin{cases} \dot{x} = V\cos(\chi) \\ \dot{y} = V\sin(\chi) \\ \dot{\chi} = \frac{a_n}{V} \end{cases} \tag{1.1}$$

where V is the magnitude of the velocity vector $\mathbf{V}$, χ is the heading angle respect to the y-axis and a_n is the normal acceleration. In this case a xyz inertial reference frame is chosen but the analisys can be considered valid for any reference frame.

The lateral acceleration a_n are transformed into heading commands suitable to guarantee the maneuvers of the UAV to be consistent to its mechanical limitations it terms of maximum turn rate. Similarly as in most flight applications, a separate inner and outer feedback-loop control approach is assumed in this thesis. This because of its simplicity and the availability of good autopilots for vehicle motion inner-loop control such as stabilization and altitude hold.

It is important to highlight the main difference respect to the well-known system model of the unicycle [1]. In the system considered in this thesis the velocity is assumed as a fixed parameter equal to the cruise airspeed of the UAV chosen for the simulation. This constraint is necessary because the UAV has to stay at a fixed altitude if a good target tracking wants to be performed.

The system model presented in 1.1 is subjected to a pure rolling non-holomonic constraint:

$$\dot{x}\sin(\chi) - \dot{y}\cos(\chi) = 0 \rightarrow \chi = \arctan(\tfrac{\dot{y}}{\dot{x}})$$

It specifies the direction of the velocity vector. Now, considerng n as the number of the varible state and $\mathbb{M}$ the corrisponding manifold, the non-holominc constraint restricts the instantaneous motion of the system to a (n-1) dimensional space, but it is still possible to reach any configuration in $\mathbb{M}$. The analysis of this constraint will be treat later in the constraint analysis section.

The system 1.1 can be expressed from a control point of view in the following form:

$$\dot{\mathbf{x}} = f(\mathbf{x}) + g(\mathbf{x})\mathbf{u} \tag{1.2}$$

representing the kinematic model of the UAV. As it can be seen the UAV model can be considered an analytic affine control system. In this case $\mathbf{x} = [x, y, \chi]^T$ represents the n-state vector of the UAV on the manifold M and $\mathbf{u} = [u]^T$ the m-vector of input (obviously in this case n=3 and m=1). Usually, $f(\mathbf{x})$ and $g(\mathbf{x})$ are smooth vector field on the manifold M. The vector field f is referred to as the *drift* vector field and the vector field g are referred to as the *input* vector fields which in this case it is constant $[0, 0, 1]^T$.

Control system 1.2 can be considered as a special case of a drift free system of the form:

$$\dot{\mathbf{x}} = \sum_{i=0}^{m} g_i(\mathbf{x})\mathbf{u}_i \tag{1.3}$$

with the input u_0 attached to the vector field $g_0(\mathbf{x}) = f(\mathbf{x})$ and fixed at 1 (m=1).

In matrix form the system 1.1 becomes:

$$\begin{bmatrix} \dot{x} \\ \dot{y} \\ \dot{\chi} \end{bmatrix} = \begin{bmatrix} V\cos\chi & 0 \\ V\sin\chi & 0 \\ 0 & 1 \end{bmatrix} \begin{bmatrix} 1 \\ u \end{bmatrix} \tag{1.4}$$

where $g_0 = [V\cos(\chi), V\sin(\chi), 0]^T$, $g_1 = [0, 0, 1]^T$ and $u = \frac{a_n}{V}$. It can be defined also $\bar{u} = [1, u]^T$.

Controllability Analysis

A non linear control system can be considered, as it can be seen in the previous section, as a collection of vector fields parametrized by a parameter called control. The system model is represented by vector fields as they allows to perform algebraic operation on them such as taking linear combinations and taking a product called Lie bracket.

Definition 1.1. Lie Bracket of two Vector Field.

Defined $g : \mathbb{R}^n \to \mathbb{R}^n$ and given two smooth vector fields $g_0(\mathbf{x}), g_1(\mathbf{x})$ on the manifold M, a new vector field called Lie Bracket $[g_0(\mathbf{x}), g_1(\mathbf{x})]$ is defined as follows:

$$[g_0, g_1](\mathbf{x}) = \frac{\partial g_1}{\partial \mathbf{x}} g_0(\mathbf{x}) - \frac{\partial g_0}{\partial \mathbf{x}} g_1(\mathbf{x})$$

where $\frac{\partial g_1}{\partial \mathbf{x}}$ and $\frac{\partial g_0}{\partial \mathbf{x}}$ denote the Jacobi matrix of g_0 and g_1.

The Lie Bracket of two vector fields is another vector field which measures noncommutativeness of the flows of the vector fields.

In order to define the control properties of the system 1.4 it is important to give some definitions.

Definition 1.2. Distributions.

Given a set of smooth vector fields $g_0(\mathbf{x}), g_1(\mathbf{x}) \dots g_m(\mathbf{x})$ a distribution $\Delta(\mathbf{x})$ is defined as:

$$\Delta = \text{span}\{g_0(\mathbf{x}), g_1(\mathbf{x}) \dots g_m(\mathbf{x})\}.$$

Definition 1.3. Involutive Distributions.

A distribution Δ' is called involutive if for any two vector field $g_0(\mathbf{x}), g_1(\mathbf{x})$ $\in \Delta'(\mathbf{x})$ their Lie Bracket $[g_0(\mathbf{x}), g_1(\mathbf{x})] \in \Delta'$.

Besides, its involutive closure $\bar{\Delta}$ is the smallest involutive distribution containing a generic distribution Δ':

$$\bar{\Delta}=\text{span}\{g_0,\ldots,g_m,[g_1,g_2],[g_1,g_3],\ldots[g_1,[g_2,g_3]],[g_2,[g_3,g_1]],\ldots\}.$$

This variable $\bar{\Delta}$ is also known as the controllability distribution and contains valuable information about the set of the states that are accessible from a given starting point $\mathbf{x}_0$[1].

Definition 1.4. Invariance.

A distribution Δ is said to be invariant under g_0, with $g_0 \in \Delta$, if for every $\tau \in \Delta$, $[g_0, \tau] \in \Delta$.

Theorem 1.3.1. Representation Theorem.

Let Δ be a regular[2] involutive distribution of dimension d and let Δ be invariant under g_0. Then at each point $\mathbf{x}_0$ there exist a neighborhood U and coordinate transformation $\mathbf{z} = \phi(\mathbf{x})$ defined on U in which the vector field has the form:

$$\tilde{g}_0(\mathbf{z}) = \begin{bmatrix} g_{01}(z_1,\ldots,z_d,z_{d+1}\ldots,z_n) \\ \vdots \\ g_{0d}(z_1,\ldots,z_d,z_{d+1}\ldots,z_n) \\ g_{0d+1}(z_{d+1}\ldots,z_n) \\ \vdots \\ g_{0n}(z_{d+1}\ldots,z_n) \end{bmatrix}$$

This machinery is very useful to study local decomposition of control system of the form of 1.2. Let Δ be a distribution which contains $g_0, g_1, \ldots, g_m$ and is invariant under the vector fields $g_0, g_1, \ldots, g_m$ and which is involutive.

[1] It is easy to derive that the involutive distribution $\bar{\Delta}$ is also invariant under $g_0, g_1 \ldots, g_m$

[2] Regular distribution means that the rank of Δ is constant in U

Then with an easy extension of the preceding theorem it is possible to find coordinates such that the control system may be represented using suitable coordinates as:

$$\begin{aligned} \dot{\xi}_1 &= g_{01}(\xi_1, \xi_2) + \textstyle\sum_{i=1}^{m} g_{0i}(\xi_1, \xi_2)\mathbf{u}_i \\ \dot{\xi}_2 &= 0 \end{aligned} \tag{1.5}$$

A candidate for the involutive distribution Δ which satisfies the preceding requirements is the controllability distribution $\bar{\Delta}$. The discussion shows that the ξ_2 states are the uncontrollable states in that the dynamics (the ξ_2 are unaffected by the choice of the input). The number of the states ξ_2 is equal to n - dimension of $\bar{\Delta}$.

Considering equation 1.4 it results:

$$[g_0, g_1](\mathbf{x}) = \begin{bmatrix} -V\sin\chi \\ V\cos\chi \\ 0 \end{bmatrix}$$

and the dimension of $\bar{\Delta}$ is equal to 3 ($\dim(\bar{\Delta})$=3). Hence, it can be conlucled that the affine control system 1.2 is controllable because the number of states ξ_2 is zero.

Kinematic Modeling of the Tracking Problem

A mathematical model is used to describe UAV-target kinematics by using the parameters of the **LOS**. These parameters are: the distance R between UAV and target, the distance rate $\dot{R}$ and the azimuth angle σ between the north axis and the **LOS**.

With reference to figure 1.1, the geometry of homing guidance in the horizontal plane the measurable variables are:

- The distance $R = \sqrt{(x_T - x)^2 + (y_T - y)^2}$
- The **LOS** angle $\sigma = \arctan \frac{y_T - y}{x_T - x}$

The variables used to specify the position and orientation of the UAV and the target in a Cartesian reference frame are:

1. x, y, z and x_T, y_T, z_T;

2. Heading angle χ and χ_T;

3. The speed V and V_T.

The Kinematics of UAV target geometry describes the change in time of the position vector from the UAV to the target **R**. The kinematics is characterized by two pairs of kinematic equations one of which determines the relative motion of the center of the mass of the UAV and the target. Hence, the system model description considered both for the UAV and for the target is the same mathematical model described at eh beginning of section 1.3.

UAV Equations of Motion

$$\begin{cases} \dot{x} = V\cos(\chi) \\ \dot{y} = V\sin(\chi) \\ \dot{\chi} = \frac{a_n}{V} \end{cases} \tag{1.6}$$

TARGET Equations of Motion

$$\begin{cases} \dot{x}_T = V_T\cos(\chi_T) \\ \dot{y}_T = V_T\sin(\chi_T) \\ \dot{\chi}_T = \frac{a_{nT}}{V_T} \end{cases} \tag{1.7}$$

The direction along the UAV travels is dictated by an alghorithm section in the guidance processor known as the guidance law. As it is written in 1.2 many different guidance laws have been developed over the years, and with the advent of highly maneuverable airbone targets, research on improved guidance laws is continuing. Currently several guidance laws of the two-point (UAV and Target) are implemented. In the next chapter two of the most famous **LOS rate guidance** laws will be explained: **Pursuit Navigation** and **Proportional Navigation Guidance** [3].

Observing figure 1.1 the expression of the distance R can be also written

[3]The pedix T represents the positions, the heading and the speed of the Target

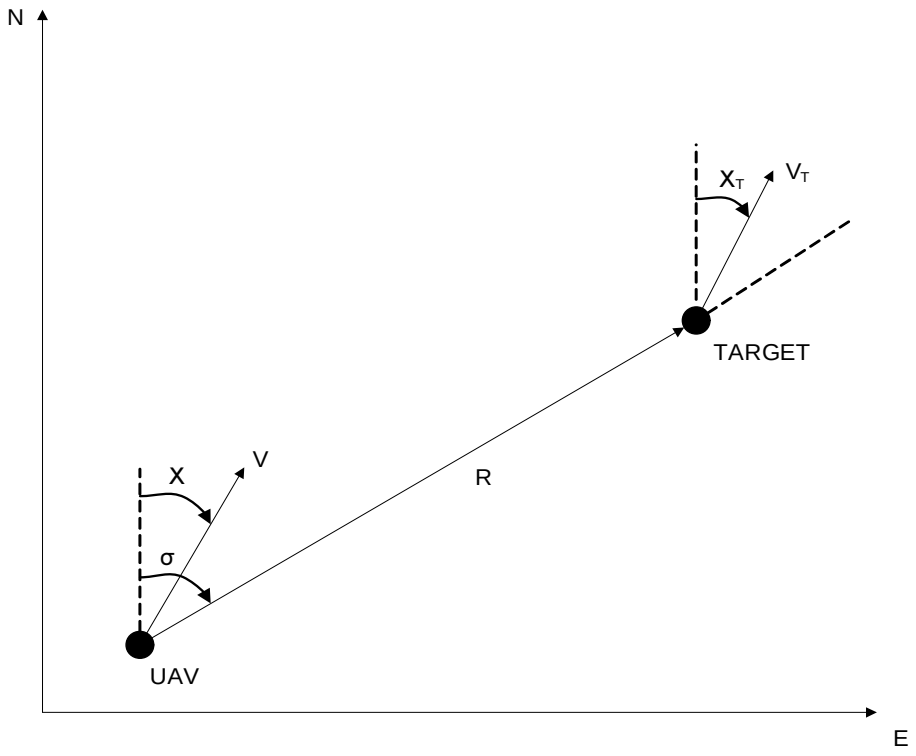

Figure 1.1: Relative Geometry for Guidance

as:

$$\begin{cases} x_T - x = R\cos(\sigma) \\ y_T - y = R\sin(\sigma) \end{cases}$$

After some substitution, the final two equations which represent the relative movement in the horizontal plane of the UAV-target couple can be easily derived.

$$\begin{cases} \dot{R} = V_T\cos(\sigma - \chi_T) - V\cos(\sigma - \chi) \\ R\dot{\sigma} = -V_T\sin(\sigma - \chi_T) + V\sin(\sigma - \chi) \end{cases} \tag{1.8}$$

Controllability analysis of the Kinematic Model of Tracking Problem

It is important to give an expression for the system 1.6 where the drift and the input vector field are highlighted. In this way the analysis of the

relative motion will be easier. A rotation χ around the Z-axes is done in order to express the relative motion along the UAV body axes. The matrix rotation is the subsequent:

$$R_I^B = \begin{bmatrix} \cos(\chi) & \sin(\chi) & 0 \\ -\sin(\chi) & \cos(\chi) & 0 \\ 0 & 0 & 1 \end{bmatrix} \tag{1.9}$$

where the sub-index I means the inertial frame while the sub-index B means the body reference frame.

Defining $\mathbf{x_{R}}_I = [x_T - x, y_T - y, \chi_T - \chi]_I^T$ it can be derived: $\mathbf{x_{R}}_B = R_I^B \mathbf{x_{R}}_I$. The error coordinates can be defined as:

$$\begin{cases} x_R = (x_T - x)\cos(\chi) + (y_T - y)\sin(\chi) \\ y_R = -(x_T - x)\sin(\chi) + (y_T - y)\cos(\chi) \\ \chi_R = \chi_T - \chi \end{cases} \tag{1.10}$$

Therefore, the tracking error model is obtained from 1.10 and 1.7 1.6 after some algebra manipulations:

$$\begin{cases} \dot{x}_R = \dot{\chi} y_R + V_T \cos(\chi_R) - V \\ \dot{y}_R = -\dot{\chi} x_R + V_T \sin(\chi_R) \\ \dot{\chi}_R = \dot{\chi}_T - \dot{\chi} \end{cases} \tag{1.11}$$

For convenience, new coordinates and inputs are defined:

$$\begin{cases} x_0 = \chi_R \\ x_1 = y_R \\ x_2 = -x_R \end{cases}$$

and

$$\begin{cases} u_0 = \dot{\chi}_T - \dot{\chi} \end{cases}$$

Equation 1.11 can be rewritten as:

$$\begin{cases} \dot{x}_0 = u_0 \\ \dot{x}_1 = x_2(\dot{\chi}_T - u_0) + V_T \sin(x_0) \\ \dot{x}_2 = V - x_1(\dot{\chi}_T - u_0) - V_T \cos(x_0) \end{cases} \tag{1.12}$$

Through this new coordinates $\bar{\mathbf{x}} = (x_0, x_1, x_2)$ the tracking problem is transformed into a stability problem. The system 1.12 is reffered to the error model of the tracking problem. Note that every coordinate trasformation used is invertible and $(x_0, x_1, x_2) = (0, 0, 0)$ is equivalent to $x = x_T$, $y = y_T$ and $\chi = \chi_T$. Hence, the tracking error model can now be expressed in an affine form $\dot{\bar{x}} = f(\bar{\mathbf{x}}) + g(\bar{\mathbf{x}})u_0$ where the drift and the input vector field results:

$$\begin{cases} f(\bar{\mathbf{x}}) = [0, V_T \sin(x_0) + x_2\dot{\chi}_T, V - V_T \cos x_0 - x_1\dot{\chi}_T]^T \\ g(\bar{\mathbf{x}}) = [1, -x_2, x_1]^T \end{cases} \tag{1.13}$$

As discussed in the precedent case, the controllability analysis of the tracking problem passes through the definition of the Lie bracket of the just presented system model. Equation 1.12 can be expressed in a form equal to equation 1.4 where the affine control system is put in a form similar to a driftless model system. In this way, considering $f(\bar{\mathbf{x}}) = g_0$ and $g(\bar{\mathbf{x}}) = g_1$ it results:

$$[g_0, g_1](\bar{\mathbf{x}}) = \begin{bmatrix} 0 \\ -V_T(\sin(x_0) + \cos(x_0)) - u_T(x_1 + x_2)) \\ -V_T \sin(x_0) - u_T x_2 \end{bmatrix}$$

where the variable $u_T = \dot{\chi}_T$.

The controllability distribution results:

$$\bar{\Delta} = \begin{bmatrix} 0 & 1 & 0 \\ V_T \sin(x_0) + u_T x_2 & -x_2 & -V_T(\sin(x_0) + \cos(x_0)) - u_T(x_1 + x_2) \\ V - V_T \cos(x_0) - u_T x_1 & x_1 & -V_T \sin(x_0) - u_T x_2 \end{bmatrix}$$

which has dimension equal to 3. Of course in this case, the model remains controllable.

It is important to underline that the solution of the Kinematic equation of the motion can be found only using the normal acceleration of the UAV. In fact, the target dynamics can be considered as an exosystem, completely autonomous from the dynamics of the airplane. Besides, in order to create

a suitable solution for the dynamics of the UAV, a saturation constraint on the normal acceleration must be considered. Only under this bound the trajectories created by the guidance law proposed can be tracked by the airplane.

The tracking problem covers two different cases:

1. V_T and u_T are equal to zero. In this case the tracking problem is reduced to a stability problem.

2. If the $\lim_{t\to\infty} V_T^2 + u_T^2 \neq 0$ the tracking problem is reduced to the so called tracking control problem.

It has to be considered that the problem of tracking a ground target can combine together the two cases just presented. However, since f is the drift vector field, which is not stereable using control input it is not completely clear in which direction it is possible to steer the control system in the distribution $\bar{\Delta}$. It is necessary to define the set of states accessible from a given state $\mathbf{x}_0$.

Accessibility analysis

Definition 1.5. Reachable Set from $\mathbf{x}_0$.

Let $R^U(\mathbf{x}_0, T) \subset \mathbb{R}^n$ be subset of all states accessible from state $\mathbf{x}_0$ in time T with the trajectories being confined to a neighborhood U of $\mathbf{x}_0$. This is called the reachable set from $\mathbf{x}_0$ (see Figure 1.2).

In order to categorize the reachable set, the accessibility Lie Algebra has to be defined.

Definition 1.6. Accessibility Lie Algebra.

The accessibility Lie Algebra A of a control system in the form 1.2 is defined to be the span over the ring of smooth function of elements in the form:

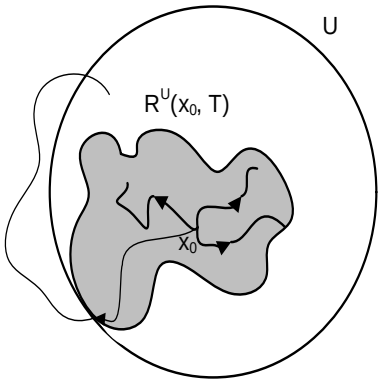

Figure 1.2: Reachable Set (shadowed figure)

$$A\text{=span}\{g_1, \ldots, g_m, [g_0, g_1], [g_0, g_2], \ldots [g_0, [g_1, g_2]], [g_0, [g_1, g_3]], \ldots\}.$$

where, respect to Definition 1.3, $\{g_1, \ldots, g_m\} \in g$ (g is the input vector field).

The distribution A is involutive and g_i invariant. The distribution A and $\bar{\Delta}$ are related by: $\bar{\Delta} = A$+span(f).

Considering the input vector $g = [0, 0, 1]^T$, which is the case of the unicycle studied in this dissertation, it is evident that the reachable subset has dimension equal to 3. This can be obviously supported because the system model is completely controllable and, as in the linear case, the states are all accessible.

The non linear control system 1.2 is locally accessible from $\mathbf{x}_0$ if $\forall U$, a neighborhood of $\mathbf{x}_0$, $\forall T \geq 0$ $\exists$ $\Omega \subset R^U(\mathbf{x}_0, T)$ with Ω some non-empty open set (see Figure 1.3).

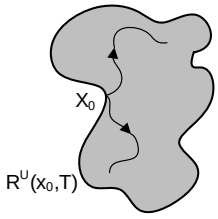

Figure 1.3: Locally Accessible Set

The locally accessible property can be checked through *Chow Theorem*.

Theorem 1.3.2. Chow's Theorem.

For drift control system of the form of 1.2 there exist admissible controls to steer the system between two given arbitrary points x_0 and $x_1 \in U$ if for some p

$$G_p(x) = T\mathbb{R}^n \cong \mathbb{R}^n$$

for all $x \in U$

It can be also defined that a non linear control system is locally accessible from $\mathbf{x}_0$ if and only if dim $\bar{\Delta}(\mathbf{x}_0) = n$ (This last sentence is also known as **accessibility rank condition** and n is equal to the number of the states).

Constraint Analysis

The configuration of a mechanical system can be uniquely described by a n-dimensional vector of generalized coordinates $\mathbf{x} = (x_1, x_2..., x_n)^T$.. The configuration space $\mathbb{M}$ is an n-dimensional smooth manifold, locally represented by $\mathbb{R}^n$. The generalized velocity at a generic point of a trajectory $x(t) \subset \mathbb{M}$ can be considered as the tangent vector $\dot{\mathbf{x}} = (\dot{x}_1, \dot{x}_2, ..., \dot{x}_n)^T$.

There are two different possible constraints:

1. **Geometric Constraints**.

   A geometric constraints may exist or be imposed on the mechanical system $h_i(x) = 0$ (i=1,...,k) restricting the possible motion to a (n-k)-dimensional submanifold.

2. **Kinematic Constraints**

   A mechanical system may also be subjected to a set of kinematic constraints, involving generalized coordinates and their derivatives $a_i^T(x, \dot{x}) = 0$ (i=1,...,k).

In most cases the constraints can be considered Pfaffian that is when $a_i^T(x)\dot{x} = 0$ (i=1,...,k) holds. A set of Pfaffian constraints is called holonomic if it is integrable; otherwise, it is called nonholonomic. Holonomic and nonholonomic constraints affect mobility in a completely different way.

For illustration, consider a single Pfaffian constraint $a^T(x)\dot{x} = 0$. If the constraint is holonomic, then it can be integraded as $h(x) = c$ $(c \neq 0)$ with $\frac{\partial h}{\partial x} = a^T(x)$ and c an integration constant. The motion of the system is confined to lie on a particular level surface of h depending on the initial condition through $c = h(x_0)$. If the constraints is nonholonomic, then it cannot be integrated: although at each configuration the instantaneous motion of the system is restricted to an (n-1) dimensional subspace, it is still possible to reach any configuration in $\mathbb{M}$.

By analysing system 1.2 it can be easily derived that it is subjected to a Pfaffian constraint described by:

$$\dot{x}\sin(\chi) - \dot{y}\cos(\chi) = 0 \tag{1.14}$$

This constraint describes the pure rolling motion of the UAV and its velocity direction. In Figure 1.4 the nonholonomic constraint is depicted using a rolling disc because the system model used for describing the trajectories of the UAV is equal to a classical unycicle model.

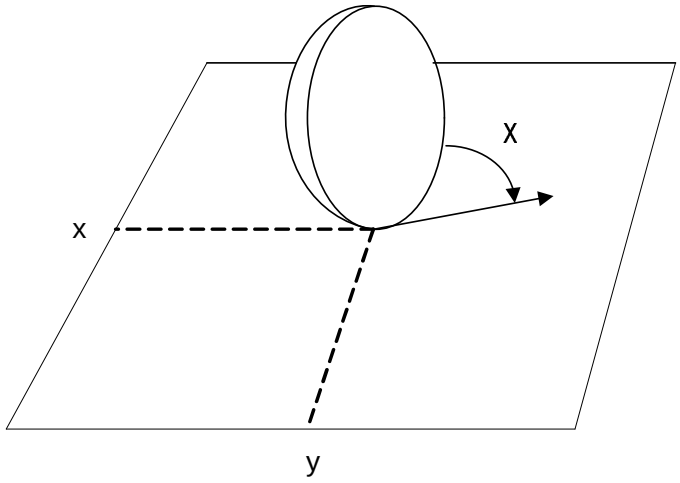

Figure 1.4: Pure NonHolomonic Constraint

The holonomy and nonholonomy of constraints may be conveniently studied through a dual approach: look at the directions in which motion is allowed rather than directions in which motion is prohibited. In fact there is a strict relationship between the capability of accessing every configuration and

nonholonomy of the velocity constraints. Hence, controllability of its whole configuration space is equivalent to nonholonomy of the original kinematic constraints.

It can be concluded that a set of k Pfaffian constraint $A(x)\dot{x} = 0$ is nonholomonic if and only if the associated kinematic model

$$\dot{\mathbf{x}} = \sum_{i=0}^{m} g_i(\mathbf{x})\mathbf{u}_i \text{ m=n-k}$$

is controllable, that is $\dim\bar{\Delta} = n$, being the involutive closure of the distribution associated with $g_1, ..., g_m$.

Chapter 2

PN and PNG Guidance Laws

2.1 Target Tracking Sensor

A tracking sensor on an aircraft is a device to detect the relative position vector of a target with respect to the pursuer. The functions of the tracking sensor is to receive external signals that are sent to the follower vehicle for the purpose of directing its heading χ. Because of its role in providing an essential communication link to the external environment, the sensor becomes the key element of the entire vehicle system.

The choice of this device is not included in this research. During the presentation of all the guidance laws the assumption of a sensor capable to detect the position and heading angle of a target is made. Different kind of sensors can be chosen relative to the variables.

Table 2.1 includes various type of targeting sensor. A particularly common type is one which measures the azimuth angle and depression angle of the pursuer-to-target LOS. Usually some type of image of the target area is displayed to the weapon system operator. The operator then selects the target by positioning a marker or a pair of crossed reticles over the target and depresses a target designating a button. The computer responds by recording the azimuth and depression angles of the target marker.

A range sensor provides two means of measuring slant range from the pursuer to the target. It should be noted that the range R, the quality of in-

Generic Type Measurement	Examples
LOS angles Azimuth σ	Gunsight, HUD, EO Display, Mapping Radar, IR, Sonar, Optical, Video Tracker
Distance **R**	Radar, Laser, Sonar, Optical Instruments, FCS, Passive Ranging Processor, On board Active sensor
LOS rate $\dot{\sigma}$	EO Tracker
Range Rate $\dot{R}$	Doppler Radar
External Reference	Ground Radar Director, LORAN, TACAN, GPS, DME

Table 2.1: Targeting sensors

formation concerning which would be very important if it were being directly utilized in the solution of Guidance Navigation Control (**GNC**) problems, is not an easily measured quantity. Thus, it is advantageous to derive guidance algorithms that do not require range information.

The great majority of angular rate sensing system that have been built so far are of the TV contrast tracker type. In addition to requiring three axis stabilization, these sensors have a response time that is scan rate limited. The TV contrast tracker is also characterized by the requirement of a single, high contrast point to track.

Determination of closing velocity V_c is done with the aid of a Doppler tracking device. Doppler frequencies, which are one of the principal outputs of the radar sensor, are proportional to V_c.

Each of these targeting sensors is a navigation aid, which locates the pursuer in an electronically generated grid or coordinate system. The rest of targeting task centers around locating the target in this same electronic grid or set of coordinates. One way in which to implement this type of targeting is to use radar ground control to direct pursuer's flight, which requires that the pursuer be within **LOS** of the ground radar. Other **LOS** positiong system

include TACAN and DME. To a large extent, acccurancy is determined by relative geometry between the pursuer and the several ground stations, also known as GDOP (geometric dilution of position). The LORAN system is capable of obtaining coverage beyond the **LOS** and at lowest altitude because it uses ground wave transmission of low frequency radio waves. When GPS is operational, it will be able to position low flying pursuers in all three dimensions since its reference stations are satellites.

2.2 LOS Rate Guidance

LOS rate guidance is defined by:

$$\dot{\chi} = \lambda \dot{\sigma} \tag{2.1}$$

$$\chi = \lambda \sigma + C \tag{2.2}$$

where χ is the commanded flight path, λ is the navigation gain and C is the initial flight path angle χ_0. Pursuit Navigation law and Proportional Navigation Guidance law, which are described in the next sections, can be implemented in a guided UAV system using LOS angle and angle rate information respectively. As it is explained the Pursuit Navigation has a limited capability to engage manuvering target. Proportional Navigation Guidance can be implemented easily and can reduce the maneuver requirements and produce good miss distance performance. It has a long history of accetable performance and has been used succesfully in several systems.

Pursuit Navigation (PN)

The first guidance law that was implemented is known as pursuit navigation, resulting in a pursuit course. The pursuer aims directly at the target throughout the encounter, like a dog chasing a rabbit. In pursuit navigation the angle between the velocity vector and the LOS to the target is driven to zero [37]. The UAV is commanded to turn at a rate equal to the difference between the LOS and the heading angle. The UAV is constantly turning

during the flight unless it is head on or tail on.

Figure 2.1a shows the diagram block of the Pursuit Navigation. The direction of the UAV velocity vector must be sensed to steer the UAV with the guidance law descripted by:

$$\chi = \sigma \tag{2.3}$$

which implies that $\lambda = 1$ and $C = 0$ in equation 2.2. Figure 2.1b shows the same engagement problem using the kinematic equations between UAV and the Target. It is evident that inside equations 1.8 there are the dynamics of the UAV and the Target. In section 1.3 it is pointed out that the input of the system is the normal acceleration of the UAV a_n.

From equation 2.3 and the definition of the Pursuit Navigation it holds:

$$\dot{\chi} = \sigma - \chi \quad \text{or} \quad a_n = V(\sigma - \chi) \tag{2.4}$$

For the following developments the assumptions of non-maneuvering target is made:

- χ_T=constant,V_T=constant,V=constant;

This hypotesis are depicted in Figure 2.2.

Inserting equation 2.3 and considering the two assuptions just made, the equations 1.8 becomes:

$$\dot{R} = V_T \cos(\sigma - \chi_T) - V \tag{2.5}$$

$$R\dot{\sigma} = -V_T \sin(\sigma - \chi_T) \tag{2.6}$$

From equation 2.6 it can be derived that:

$$\dot{\sigma} = -\frac{V_T \sin(\sigma - \chi_T)}{R} \tag{2.7}$$

Note that $\dot{\sigma} = 0$ if $\sigma = \chi_T$ or $\sigma = \chi_T + \pi$. Therefore a_n will always be varying unless $\chi = \chi_T$,$\chi_T + \pi$ which implies a head-on or a tail-on path.

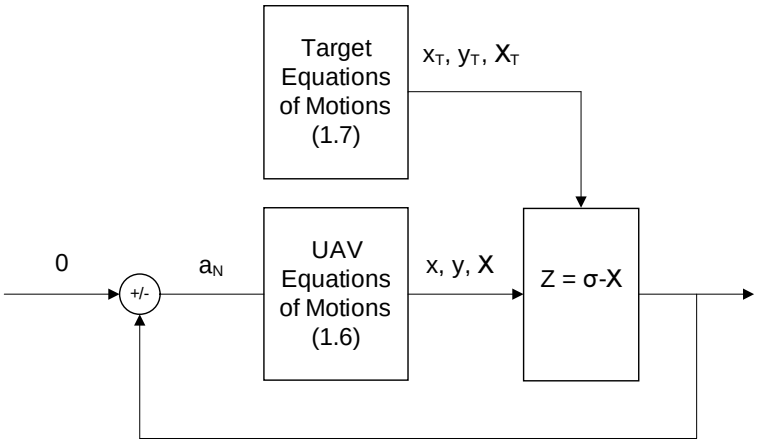

(a) Kinematic Equations of Motions

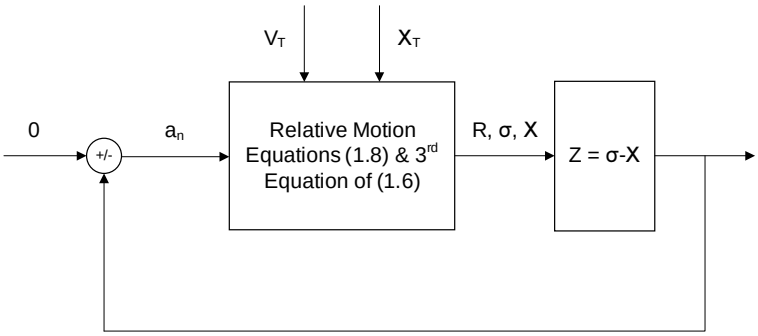

(b) Kinematic Equations of Relative Motion

Figure 2.1: Block Diagrams of Pursuit Navigation

Consequently, since equation 2.4, the UAV must be continuously turning if $\chi \neq \chi_T, \chi_T + \pi$.

The pursuit equations are solved as:

$$\frac{\dot{R}}{R\dot{\sigma}} = -\frac{\cos(\sigma - \chi_T)}{\sin(\sigma - \chi_T)} + \frac{V}{V_T \sin(\sigma - \chi_T)}$$

hence:

$$\frac{dR}{R} = (-\cot(\sigma - \chi_T) + \frac{V}{V_T}\csc(\sigma - \chi_T))d\sigma \tag{2.8}$$

Integrating equation 2.8 results:

$$\ln(R) = -\ln(\sin(\sigma - \chi_T)) + \mu \ln\left(\tan(\frac{\sigma - \chi_T}{2})\right) + C \tag{2.9}$$

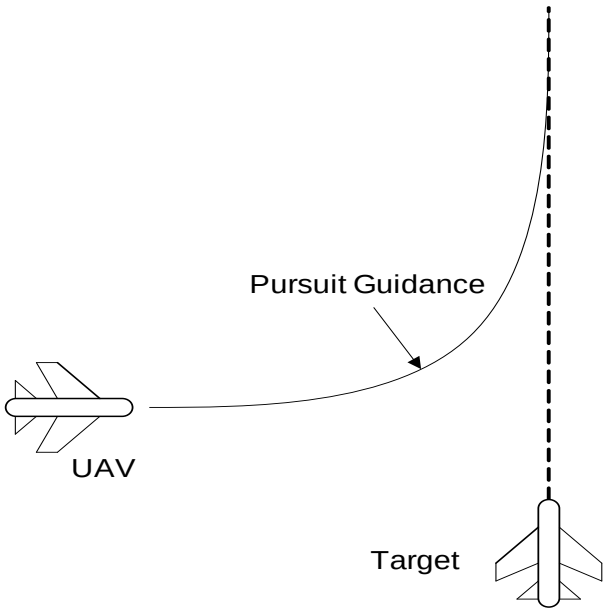

Figure 2.2: Pursuit Navigation

where $\mu = \frac{V}{V_T}$.

It has to be considered that if $\chi_T \leq \sigma \leq \chi_T + pi$ the target is essentially assumed to be in front of the UAV while if $-\pi - \chi_T \leq \sigma \leq \chi_T$ the target is behind the pursuer.

Operating on equation 2.9 it can be derived:

$$\frac{R\sin(\sigma - \chi_T)}{(\tan(\frac{\sigma-\chi_T}{2}))^{\mu}} = C \tag{2.10}$$

Hence, considering equation 2.6 and using equation 2.10 it results:

$$\dot{\sigma} = -\frac{V_T C(\tan(\frac{\sigma-\chi_T}{2}))^{\mu}}{R^2} \tag{2.11}$$

If the target is assumed to be in front of the target this relation leads to the property of Pursuit Navigation which terminates in a tail chase which means $\sigma(t_f) = \chi(t_f)$ for all cases except the head-on case.

If the target is assumed to be behind the pursuer it is assumed that: $\cot(\sigma) = -\cot|\sigma|$ and $\csc(\sigma) = -\csc|\sigma|$. With these hypothesis it can be derived in the same way that $\sigma(t_f) = \chi(t_f) = 0$.

For the non head-on pursuit, the UAV must go faster than the Target to be able to catch it in a tail case, thus $\mu \geq 1$.

Figure 2.2 shows Target interception based on a Pursuit Navigation. In the Pursuit Navigation law the UAV is commanded to turn at a rate equal to the LOS rate.

Assuming a nonhead-on mission and analyzing equation 2.11, a_n has the following range of values in the neighborhood of the terminal time:

$$a_n = \begin{cases} \infty & \text{if } \mu > 2, \\ 0 & \text{if } \mu < 2. \end{cases}$$

Limits of Pursuit Navigation

The guidance law described by equation 2.3 creates errors even in absence of wind due to the curvilinear nature of the UAV's heading trajectory, and the fact that the vector speed of the UAV $\mathbf{V}$ and the velocity vector respect to the ground $\mathbf{V_g}$ are not always coincident due to the wind effect.

Figure 2.4 depicts the geometry of guidance with the wind effect. σ_{LEAD} is the lead angle between the projections of the line of sight and the required aircraft ground velocity vector V_g into the horizontal plane. The best results are obtained using Velocity Pursuit Navigation, or pure guidance, as it is called. The angle σ_{LEAD} has been defined in [22] as:

$$\sigma_{LEAD} = \gamma - \alpha \sin(\phi) \tag{2.12}$$

where $\gamma = (\sigma - \chi)$. α denotes the angle of attack and ϕ denotes the roll angle.

The pure guidance law can be described by:

$$\chi_g = \sigma_{LEAD} \tag{2.13}$$

The essence of this guidance process is to align the aircraft's ground velocity vector with the LOS. Equation 2.13 shows that the velocity Pursuit Navigation needs the measurements of the angle σ_{LEAD}, α and ϕ. The last two are measured rather easily.Besides, it is important to underline that

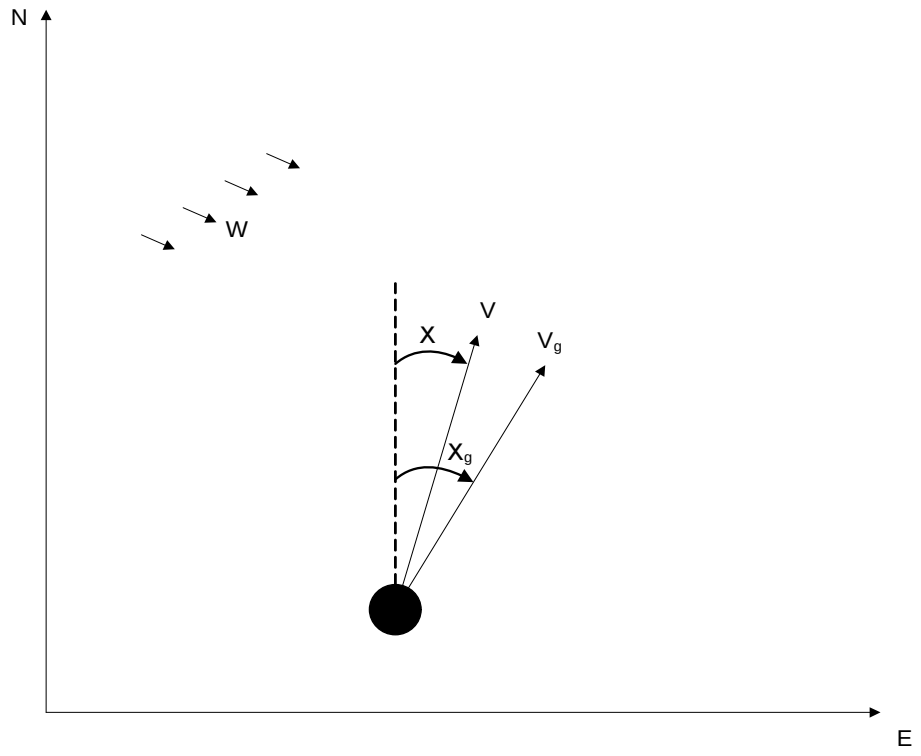

Figure 2.3: Wind Geometry

also the use of a GPS receiver provides directly the direction of the ground velocity vector χ_g. Hence equation 2.12 can be written as: $\sigma_{LEAD} = \sigma - \chi_g$.

Observing Figure 2.4 and using equations 2.12 it can be derived that $\chi_g = \chi + \alpha \sin(\phi)$. Hence the guidance law 2.13 means that $\chi = (\sigma - \sigma_{LEAD}) - \alpha \sin(\phi)$. The scheme represented in 2.5 represents the block diagram that can be used in order to avoid the effect of the wind in the Pursuit Navigation law.

Generally, pursuit navigation is not used to guide a UAV for rendezvous problem or interception if the velocity of the UAV becomes teo times greater than the target velocity because the guidance forces tends to be too high when the relative distance between the UAV and the target becomes zero. Those problem will not occur for a chasing purpose if a reference target with the same constant velocity of the UAV can be created. In both Pursuit Navigation and velocity pursuit, the UAV is constantly turning unless it is tail

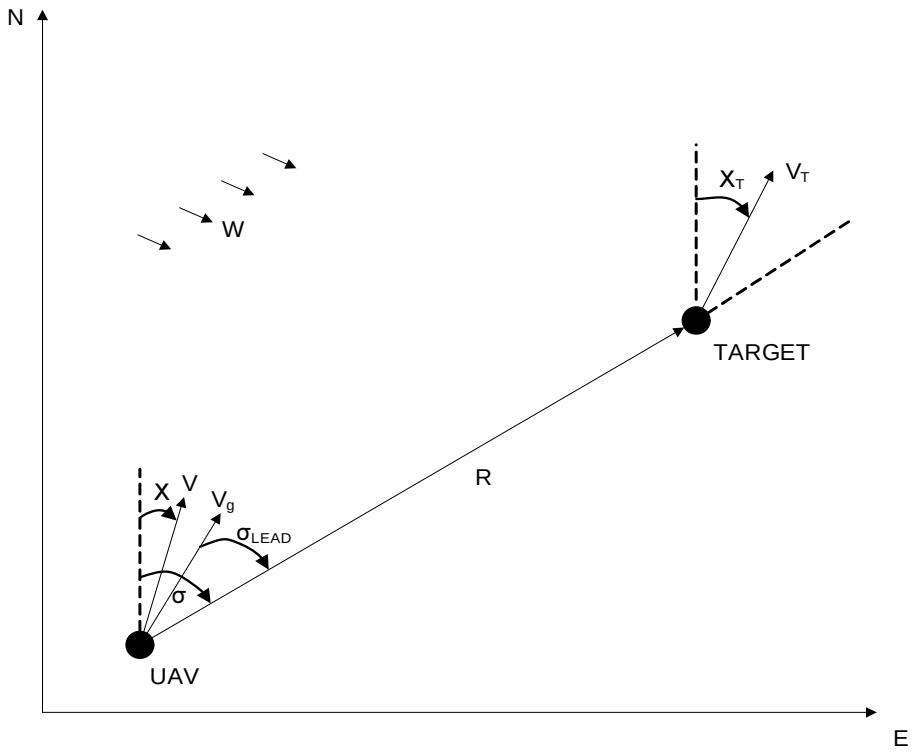

Figure 2.4: Relative Geometry for Guidance with Wind Effect

on or head on respect to the target. While it permits a simple implementation and it is less sensitive to noise, pursuit navigation and velocity pursuit are considered impractical as a homing guidance law against moving target owing to the high maneuver requirement when the UAV is close to the target.

Besides it is not possible to use this kind of guidance laws when the target is supposed to be fixed because once it is reached the UAV continuates to follow the LOS.

Proportional Navigation Guidance (PNG)

Proportional Navigation Guidance is a guidance law where the pursuer heading rate is made proportional to the rate of the LOS. The purpose of such a course is to counter the tendency for the LOS to rotate and to approximate a constant-bearing course.

Consider the UAV pointed towards the target: if the latter is considered

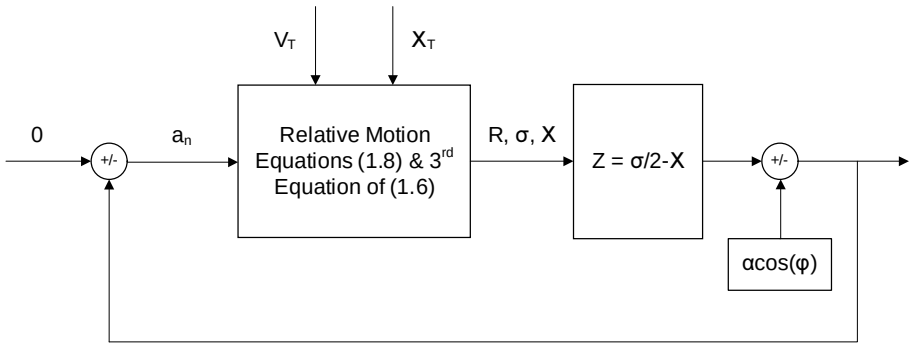

Figure 2.5: Guidance Pursuit with wind effect

non-maneuvering and the UAV and Target velocities remain unchanged, the UAV will continue on a collision course, having achieved a constant-bearing navigation. If it happens that the UAV is not launched on a collision course, there will be some curvature associated with the resulting trajectory that depends on a navigation constant λ.

The analysis of the navigation constant is very important to understand the behavior of the UAV during the flight. For small λ values the UAV corrections are small early in the flight while they begin to be larger as the UAV get closer to the Target. The situation is reversed for high values of λ, where the collision course errors are corrected early on in flight and maneuvers consequently are kept at reasonable levels in the terminal phase. A reasonable value of λ based on experience is usually set between 2 and 4.

The proportinal navigation guidance turns the relative velocity vector $\mathbf{V_r}$ between the UAV and the target on the LOS through the guidance law:

$$\dot{\chi} = \lambda\dot{\sigma} \quad \text{or} \quad a_n = V\lambda\dot{\sigma} \tag{2.14}$$

Defining $\mathbf{V_r} = [\dot{y}_T - \dot{y}, \dot{x}_T - \dot{x}, 0]^T$ and $\mathbf{R} = [y_T - y, x_T - x, 0]^T$ as, respectevely, the relative velocity vector and the distance vector, the rate of the LOS angle can be also expressed by:

$$\dot{\sigma} = \frac{\mathbf{V_r} \times \mathbf{R}}{R^2} \tag{2.15}$$

Figures 2.6a and 2.6b represent the block diagrams of the proportinal

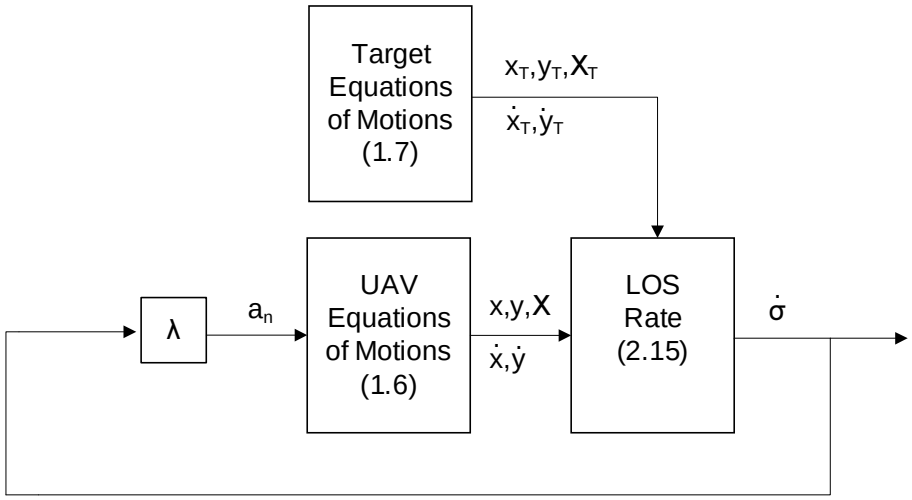

(a) Equations of Motions

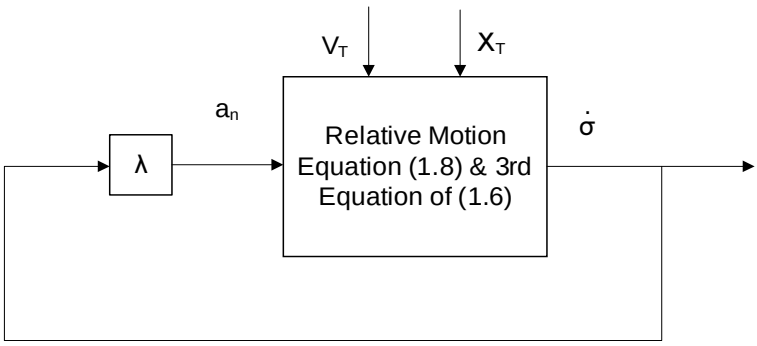

(b) Kinematic Equations

Figure 2.6: Block Diagrams of PNG Guidance

guidance navigation. They are slightly different respect to figures 2.1a and 2.1b especially for the presence of the navigation factor λ. In order to analyse the property of this guidance law, the same assumptions chosen for the pursuit navigation are made (constant velocities, target nonmaneuvering, $\chi_T = 0$). Considering these hypothesis equations 1.8 becomes:

$$\dot{R} = V_T \cos(\sigma - \chi_T) - V \cos(\sigma - \chi) \tag{2.16}$$

$$R\dot{\sigma} = -V_T \sin(\sigma - \chi_T) + V \sin(\sigma - \chi) \tag{2.17}$$

Differentiation of equation 2.17 and the introduction of 2.14 leads to:

$$R\ddot{\sigma} + \dot{\sigma}\left[2\dot{R} - V\cos(\sigma - \chi)\lambda\right] = 0 \tag{2.18}$$

In order to simplify this equation the followiong guidance factor is considered: $\lambda = \frac{K\dot{R}}{V\cos(\sigma-\chi)}$. In this way it highlighted that equation 2.18 can be solved analytically and the results is:

$$\dot{\sigma} = \dot{\sigma}_0 \left(\frac{R}{R_0}\right)^{K-2} \tag{2.19}$$

For the purser target closing, $\dot{R}(t) < 0$, equation 2.19 shows that $\dot{\sigma}(t)$ decreases linearly to zero if $K = 3$ and approaches the value of zero asymptotically to zero for $K > 3$. The collision course condition $\dot{\sigma}(t) = 0$ is satisfied exactly at the final point $R = 0$ with $a_n = 0$.

Comparasion between PN and PNG

Different simulations for the Pursuit Navigation and the Proportional Navigation Guidance are shown in order to better understand the behaviour of these two guidance laws. It is important to underline that these two laws have been created to intercept or following a moving target. However figure 2.7 shows the trajectories travelled by the UAV when a fixed target is considered.

In these two simulations the intial position of the UAV is in (500,500) and with a heading angle initially pointed west. No wind effects are considered. The target is placed at the origin of the system (0,0). The navigation factor λ has been chosen equal to 4. The UAV speed is equal to $35[m/s]$. Figure 2.8 plots the relative distance between the UAV and the target and the normal acceleration of the airplane.

For the Pursuit Navigation the angle $\sigma - \chi$ is calculated through the *wrap angle* function. This function is defined as: $(\sigma - \chi)_{wrap} = mod((\sigma - \chi) + \pi, 2\pi) - \pi$ where *mod* is the modulus after division function.

Case 1: Fixed Target

As it can be seen in figure 2.7 in this first simulation only a interception

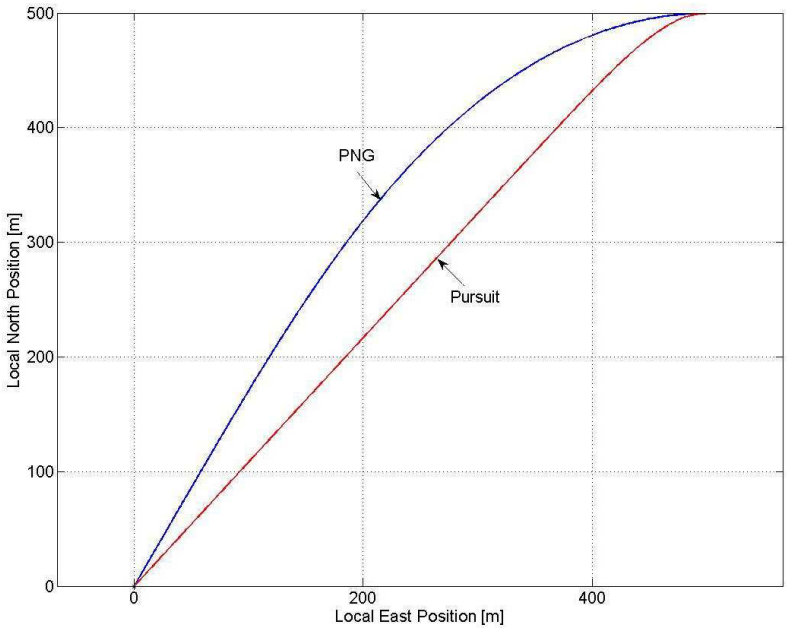

Figure 2.7: Trajectories of the UAV

case is shown. This is due to the fact that when the UAV reaches the target the PNG guidance law gives an infinite acceleration command because the distance R is equal to zero. After this point is not really significative. On the contrary, the PN is not affected by this problem and it ends in a loitering circle (even if it is not shown in the figure) around the target position. However, the normal acceleration on this circle is too high for an UAV. Figure 2.8 shows that the PN is faster than the PNG to reach the target but is gives an higher acceleration command.

Case 2: Moving Target ($V_T \leq V$)

In this second case the target it is not considered fixed but with a constant velocity slower than the target ($10[m/s]$) and with a fixed heading angle ($\chi_T = 0$). The initial conditions of the UAV are the same of *Case 1.*

Figure 2.9 shows the different trajectories created by the PNG and the PN. The paths are granted respect to the explanation of the guidance law given in section 2.2. In figure 2.10 the reader can see that when the UAV is approaching the target the required normal acceleration increases.

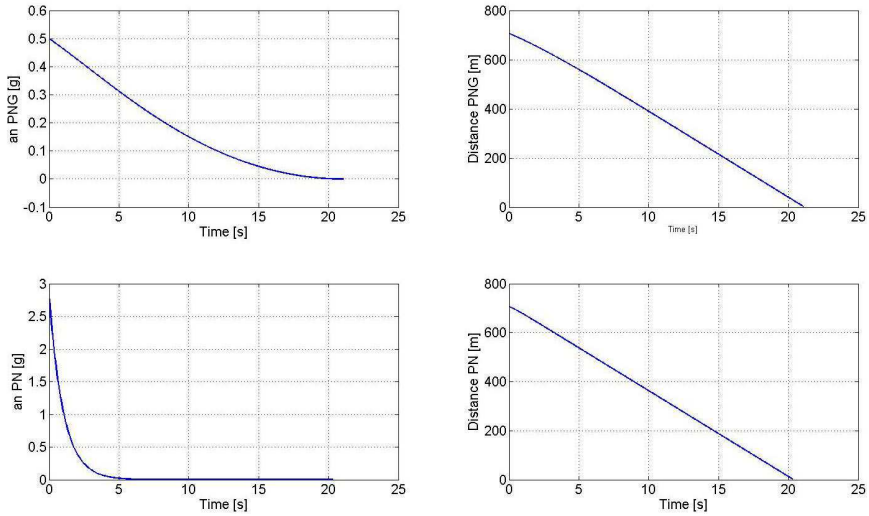

Figure 2.8: Normal Acceleration and Distance with fixed target using PNG and PN Guidance Laws

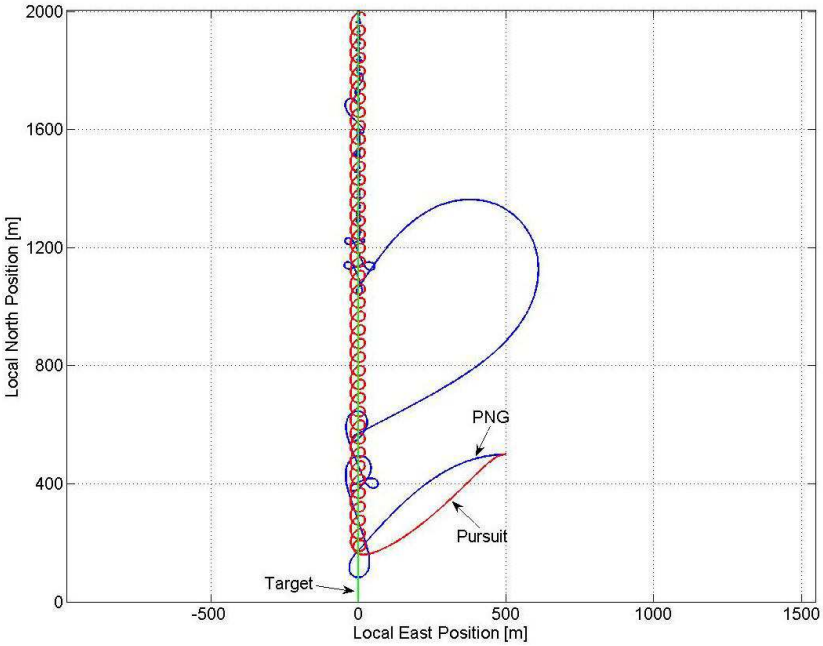

Figure 2.9: Trajectories of the UAV (Case 2)

Pursuit Navigation permits the UAV to stay around the target. However, even in this case, it is impossible to control the value of the distance and consequently the normal acceleration required seems to be too high for the UAV to perform.

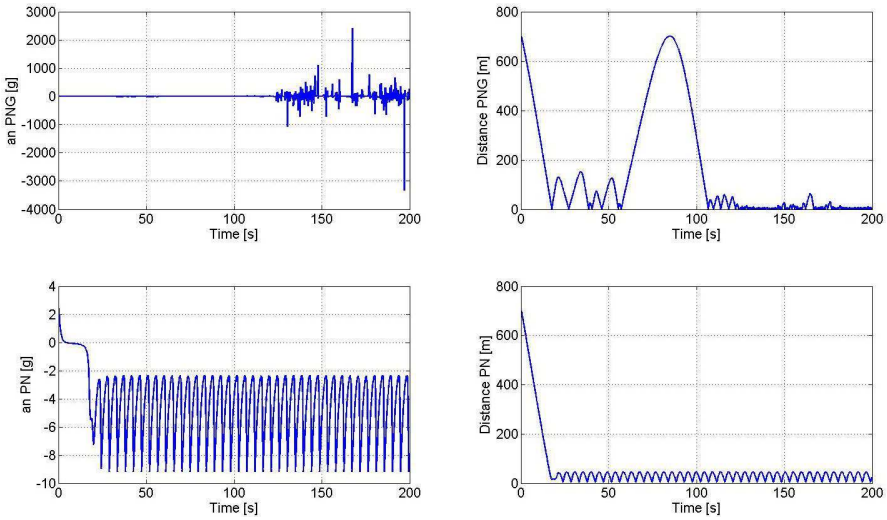

Figure 2.10: Normal Acceleration and Distance with fixed target using PNG and PN Guidance Laws (Case 2)

In this case one of the limit of the PNG is highlighted. It can not be considered suitable for surveillance purpouse. On the contrary, the Pursuit Navigation has a better behaviour under this point of view. However, even for this guidance law, an improvement has to be done in order to create a trajectory feasible for the UAV.

Case 3: Moving Target ($V_T = V$)

This last case shows the fundamental limit of the Proportional Navigation Guidance. A target with a north constant heading angle and with the same speed of the UAV is considered. The initial position of the UAV are the same as in the previous cases.

In figure 2.11 the UAV commanded with the PNG guidance law goes straight also when it intercepts the target. This is due to the nature of this guidance which consider only the rate of the LOS angle. Hence, considering a target with the same speed of the UAV, $\dot{\sigma}$ will not change and consequently

the UAV will not turn. The distance between the target and the UAV will increase linearly. Figure 2.12 shows that the normal acceleration a_n is zero during all the simulation.

The pursuit navigation, which is represented by the red line, has a smarter behaviour: it flies behind the target and the distance will be constant. In this case the normal acceleration seems to be acceptable for the UAV.

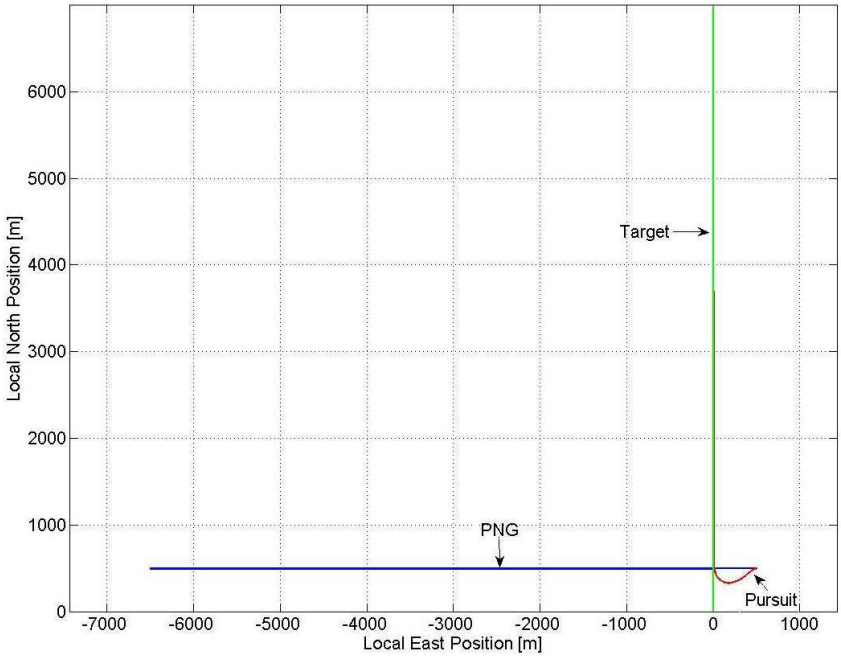

Figure 2.11: Trajectories of the UAV (Case 3)

Even considering *Case 2*, the PNG shows another limit which gives this guidance law unsuitable for monitoring or following a target.

This last case is very important when a 'ghost' target will be created in the next section. A new guidance law, which will have some properties of the Proportional Navigation Guidance and the Pursuit Navigation, will be created in the next section in order to avoid this limit but always considering the rate of the LOS angle $\dot{\sigma}$.

Summary of the PN and PNG criticalities

PNG

1. Unbounded lateral acceleration.

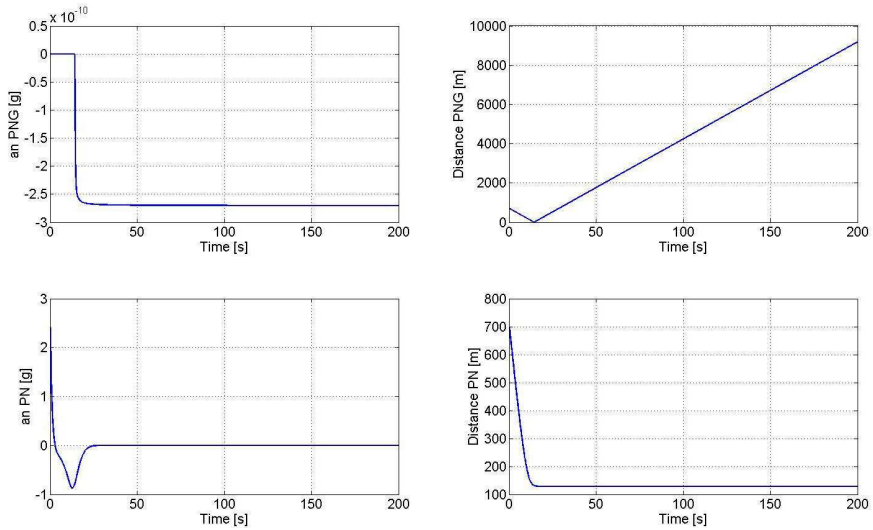

Figure 2.12: Normal Acceleration and Distance with fixed target using PNG and PN Guidance Laws (Case 3)

2. $\dot{\sigma} \to \infty$ when $R \to \infty$.

3. Steady state tracking error not error in certain situations.

4. Unbounded tracking error after interception.

PN

1. After interception there is a loitering around target behaviour.

2. Moving target causes tracking to be slow.

2.3 Tracking Targets by Lyapunov Guidance

The guidance law considered in this section forces the pursuer UAV to follow a target by keeping a certain distance from it even in presence of target unpredicted motion and wind. Moreover, the pursuer has to maintain an airspeed not lower than the one it needs to have sufficient lift and to avoid stall. The guidance law is a nonlinear law designed by means of a Lyapunov based method that provides the stabilizing control input for correct tracking.

The feedback nature of the guidance law lets it to be effective also in presence of wind. Global stability of tracking law is demonstrated by Lyapunov analysis in the close loop system in the case the velocity of the pursuer is not higher than that of the target. In this case the guidance law produces a stable behaviour always pointing to the target also in case of wind and moving target while maintaining the UAV desired speed. Simulations in different conditions show good tracking performances.

2.3.1 Description of the mathematical model

In this section the airspeed, i.e. the speed of the UAV with respect to air flow, is assumed to be constant. Constant speed assumption, also made in others papers ([26], [30] and [27]), is consistent with typical tracking requirements because fixed-wing aircraft velocity changes are generally considered undesirable, in order to avoid altitude variations due to changes in lift. Therefore, according to the scopes and objectives of most guidance problems, it is possible to describe the translation motion of the air vehicle as a mass-point moving in a two dimensional plane. An orthogonal Cartesian frame description of UAV dynamical motion is as follows (see also Figure 2.13):

$$\begin{aligned} \dot{x} &= V\cos(\chi) + W\cos\chi_w \\ \dot{y} &= V\sin(\chi) + W\sin\chi_w \\ \dot{\chi} &= \tfrac{a_n}{V} \end{aligned} \tag{2.20}$$

where $\mathbf{x} = [x, y]^T$ is the position vector of the UAV. The angle χ is positive in an anti-clockwise sense and it represents the angle between the x axis and the direction of the UAV airspeed vector $\mathbf{V}$; $\mathbf{V}$ is supposed to lie along the aircraft longitudinal axis. V is the modulus of $\mathbf{V}$; W is the modulus of the wind velocity vector $\mathbf{W}$; χ_w is defined as the wind course angle. a_n is the single input signal of the model and represents the value of lateral acceleration. No longitudinal acceleration respect to the air flow is considered because V is assumed constant.

The velocity vector of the UAV respect to the ground is represented by

$\mathbf{V_g} = \mathbf{V} + \mathbf{W}$.

Figure 2.13 shows the angles and the velocity vectors defined above; β, the angle between the ground velocity $\mathbf{V_g}$ and the airspeed vector $\mathbf{V}$, is:

$$\beta = \arctan \frac{(\mathbf{V} \times \mathbf{V_g}) \cdot \hat{\mathbf{k}}}{\mathbf{V} \cdot \mathbf{V_g}} \tag{2.21}$$

where $\hat{\mathbf{k}}$ represents the z-axis unit vector orthogonal to the plane x-y. $\times$ and $\cdot$ are the usual symbols denoting cross and inner product, respectively.

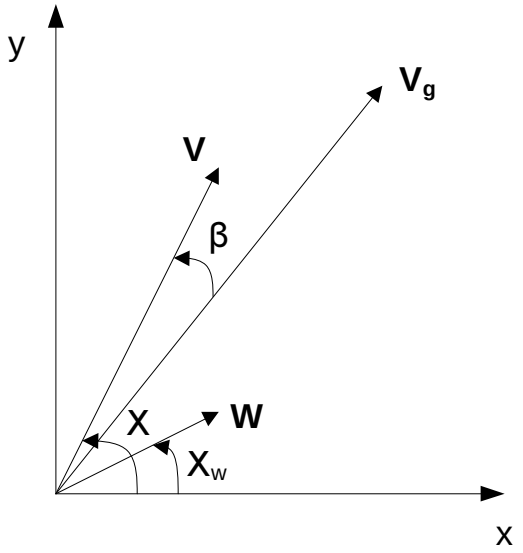

Figure 2.13: Vectors and angles involved

Figure 2.14 shows the direction of the lateral acceleration; its effect is to cause a change in the rate of turn while leaving the airspeed unchanged.

In this section as, it was explained at the beginning of this thesis, it is assumed that the position of the target is known by the pursuer guidance system. In [39] and [3] a description of typical sensors useful for this scope are given.

Moreover, another important assumption is that intensity and direction of the wind are known. This is a easy to assume hypothesis because a position-velocity sensor (i.e. a satellite receiver) and a Pitot tube are standard equipments usually installed on-board an UAV: they allow for an easy on-board

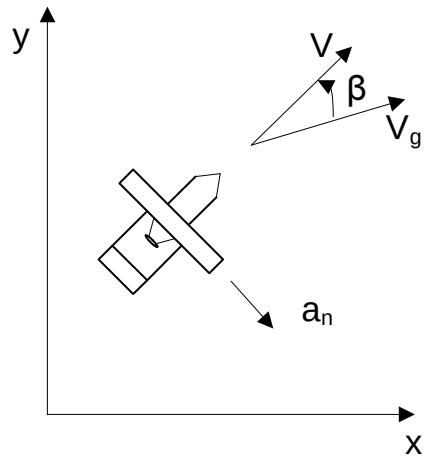

Figure 2.14: Control input, ground and air velocity

airspeed and wind velocity vector computation.

These assumptions allow for the on-board computation also of the rate of change of β that, under the hypothesis of constant wind velocity, is easy to demonstrate that is given by:

$$\dot{\beta} = \frac{\dot{\mathbf{V}} \times \mathbf{W} \cdot \hat{\mathbf{k}} \left(\mathbf{V} \cdot \mathbf{W} + V^2\right) - \mathbf{V} \times \mathbf{W} \cdot \hat{\mathbf{k}} \left(\dot{\mathbf{V}} \cdot \mathbf{W}\right)}{\left(1 + \tan^2 \beta\right) \left(V^2 + \mathbf{V} \cdot \mathbf{W}\right)^2} \tag{2.22}$$

The derivative of airspeed velocity vector respect with time is

$$\dot{\mathbf{V}} = V\dot{\chi}\hat{\mathbf{n}} = a_n\hat{\mathbf{n}} \tag{2.23}$$

where $\hat{\mathbf{n}}$ is the unity vector orthogonal to velocity $\mathbf{V}$.

In next section the computation of $\dot{\beta}$ will be demonstrated to result useful for the proposed guidance law: in fact it lets to compensate for the negative effects of the wind during reference tracking.

2.3.2 Proposed Guidance Law

The objective of the proposed guidance law is to allow the pursuer UAV for tracking a target. This aim is achieved by providing the pursuer guidance system with a reference command obtained as the line of sight (LOS) between

the pursuer UAV and a virtual target. The virtual target, that actually behaves as the main target for the UAV, is defined in such a way as to always stay at a fixed distance from the pursuer. The course angle of the virtual target (i. e. the direction of its ground velocity) has to be selected in order to point to the real target, except when virtual target is passing before real one. In fact, in this case there would be an abrupt change in virtual-real target LOS that could result in unacceptable rate of turn of the UAV. This situation could happen when UAV velocity is higher than real target velocity. Planning of virtual target motion in these cases is not discussed in this paper.

The aim of this section is to describe how the proposed guidance law can be designed by means of a procedure based on a general Lyapunov function. In figure 2.15 the geometry of the problem is sketched. As stated before, what is indicated as the target now is actually the center of oscillation: the guidance law is based on tracking of it. Consider the following scalar function:

$$V_L = V_L(\mathbf{x}) = \frac{1}{2}\left[h(\mathbf{x}) - g(h(\mathbf{x}))\right]^2 \tag{2.24}$$

where

$\mathbf{x} \in \mathcal{R}^n$, $h(\mathbf{x}) := \mathcal{R}^n \to \mathcal{R}$ and $g(h) := \mathcal{R} \to \mathcal{R}$ are scalar smooth functions and

$$g(h(\mathbf{x})) = 0 \text{ when } h(\mathbf{x}) = 0.$$

It can be seen that V_L is a positive semidefinite function. Moreover, after some algebra, the rate of change of V_L results to be:

$$\dot{V}_L = \left[h(\mathbf{x}) - g(h(\mathbf{x}))\right]\left(1 - \frac{\partial g}{\partial h}\right)\nabla h \cdot \dot{\mathbf{x}} \tag{2.25}$$

If the following relationship holds

$$\nabla h \cdot \dot{\mathbf{x}} = -K_1\left[h(\mathbf{x}) - g(h(\mathbf{x}))\right] \tag{2.26}$$

where K_1 is a scalar positive constant, then $\dot{V}_L \leq 0$ (because the term $\left(1 - \frac{\partial g}{\partial h}\right)$ can be assumed to be always positive) and the system state trajec-

tory converges to a stable domain. Equation (2.26) can be adapted to the guidance problem considered in this work. Hence, it becomes

$$V\frac{\partial h}{\partial x}\cos\chi + V\frac{\partial h}{\partial y}\sin\chi + \frac{1}{V}\frac{\partial h}{\partial \chi}a_n = K_1\left(g\left(h\left(\mathbf{x}\right)\right) - h\left(\mathbf{x}\right)\right) \tag{2.27}$$

Now, consider the line of sight UAV-virtual target angle σ (see figure 2.15 for a visualization of the involved geometry). Having defined function $h(\mathbf{x}) = \chi - \sigma$, it is easy to demonstrate that:

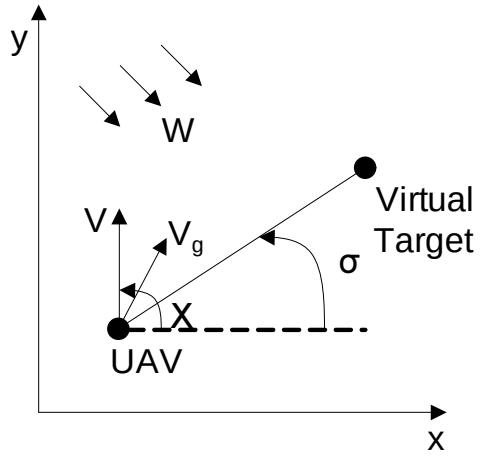

Figure 2.15: Geometry of the tracking problem

$$\tan\sigma = \left(\frac{y_R}{x_R}\right) \tag{2.28}$$

$$\dot{\sigma} = \frac{\dot{\mathbf{R}} \times \mathbf{R}}{R^2} \tag{2.29}$$

where $\mathbf{R} = [x_R, y_R]^T$ is the vector representing the relative pursuer-virtual target position coordinates, $R = \|\mathbf{R}\|$ is constant due to the definition of Virtual target. Hence, it is possible to derive a stabilizing guidance law in terms of normal acceleration that has to be provided as input to the pursuer UAV. In fact, by developing substitutions in (2.27), it holds

$$\frac{a_n}{V} = \dot{\sigma} + K_1 \left(\sigma - \chi + g\left(\sigma - \chi\right)\right) \tag{2.30}$$

The choice of function $g\left(\right)$ can be accomplished with a certain degree of arbitrarily under the assumption $g\left(0\right) = 0$. In particular, the following choice has been made in this work:

$$g\left(h\right) = K_2 \tanh\left(K_3 h\right) \tag{2.31}$$

where K_2 and K_3 are constants to be tuned during calibration of the guidance law in order to improve the readiness of the close loop system performance.

2.3.3 Simulation and Analysis Results

The aim of this subsection is to evaluate the different performances and behaviors of the proposed guidance law respect to the PNG. In particular three different cases are investigated in the following numerical simulations:

1. Moving target at constant velocity equal to the UAV and with a heading pointed constantly west. Initial position of the target at $(0, 0)$. Initial position of the UAV at $(500, 500)$ with heading pointed West. No wind effect.

2. Moving target at constant velocity 10 (m/s) and fixed West direction. Initial position of the target at $(0, 0)$. Initial position of the UAV at $(500, 500)$ with heading pointed West. Wind intensity of 5 (m/s) with North-East Direction.

3. Moving target at constant velocity 35 (m/s) with a circle trajectory. Initial position of the target at $(0, 0)$ and initial heading pointed in a west direction. Initial position of the UAV at $(0, 500)$ with heading pointed West. No wind effect.

The airspeed of the UAV is fixed at 35 (m/s). The gains are always chosen as cited in section 2.3.2: $K_1 = 0.1$, $K_2 = \frac{\pi}{4}$. Just to remind the PNG guidance law is described by $\dot{\chi} = \lambda\dot{\sigma}$ where λ is navigation gain. The variable

λ is always set to 4. In figure 2.16 the dashed line represents the trajectory of the UAV with the proposed guidance law while the continuous line is the trajectory with the Proportional Navigation Guidance. The dot line is the position of the ghost target created at a fixed distance on the line of sight.

Case 1

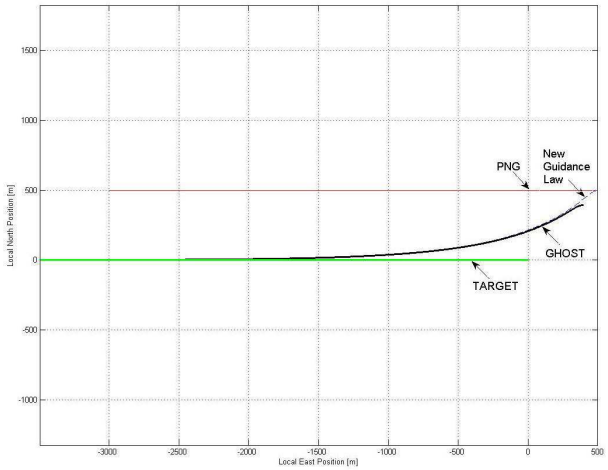

Figure 2.16: Comparison between guidance law behaviors (Case 1)

In this case, where the target and the UAV have the same speed, the new guidance law avoid the lateral error and try to chase the target. The proportional navigation guidance does not give an acceleration command because the rate of the LOS angle remains constant ($\dot{\sigma} = 0$). Hence, this simulation shows that the PNG is not designed for following a moving target.

Case 2

Figure 2.17 highlights the different aim between the two guidance laws. The guidance law designed in this paper tries to chase a moving target while the classical PNG is designed to intercept it. The new guidance law drives the UAV towards the target with a smoother trajectory. As in the PNG guidance law there is a singularity point when the distance between the target and the UAV goes to zero. It is not the object of this article to investigate this

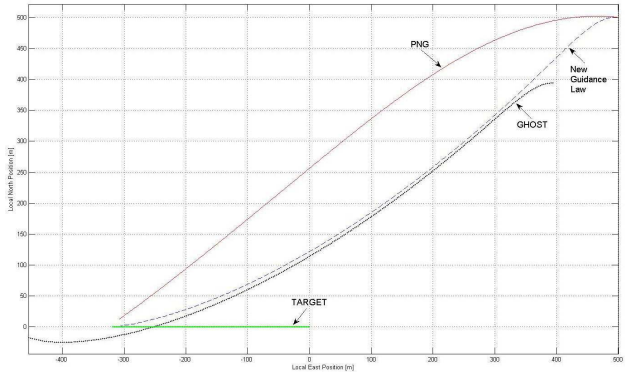

Figure 2.17: Comparison between guidance law behaviors (Case 2)

problem but a suitable ghost trajectory can be created in order to drive the UAV behind the target again.

In Figure 2.18 the same parameters chosen for 2.17 is used but with a speed of the target equal to the UAV (35 m/s). In this case the PNG diverges respect to the trajectory of the target instead of what the new guidance does. This is one of the great advantage to use this guidance law for following a moving target.

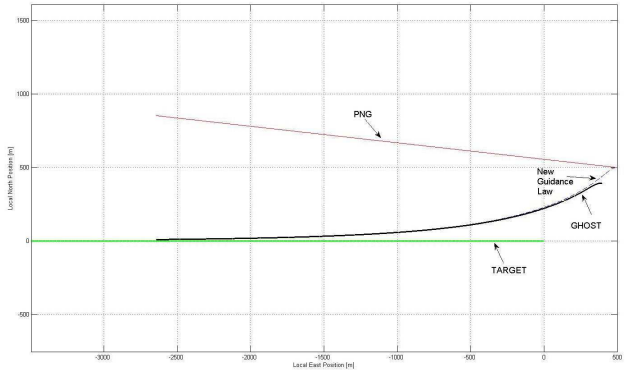

Figure 2.18: Comparison between guidance law behaviors (Case 2)

Case 3

Figure 2.19 shows how the UAV follows a circle trajectory. The dot line which represents the ghost target is outside the circle created by the

target because a fixed distance of 150 (m) is chosen for all the simulations. However the new guidance law drives the UAV close to the target without high acceleration command. Figure 2.19 shows the behavior of the UAV with the PNG guidance. Even if with this guidance law the UAV is driven to the circle, when the distance R is close to zero the corrections of the UAV becomes really pronounced. This situation is not correctable with a different choice of the constant navigation λ. In fact, if a higher gain is chosen, the corrections of the UAV becomes impossible early in the flight.

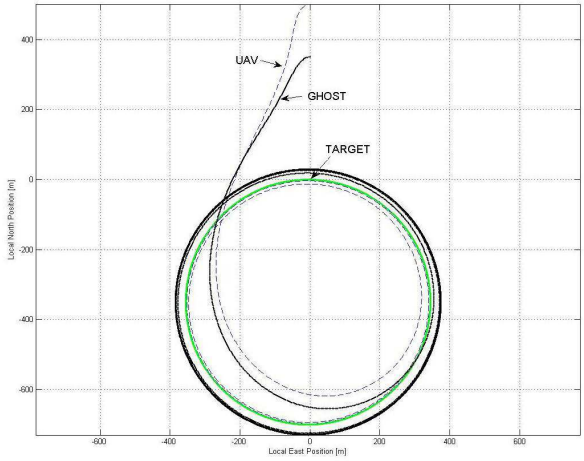

Figure 2.19: UAV circling trajectory with proposed guidance law (Case 3)

Application of New Guidance Law for inspection of different waypoints

This subsection is dedicated to show the behavior of the guidance law when a tour planning for an UAV is prefixed. A similar problem can be seen in [6] and[24] where an optimal solution is given to find a trajectory for inspection of different waypoints in wind conditions. In all these articles a predefined trajectory is calculated in order that the resulting path can be followed easily by an inner autopilot. In this approach, the target is commanded to create a trajectory around the waypoints. Figure 2.21 and figure 2.22 shows how the proposed guidance law tracks this type of trajectory. The four different waypoint are located at:

- WayPoint 1: $(500, 0)$

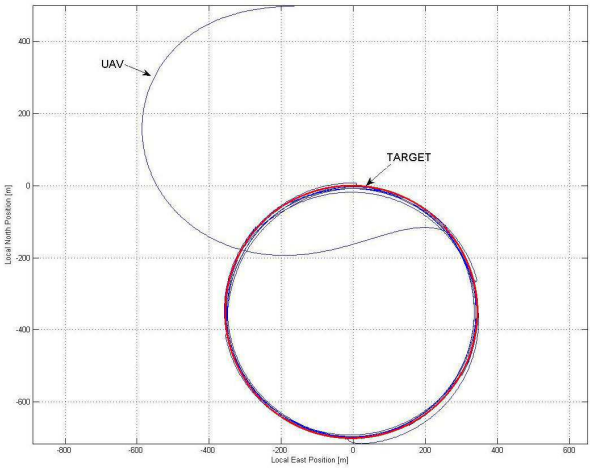

Figure 2.20: UAV circling trajectory with PNG (Case 3)

- WayPoint 2: $(-200, 0)$
- WayPoint 3: $(-200, 500)$
- WayPoint 4: $(500, 500)$

The velocity of the UAV is always setted to 35 (m/s) while the wind has a constant magnitude of 2 (m/s) in north east direction.

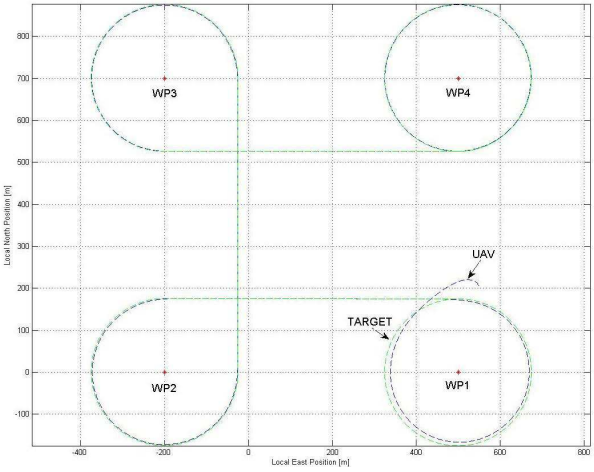

Figure 2.21: Inspection of WayPoints (No Wind)

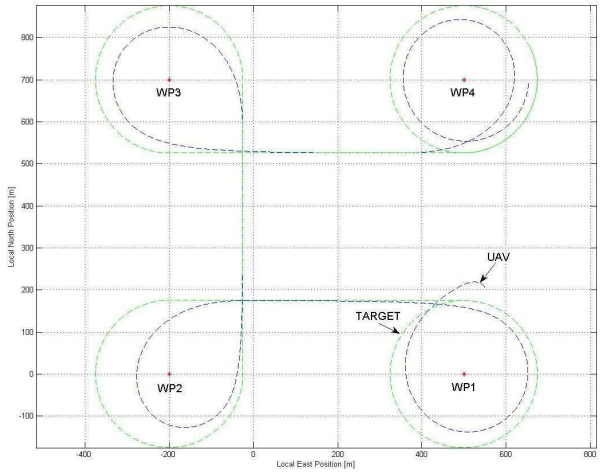

Figure 2.22: Inspection of WayPoints (Wind)

It is important to underline that, using the proposed guidance law, the trajectory will not be an optimal solution. However if an optimal solution is given by an external algorithm or is calculated off-line, it is possible to create a target which tracks that kind of trajectory with the same speed of the UAV. In this case the proposed guidance law can be used to track the moving target.

2.3.4 Conclusion

In this section a new nonlinear guidance law for target tracking is presented. The guidance law forces the UAV to track a virtual target at constant distance from the pursuer. The guidance law is obtained by following a quite simple design method based on the definition of a suitable Lyapunov function. The same method can be exploited in order to generate other guidance laws by modifying the selected Lyapunov function.

From simulation tests it results that, by comparing the performances of the proposed guidance law with the classic proportional navigation (PNG) one, the nonlinear law behaves better than the PNG in case of wind and in case of moving target. Hence it can be concluded that the proposed law has good features in terms of robustness to disturbances, tracking performances,

simplicity of derivation and adaptability to different scenarios.

This page is intentionally left blank.

Chapter 3

Nonlinear Guidance Law

3.1 Introduction

This section presents a new non-linear two dimensional (2D) guidance law for an aerial pursuer, such as an unmanned air vehicle (UAV) tracking a ground moving target. In particular, the problem consists in steering the pursuer for flying over or at a minimum distance from a target, tracking it whether the target is moving or it is keeping still. Moreover, the pursuer has to maintain an airspeed not lower than the one it needs to have sufficient lift and to avoid stall. Beside this, the rate of turn of the aircraft cannot exceed an upper bound required by its flight performances. The trajectory of the target is not a priori known by the pursuer, and the one of the pursuer has to be adaptively generated by the feedback guidance loop.

The presented guidance law drives the pursuer to fly over the target or to pass close to it at the minimum desired distance, the first time, and subsequently to loiter around it by following a curve that asymptotically becomes a circumference centered on the target. If the minimum pre-set distance is greater than that of the minimum turn radius required by the aircraft, the first one is that followed by the aircraft.

The feedback nature of the guidance law lets it to be effective also in presence of wind and/or unpredicted target maneuvers. Global stability of the presented non-linear guidance law is demonstrated by Lyapunov analysis

in the close loop system in the case of no wind and no moving target. In this case the guidance law produces stable behavior converging to a stable point in the state space or a circle in the configuration space.

Simulations show good tracking capabilities of the guidance law also in case of background wind and moving target while maintaining the pursuer desired air speed. Hence, this law is well suitable for problems like continuous live sensing from around and ahead of friendly, adversarial or unidentified targets.

3.2 Model System Dynamics

The system dynamics in this particular section is described by the following kinematic model as exoressed to a fixed reference frame:

$$\begin{cases} \dot{x}_R = V\cos(\chi) + W_x - V_{Tx} \\ \dot{y}_R = V\sin(\chi) + W_y - V_{Ty} \\ \dot{\chi} = \frac{a_n}{V} \end{cases} \tag{3.1}$$

This model is used to describe the geometry of the movement of a mobile point, regardless of the forces acting on it. In equation 3.1, $[x_R, y_R]^T$ is the position of the target relative to the pursuer, $[V_{TN}, V_{TE}]^T$ is the absolute velocity vector of the target and $[W_N, W_E]^T$ are the components of the wind velocity. The other variables are defined in the nomenclature section.

By referring to figure 1.1, model 3.1 can also be expressed in polar coordinates as the model described in 1.8 and it becomes:

$$\begin{cases} \dot{R} = V_T\cos(\sigma - \chi_T) - V\cos(\sigma - \chi) \\ R\dot{\sigma} = -V_T\sin(\sigma - \chi_T) + V\sin(\sigma - \chi) \\ \dot{\chi} = \frac{a_n}{V} \end{cases} \tag{3.2}$$

In these equation is preferable to consider the pursuer velocity and its course angle instead of the magnitude of the UAV airpseed. It is better to define the component of the velocity vectors as follow:

1. Speed components of the UAV velocity vector

$$\mathbf{V} = \begin{bmatrix} V\cos(\chi) \\ V\sin(\chi) \end{bmatrix} \tag{3.3}$$

2. Speed components of the Target velocity vector

$$\mathbf{V}_T = \begin{bmatrix} V_T\cos(\chi_T) \\ V_T\sin(\chi_T) \end{bmatrix} \tag{3.4}$$

3. Speed components of the Wind velocity vector

$$\mathbf{W} = \begin{bmatrix} W\cos(\chi_W) \\ W\sin(\chi_W) \end{bmatrix} \tag{3.5}$$

Observing figure 3.1 it holds $\mathbf{V}_P = \mathbf{V} + \mathbf{W}$ and consequently it can be defined:

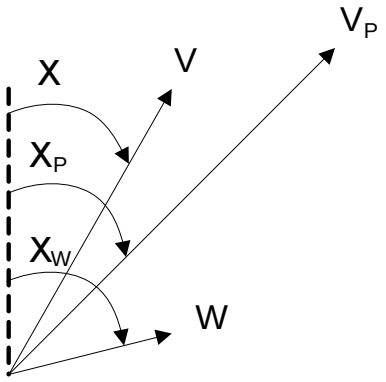

Figure 3.1: Difference between $\mathbf{V}$ and $\mathbf{V}_p$

$$\mathbf{V}_P = \begin{bmatrix} V\cos(\chi) + W\cos(\chi_W) \\ V\sin(\chi) + W\sin(\chi_W) \end{bmatrix} \tag{3.6}$$

The new velocity vector $\mathbf{V}_P$ is called velocity vector of the Pursuer. Using this new vector equation 3.2 can be also defined:

$$\begin{cases} \dot{R} = V_T \cos(\sigma - \chi_T) - V_P \cos(\sigma - \chi_P) \\ R\dot{\sigma} = -V_T \sin(\sigma - \chi_T) + V_P \sin(\sigma - \chi_P) \\ \dot{\chi} = \frac{a_n}{V} \end{cases} \tag{3.7}$$

Wind and target velocity enter equation 3.1 in the same way, so it is convenient to consider a single velocity term:

$$T_N = V_{TN} - W_N \tag{3.8}$$

$$T_E = V_{TE} - W_E \tag{3.9}$$

After some algebra equation 3.7 becomes:

$$\begin{cases} \dot{R} = T_N \cos(\sigma) + T_E \sin(\sigma) - V \cos(\sigma - \chi) \\ R\dot{\sigma} = -T_N \sin(\sigma) + T_E \cos(\sigma) - V \sin(\sigma - \chi) \\ \dot{\chi} = \frac{a_n}{V} \end{cases} \tag{3.10}$$

It now results useful to define the following alpha angle α as:

$$\alpha = \sigma - \chi \tag{3.11}$$

Hence, model 3.10 can be written in the following more suitable form:

$$\begin{cases} \dot{R} = T_N \cos(\sigma) + T_E \sin(\sigma) - V \cos(\sigma - \chi) \\ \dot{\alpha} = \frac{-T_N \sin(\sigma) + T_E \cos(\sigma) - V \sin(\alpha)}{R} - \frac{a_n}{V} \\ \dot{\sigma} = \frac{-T_N \sin(\sigma) + T_E \cos(\sigma) - V \sin(\alpha)}{R} \end{cases} \tag{3.12}$$

3.3 Guidance Law

In this section a guidance law for the UAV vehicle is described. The objective of the law consists of allowing it tracking a ground target. In particular, target tracking is here assumed as the possibility to loiter near a target by circling around it at a radius not lower than a prescribed one. Eventually, the vehicle can over-flight the target a first time by setting up a prescribed radius of zero length. In the following the UAV vehicle is also indicated as

the pursuer.

Assumption

From now on it is assumed that the target has a ground speed lower than that of the pursuer: this in order to avoid problems that can occur in case of target-pursuer relative speed equal to zero.

Moreover, the flight of the vehicle has to be performed under the requirements of a maximum rate of turn and with a constant airspeed, in order to avoid loss of lift.The latter requirement is fulfilled by considering a guidance law that acts only on the lateral acceleration, i.e. the acceleration perpendicular to the vehicle velocity respect to air, while leaving the longitudinal acceleration at zero.

Now, by defining R_D as the minimum radius of a circle centered over the target position and such that the pursuer-target distance cannot be lower, it results (see figure 3.2)

$$\sin(\phi) = \frac{R_D}{R} \tag{3.13}$$

if $R \geq R_D$ where R is the tangent-pursuer distance;ϕ is the angle between the target-pursuer line of sight and the direction of the tangent to the circle with radius R_D taken from the pursuer position.

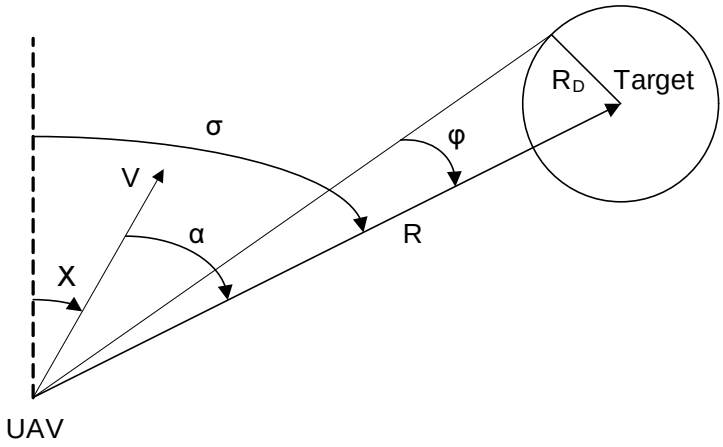

Figure 3.2: Geometry of the Guidance Law

If the pursuer is inside the circle, and expression 3.13 is not defined. In

this case ϕ is arbitrarily set to $\frac{\pi}{2}$, the value it has over the circumference. Summarizing, it holds:

$$\begin{cases} \phi = \arcsin\left(\frac{R_D}{R}\right) & R \geq R_D \\ \phi = \frac{\pi}{2} & R \geq R_D \end{cases} \tag{3.14}$$

The aim of the guidance law is to force the pursuer to steer toward the closest tangent-to-circle direction, that can be

$$\sigma - \phi \quad \text{or} \quad \sigma + \phi \tag{3.15}$$

or, depending on the direction of the pursuer velocity vector. For the description of the proposed guidance law it is now useful to define the following two-level sign function:

$$sign_2 : \mathbb{R} \to \mathbb{R}, \quad sign_2(x) = \begin{cases} 1 & x \geq 0 \\ -1 & x < 0 \end{cases} \tag{3.16}$$

that is a slight modification of the usual well known sign function (often indicated as "sgn"), that assumes value of zero when $x = 0$.

Now by setting

$$s = sign_2(\sin(\alpha)) \tag{3.17}$$

it is easy to see that s allows to select between the two sides of the horizontal plane that are cut by the LOS.

It is now quite easy to write down an unique formula for the reference direction that comprises the two expressions given in 3.15:

$$\sigma - s\phi \tag{3.18}$$

The feedback control law considered for the normal acceleration a_n an has the following analytical expression:

$$a_n = K sign_2[\sin(\alpha - s\phi)] \left|\sin\left(\frac{\alpha - s\phi}{2}\right)\right| \tag{3.19}$$

where K is an arbitrary scalar gain.

It is straightforward to note that the maximum possible absolute value for the normal acceleration is K; hence, the acceleration is bounded and similarly the maximum turn-rate of the vehicle. Therefore the gain can be chosen in a way such to fulfill the structural requirements of the vehicle.

Moreover, it is possible to note that the expression of the acceleration consists, apart from the gain, of two factors.

The first one is responsible of the side of the acceleration (it can only be -1 or +1). Its role is that of steering the pursuer to right or left in order to point to the selected reference direction.

The second one causes a continuous modulation of the gain between 0 and 1: no acceleration when angle α coincides with the reference direction sϕ; maximum lateral acceleration when α differs 180 from sϕ, hence forcing the vehicle that was going in the opposite way for gradually heading toward the reference direction.

Pursuer over the Target

It is worth observing that angle σ, the LOS angle, is not defined when $R = 0$. As a consequence, the same is for the guidance law. This is not a problem because the pursuer-target relative speed is always assumed grater than zero. So, the pursuer-target geometry cannot permanently have zero LOS angle but only in a numerable set of instants. When this happens, i.e. when R is zero, the commanded normal acceleration can be conventionally set to zero.

Behaviour of the closed loop system

The following two figures show the effect of the described guidance law in two different cases, A and B respectively. The gain K has been chosen such that normal acceleration cannot exceed a prescribed maximum value, i.e. that required by the structural limits of the vehicle.

In case A (figure 3.3), the pursuer starts from point (800,800), heading North-East, and the target is fixed at (0,0). It is specified a minimum circling radius $R_D = 500$ and, as can be seen, the pursuer directs toward the corresponding circumference and loiters around it.

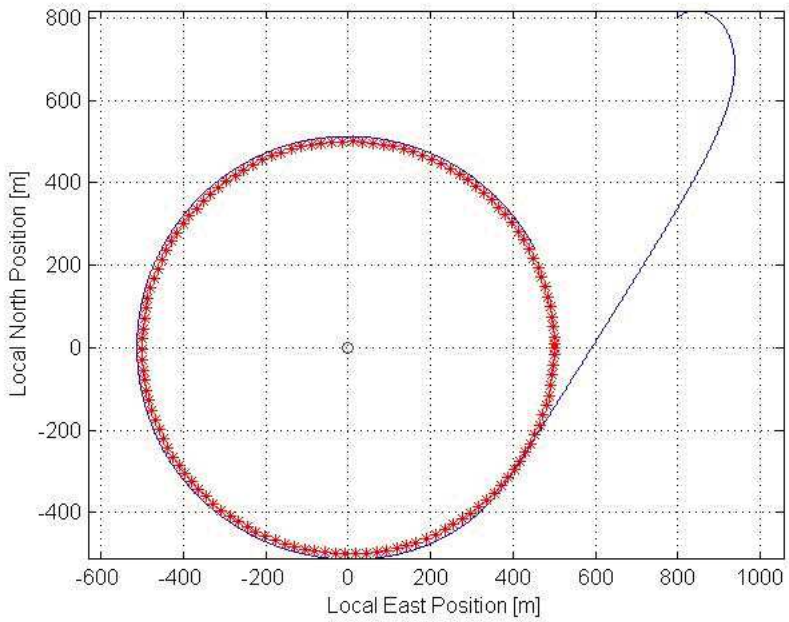

Figure 3.3: Trajectory of the Pursuer case A

In case B (Figure 5), the pursuer starts with heading North-East, and the target is fixed at (0,0). In this case a low circling radius is imposed: $R_D = 20$. This radius is too low and would require a too high turn-rate: hence, as can be seen, the pursuer directs toward the corresponding circumference but then it automatically finds and stabilizes on a greater circumference where the turn rate is sustainable by the vehicle.

3.4 Stability Analysis

Bounds on state Derivatives

In this section a Lyapunov function is developed that ensures stability of the nonlinear guidance law for the model that is represented in 3.10 but with the characteristic of no wind and no target speed. Moreover, the demonstration is presented here for the special case of $R_D = 0$. In this special case model 3.12, with the insertion of the described acceleration law, becomes:

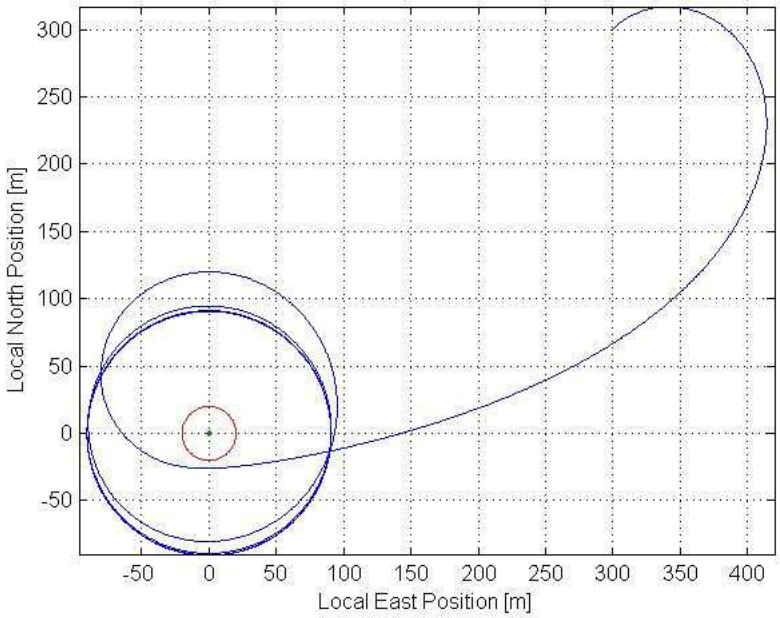

Figure 3.4: Trajectory of the Pursuer case B

$$\begin{cases} \dot{R} = -V\cos(\alpha) \\ \dot{\alpha} = \frac{V\sin(\alpha)}{R} - \frac{Ksign_2[\sin(\alpha - s\phi)]\left|\sin\left(\frac{\alpha}{2}\right)\right|}{V} \end{cases} \tag{3.20}$$

The basic ideas for the development of this section builds on the results of [4] and [28].

Consider now the regions where the state derivatives of model 3.20 are zero. From the second of equations 3.20, after the application of half-angle formula, is:

$$\dot{\alpha} = sign_2\left[\sin(\alpha)\right] \times \left[\frac{2V}{R}\left|\sin\left(\frac{\alpha}{2}\right)\right|\left|\cos\left(\frac{\alpha}{2}\right)\right| - \frac{K}{V}\left|\sin\left(\frac{\alpha}{2}\right)\right|\right] \tag{3.21}$$

and

$$\dot{\alpha} = \frac{K}{V}sign_2\left[\sin(\alpha)\right] \times \left|\sin\left(\frac{\alpha}{2}\right)\right|\left[\frac{2V^2}{RK}\left|\cos\left(\frac{\alpha}{2}\right)\right| - 1\right] \tag{3.22}$$

Now, $\dot{\alpha} = 0$ if $\left|\sin\left(\frac{\alpha}{2}\right)\right| = 0$ that is $\alpha = -2\pi, 0, 2\pi \ \forall$ R or

$$\frac{2V^2}{\overline{R(\alpha)}K}\left|\cos\left(\frac{\alpha}{2}\right)\right| - 1.$$

that is

$$\overline{R}(\alpha) = \frac{2V^2\left|\cos\left(\frac{\alpha}{2}\right)\right|}{K} \tag{3.23}$$

Moreover, analyzing equation 3.23, it results:

$$\dot{\alpha} \Leftrightarrow \begin{cases} R < \overline{R}(\alpha) & \text{and} \quad sign_2\left[\sin\left(\alpha\right)\right] < 0 \\ \text{or} & \\ R > \overline{R}(\alpha) & \text{and} \quad sign_2\left[\sin\left(\alpha\right)\right] > 0 \end{cases} \tag{3.24}$$

$$\dot{\alpha} \Leftrightarrow \begin{cases} R > \overline{R}(\alpha) & \text{and} \quad sign_2\left[\sin\left(\alpha\right)\right] > 0 \\ \text{or} & \\ R > \overline{R}(\alpha) & \text{and} \quad sign_2\left[\sin\left(\alpha\right)\right] < 0 \end{cases} \tag{3.25}$$

In figure 6 these conditions on $\dot{\alpha}$ are summarized on the on system state space.

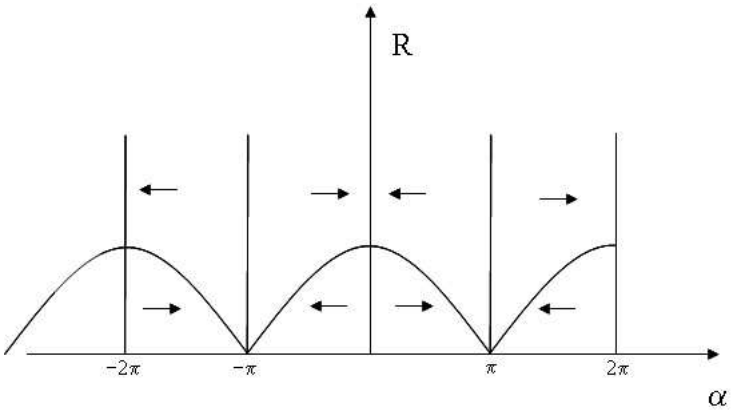

Figure 3.5: Direction of $\dot{\alpha}$

Similar condition on $\dot{R} = 0$ in the first equation of 3.20 brings to:

$$\dot{R} = 0 \Rightarrow \alpha = \pm\frac{\pi}{2}; \pm\frac{3\pi}{2} \tag{3.26}$$

and

$$\dot{R} < 0 \Rightarrow -2\pi < \alpha < \frac{-3\pi}{2}; -\frac{2\pi}{2} < \alpha < \frac{2\pi}{2}; \frac{3\pi}{2} < \alpha < 2\pi \tag{3.27}$$

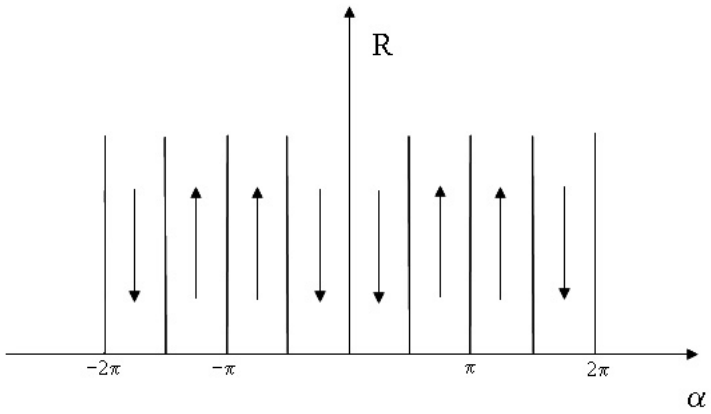

Figure 3.6: Direction of $\dot{R}$

All the conditions expressed by 3.25, 3.26 and 3.27 impose restrictions on the direction that state space trajectory can take. Figure 3.7 summarizes all these condition.

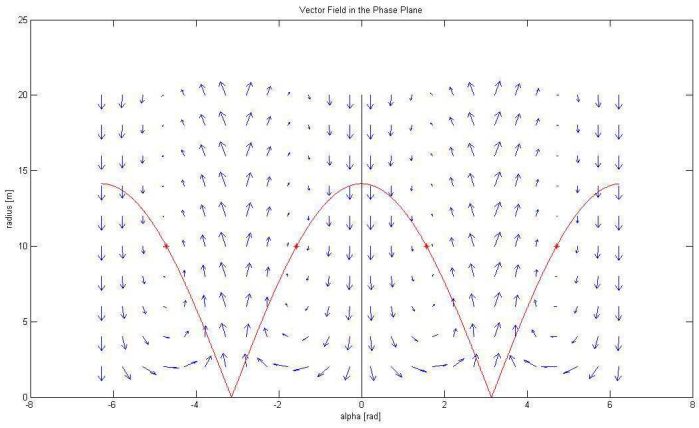

Figure 3.7: Vector Field of the Guidance Closed Loop

The arrows indicate the possible direction that the state variables can take during their evolutions. It is important to note that the purser approaches

the target when $\alpha = \lambda - \chi = 0$. When the pursuer over flies the target there is a significant change in the controlled acceleration that passes from the minimum value to maximum one. There are four equilibrium points: these are represented on the figure by a star and their coordinates are:

$$P_{e1} = \left(\frac{-3\pi}{2}; \frac{\sqrt{2}V^2}{K} \right) \tag{3.28}$$

$$P_{e2} = \left(\frac{-pi}{2}; \frac{\sqrt{2}V^2}{K} \right) \tag{3.29}$$

$$P_{e3} = \left(\frac{pi}{2}; \frac{\sqrt{2}V^2}{K} \right) \tag{3.30}$$

$$P_{e4} = \left(\frac{3\pi}{2}; \frac{\sqrt{2}V^2}{K} \right) \tag{3.31}$$

Moreover the arrows in the figure indicate that, from every initial state, trajectories proceed in a clockwise or anti-clockwise fashion to one of the equilibrium points. It is evident that in the state space there are four sections and for each one there is a corresponding equilibrium point.

- Section 1: $-2\pi < \alpha < -\pi$
- Section 2: $-pi < \alpha < 0$
- Section 3: $0 < \alpha < \pi$
- Section 4: $pi < \alpha < 2\pi$

The following considerations are referred to Section 3: because of symmetry, the other sections can be handled in a similar way. By examining Section 3 ($0 < \alpha < \pi$), a bound for the maximum value of R that can be reached from any point of the Section can be found by analyzing the value of $\frac{\dot{R}}{\dot{\alpha}}$ and its derivatives.

Then, the vector field slope is described by:

$$\frac{\dot{R}}{\dot{\alpha}} = \frac{-\cos(\alpha)}{\frac{\sin(\alpha)}{R} - \frac{K\sin\left(\frac{\alpha}{2}\right)}{V^2}} \tag{3.32}$$

By studying function 3.32 it is possible to find that, after the system has just over flown the target and hence $\dot{R} = 0$, the minimum value of this ratio is obtained at $\alpha = \pi$ and it is:

$$\frac{\dot{R}}{\dot{\alpha}_{(\alpha=\pi)}} = -\frac{V^2}{K} \tag{3.33}$$

As a consequence, the farest point from the target that can be reached (maximum R after overflight) is:

$$R_max = -\frac{V^2\pi}{2K} \tag{3.34}$$

In order to demonstrate the asymptotic stability of the system, it is useful to consider its behavior along some reference curves, as depicted in 3.8.

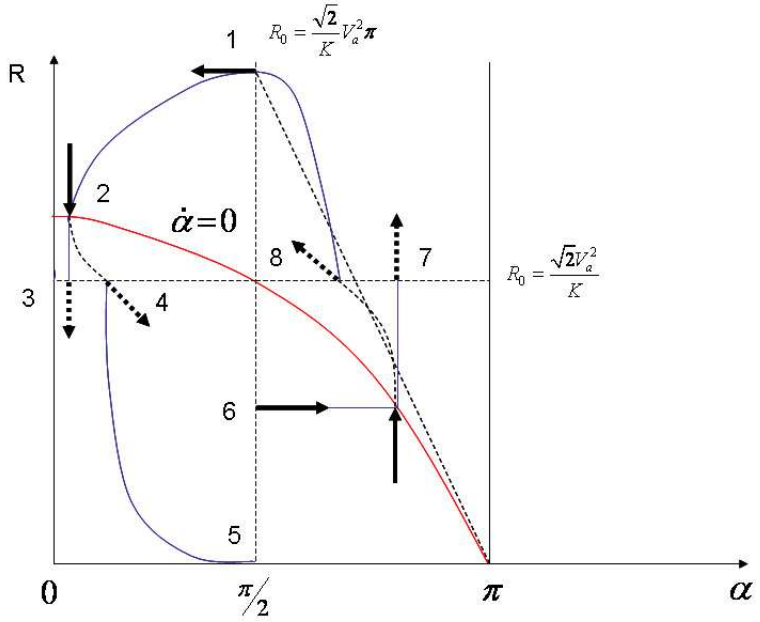

Figure 3.8: Arcs Bounding State Trajectory

In particular, the slope of tangent lines to arcs of ellipses and straight lines has been compared to the slope of the system vector field along the

same arcs.

The slope of an ellipse tangent line is $\frac{a^2(\alpha-\alpha_0)}{b^2(R-R_0)}$ with:

- a, b ellipse semi-axes
- $a_0 = \frac{\pi}{2}$,$R_0 = \frac{\sqrt{2}V^2}{K}$: equilibrium coordinates.

More precisely, the curve from point 1 and point 2 is an arc of ellipse. 2 and 3 are connected by a vertical straight line. From point 4 to 5 there is another ellipse, with a minor axis that is smaller than the one of the previous ellipse. 6 and 7 are connected by two straight line segments. Finally, curve connecting 8 and 1 is another arc of ellipse whose major axis is the same as the first ellipse. Dotted arrows represent the real directions of the vector field and emphasize that the state trajectory is heading inner points.

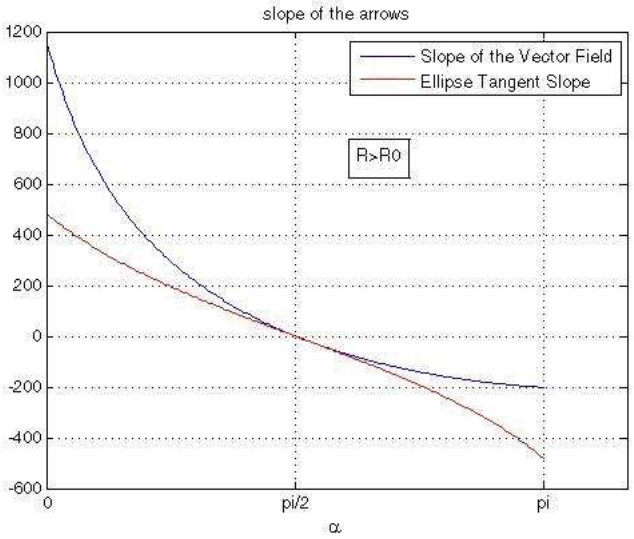

Figure 3.9: Arcs Bounding State Trajectory

This comparison shows that, by starting from an initial point denoted by 1, the evolution of the system state proceeds pointing to the interior of the figure bounded by the arcs. This is due to the direction of the vector field that forces the system state to leave the arcs of the figure because of the values in their tangent line slopes respect to the corresponding values of the arc tangent line slopes. After a complete anti-clockwise turn, the position of

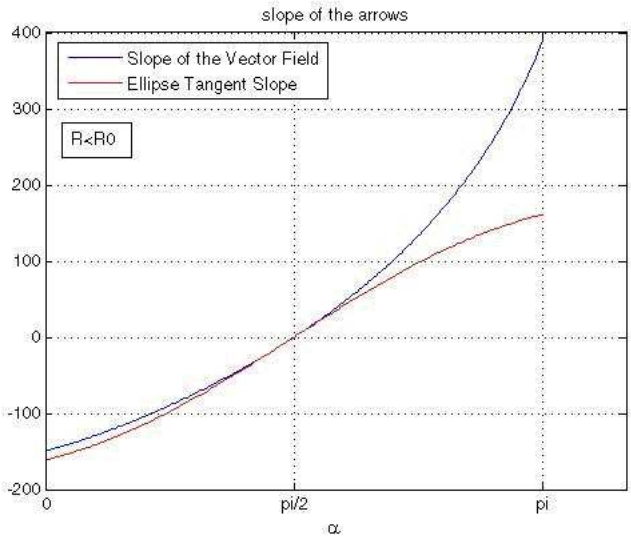

Figure 3.10: Arcs Bounding State Trajectory

the system state is in a point that is closer to the equilibrium point than the initial position. Consequently, the resulting system state can be considered as a new initial point and the reasoning can be repeated now for a smaller area figure. The area of each figure defined by the system position in the state plane can be considered a Lyapunov function, because it is a strictly decreasing positive definite function.

3.5 Simulation Results

The aim of this paragraph is to evaluate the different performances and behaviors of the proposed guidance law in two different forms, i.e. $R_D = 0$ and $R_D \neq 0$. In particular three different case studies are presented in the following numerical simulations:

1. Not moving target, located at $(0, 0)$, initial position of the pursuer at $(800, 800)$, heading North.

2. Not moving target, located at $(0, 0)$, initial position of the pursuer at $(800, 800)$, heading the target.

3. Moving target at constant velocity, initial position of the pursuer at $(800, 800)$, initially heading to the target.

All the simulation last 1000 sec and the airspeed of the pursuer is 20 m/s. In the third case the speed of the target is 5 m/s, less then the pursuer, as stated in an initial assumption. Obviously, the K gain value has been chosen so that the aircraft turn rate maximum value is never exceeded. Moreover, the minimum radius chosen for the general guidance law case is $R_D = 500$ [m].

A comparison of the two guidance law forms shows the main differences among them. In the case (1), with $R_D = 0$, the pursuer tends to intercept the target and, only after this attempt, it moves on a loitering circle with radius of $\frac{\sqrt{2}V^2}{K}$. In this case the pursuer does not perfectly flies over the target, due to its initial condition, however the aim of the law is to fly it as close as possible to the target.

With $R_D \neq 0$ the UAV heads directly to the loitering circle.

A similar behavior features case (2) even if the initial pursuer heading is very different from case (1) (see figures 3.13 and 3.14). The $R_D = 0$ guidance law has a little change respect to the previous case in fact the UAV over flies the target instead of flying only near it. In case (3) the behavior of both guidance law is very similar. The only difference is the maximum distance between the target and the UAV that, for the $R_D \neq 0$ guidance law form can be changed (see figure 3.14 and 3.15).

3.6 Conclusion

A new non-linear two dimensional (2D) guidance law for an aerial pursuer, such as an unmanned air vehicle tracking a ground moving target. The law forces the pursuer to intercept at least one time the target, differently from what other guidance laws do. Moreover, after a first over-fly or fly-by of the target, starts loitering around it. Stability demonstration of a special case of the presented law in the feedback loop, together with numerical simulations of its performances are given in this work.

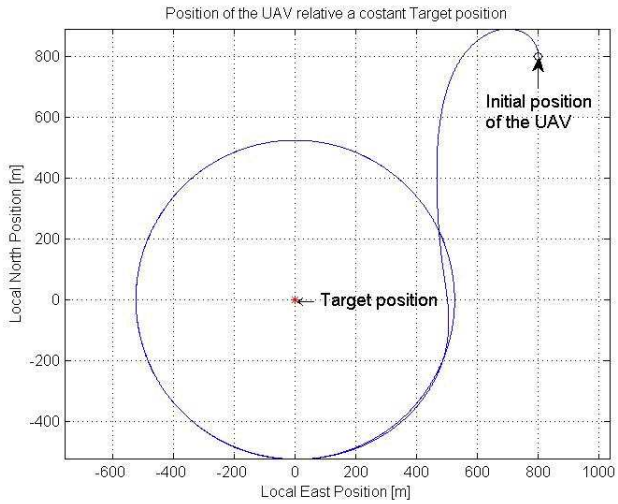

Figure 3.11: Position of the UAV relative to a fixed target $R_D = 500$

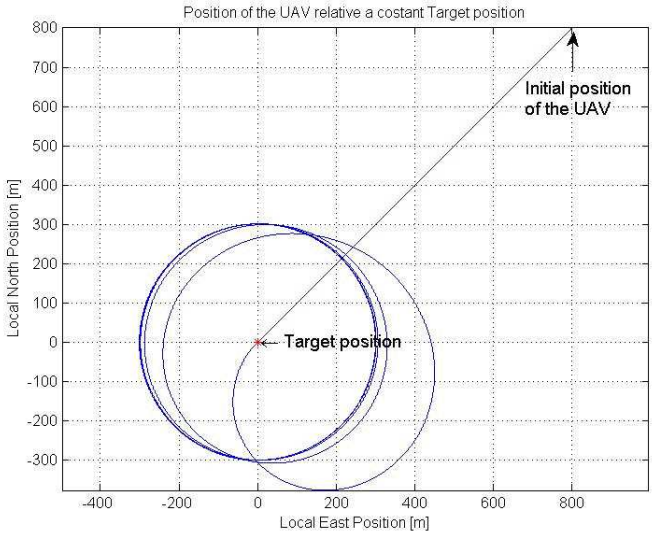

Figure 3.12: Position of the UAV relative to a fixed target with different initial condition $R_D = 0$

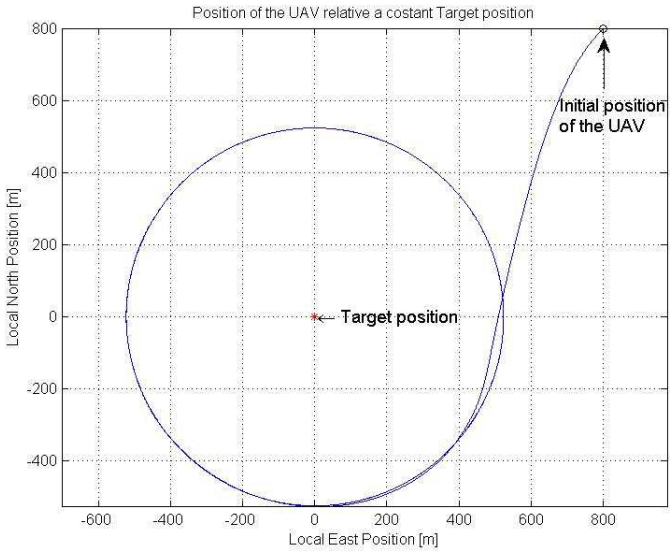

Figure 3.13: Position of the UAV relative to a fixed target with different initial condition $R_D = 500$

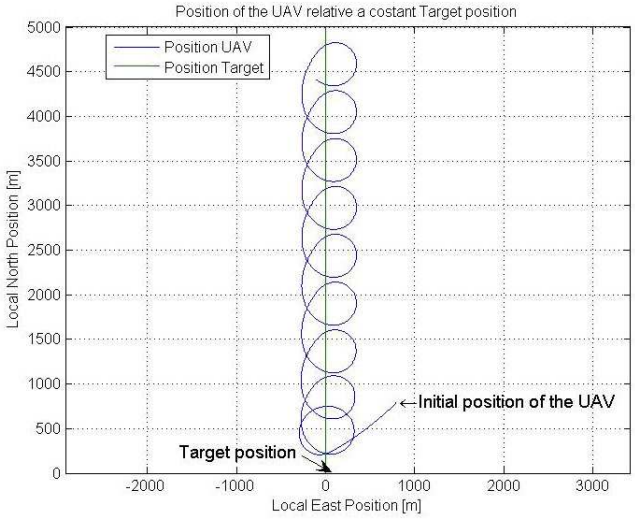

Figure 3.14: Position of the UAV relative to a moving target $R_D = 0$

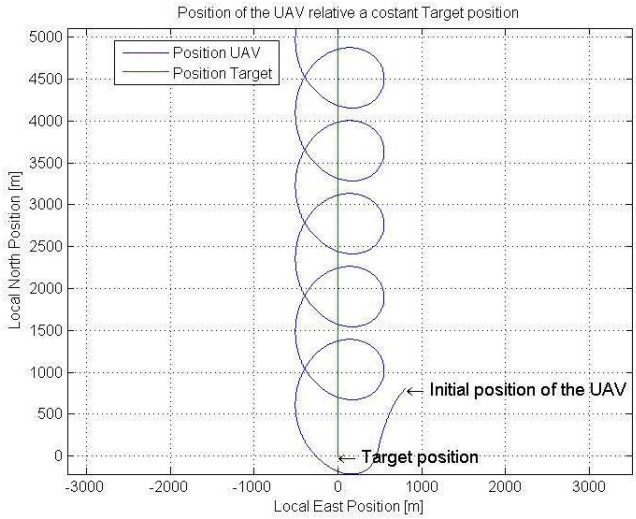

Figure 3.15: Position of the UAV relative to a moving target $R_D = 500$

An advantage of this guidance law is that the maximum value of the lateral acceleration can be chosen by the user simply acting on the gain . Another advantage consists on the fact that in every situation the airspeed of the aircraft is kept above a fixed threshold. The main limitation is that it is difficult to predict the exact behavior of the UAV when one decides to intercept the target. In fact there are some initial condition that cannot allow the vehicle for flying over the target due to the upper bound on the lateral acceleration. Hence the pursuer directly heads for the loitering circle.

Applications of the results. The capability of the guidance law to pass over the target and then to loiter around this at a stand-off distance is highlighted, both when the target is moving and when it is not. So this law is well suitable for problems like continuous live sensing from around and ahead of friendly, adversarial or unidentified targets.

Further investigations are needed in order to find an analytical proof of the stability of the general case of the proposed guidance law. Moreover, modifications of the law in order to face situations where many transits over the target are possible, as well as situations where better performances are assured with respect to wind and more general target motions, necessitate to be considered.

This page is intentionally left blank.

Chapter 4

Lyapunov Vector Field

4.1 Introduction

This paper proposes a 2D guidance law for an aerial pursuer tracking a ground moving target and subject to kinematic constraints in order to be consistent to its flight performances. Several scientific papers cope with problems of target tracking, trajectory tracking and trajectory planning for unmanned air vehicle (UAV).

The problem of target tracking has been studied for a long time. The most famous guidance laws are "LOS angle guidance" and "LOS rate Guidance", see [21]. A different guidance law has been recently presented, see [28]. This second approach shows a number of benefits over the first one and it is designed for following any circular path or, as a specific case, a straight line. Both these guidance laws are not suitable if the aim is to pass over the target or to track a fixed target.

The trajectory tracking has been studied for more time in the robot application than in the aeronautical field. See [38] for some example. Both the articles presented the trajectory tracking utilizing the Lyapunov vector field technique.

The trajectory planning is a slightly different study field. Almost the articles are more focused on the optimization of a path defined by a several numbers of waypoints see [25]. The main source of this technique Has been

proposed by Dubins in one of his most famous article see [8].

In this chapter the target tracking is performed by forcing the UAV to loiter around the target by going through a suitable path whose shape is a priori decided according to pre-established needs. In particular, the emerging Lyapunov vector field approach is followed: a loitering trajectory is defined as stable limit cycle in the system state space. Moreover, the guidance law forces the UAV velocity vector to align with the vector field directions and, hence, to direct towards the limit cycle.

Reliability and simplicity motivate the development of this approach: it provides a simple, yet highly capable basis, for higher level algorithms that adjust the parameters of the vector field to accomplish complex autonomous UAV behaviour. An inner feedback control loop is assumed to ensure the vehicle tracks the vector field by actuating the aircraft control surfaces in order to produce aerodynamics moments to achieve the desired vehicle attitude and altitude hold mode. The direction and the magnitude of the computed vector field velocity are transformed by the guidance outer loop into heading commands, suitable to assure the maneuvers of the UAV to be consistent to its flight performances in terms of minimum required air-speed and maximum turn-rate.

Several Lyapunov vector field guidance laws have been proposed in literature but the capability to fly over the target and to have a continuous live sensing on it from around and ahead of friendly, adversarial or unidentified targets has not yet been explored. The first solution was to follow a straight line see [26]. In this work also the solution of a circle has been proposed but it has been improved later see [20]. Slightly different works have been focused on the use of Lyapunov vector for a cooperative tracking of by two or more UAV see [10]. In last cited paper the shape chosen for the two UAV when the target is not moving was always a circle. The new aspect of this last work was the presence of two UAV monitoring a target on the same Lyapunov vector field.

In this chapter a novel application of vector field-derived guidance law is presented: the proposed law drives the pursuer UAV to fly over the target by following a bow-shaped loitering path centered on the target, a sort of petal-

shaped trajectory. This guidance law is designed for a continuous overflight of a fixed target The main difference with respect to other guidance laws is given by the particular figure chosen. This bow shaped trajectory allows for the possibility to pass more than one time over the target and to surveillance its state. In this way the best applications of this guidance law are for aims as: continuous overflight of a ship with damages or for rescue of people lost in any environment. This goal is accomplished by defining a Lyapunov function whose zero-level set defines a Bernoulli Lemniscate curve. The exact shape of the lemniscates are tunable by setting the parameters of the Lyapunov function according to the aircraft flight performances. The lemniscates represents a stable limit cycle that defines the loitering trajectory around the target. A reference vector field that drives the system towards this limit cycle has been proposed and, based on it, a simple feedback control loop has been defined. Theoretical considerations about global stability of the guidance law are also provided. They have been inspired by several works on the Lyapunov stability global see [15].

The feedback nature of the guidance law allows it for being effective also in presence of wind. The basic algorithm is presented for a stationary target in the absence of wind and then a modification is described that accounts for known constant target velocity and known constant background wind. In these cases the capability of the guidance law to pass over the target and then to loiter is highlighted by means of simulation results both when the target is moving and when it is fixed.

4.2 Lyapunov Vector Field Construction

For vehicle guidance, a vector field can be represented by:

$$\dot{\overline{r}}_d = h\left(\overline{r}, \theta\right) \tag{4.1}$$

parameterized by a coefficient array θ. This provides a desired velocity vector $\dot{\overline{r}}_d$ at each vehicle position $\overline{r}$ (see figure 4.1) that can be used as a reference for middle level control of vehicle acceleration. If global behavior

of this vector field can be specified to be simple and robust for all values of θ, then management of the vehicle can be accomplished at a higher hierarchical level by relatively infrequent manipulation of the parameters in θ. This promotes a high degree of autonomy in the vehicle, and reduced communication bandwidth to centralized command and control systems.

Desired asymptotic behavior is produced via an attractor, which consists of a path or equivalently a set of desired positions to which the vehicle should converge. In many other applications, this set could be a single equilibrium point, which implies an asymptotically fixed position (zero velocity). For airplane UAVs, however, this is not possible since they must maintain airspeed to remain aloft. Here we are interested in attractors that allow asymptotic motion with non-zero velocity. Such attractors are continuous curves in configuration space, and can take many forms, including chaotic strange attractors [14]. To provide well-understood vehicle behavior, we focus on the simplest of these attractors, i.e. limit cycles. In this application, these are closed, non-intersecting curves $C \ni \mathbb{R}^3$ which contain no equilibrium points. The problem is then to construct a vector field $h(\overline{r}, \theta)$ that causes vehicle motion to be globally attracted to this set C.

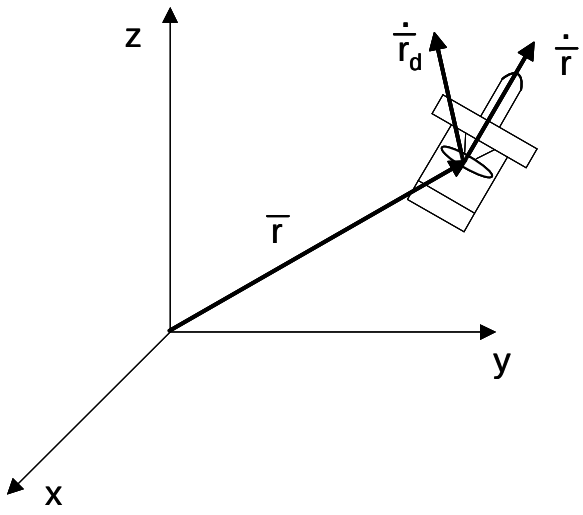

Figure 4.1: UAV inertial position and velocity, along with the desired velocity defined by the Lyapunov vector field

Lyapunov stability theory is used to construct a vector field, rather than to analyze a given vector field. In this approach, the desired attractor C is specified as a zero-level set of an otherwise positive potential function $V_F(\overline{r})$. That is, $V_F(\overline{r})$ is positive definite on C . We also require that $V_F(\overline{r})$ is radially unbounded, i.e. $\overline{r} \to \infty$ implies that $V_F(\overline{r}) \to \infty$, that the gradient of $V_F(\overline{r})$ is finite, i.e. that $\frac{\partial V_F}{\partial \overline{r}}$is bounded whenever $\overline{r}$ is bounded, and that $\frac{\partial V_F}{\partial \overline{r}} \to 0$ implies that $V_F(\overline{r}) \to 0$. The time derivative of $V_F(\overline{r})$ is given by:

$$\dot{V}_F(\overline{r}) = \frac{\partial V_F}{\partial \overline{r}}\dot{\overline{r}} = \frac{\partial V_F}{\partial \overline{r}} h(\overline{r}, \theta) \tag{4.2}$$

Assume for the moment that the vehicle motion $\dot{\overline{r}}$ can be specified to equal any desired vector field $\dot{\overline{r}}_d$.Then choose the following vector field:

$$\dot{\overline{r}} = \dot{\overline{r}}_d = h(\overline{r}, \theta) = -\left[\frac{\partial V_F}{\partial \overline{r}}\Gamma(\overline{r})\right]^T + S(\overline{r}) \tag{4.3}$$

where $\Gamma(\overline{r})$ is any symmetric positive definite matrix function such that $\frac{\partial V_F}{\partial \overline{r}}\Gamma(\overline{r})$ is bounded whenever $\overline{r}$ is bounded, $\frac{\partial V_F}{\partial \overline{r}}\Gamma(\overline{r})\left[\frac{\partial V_F}{\partial \overline{r}}\right]^T \to 0$ implies that $\frac{\partial V_F}{\partial \overline{r}} \to 0$ and $S(\overline{r})$ satisfies:

$$\frac{\partial V_F}{\partial \overline{r}} S(\overline{r}) = 0 \tag{4.4}$$

Then

$$\dot{V}_F(\overline{r}) = \left(\frac{\partial V_F}{\partial \overline{r}}\right)\Gamma(\overline{r})\left(\frac{\partial V_F}{\partial \overline{r}}\right)^T \tag{4.5}$$

Since $\dot{V}_F(\overline{r}) \leq 0$, $V_F(\overline{r})$ is bounded and converges. Since $V_F(\overline{r})$ is radially unbounded, $\overline{r}$ is bounded. Then by the assumption on $\Gamma(\overline{r})$ and 4.4, $\dot{V}_F(\overline{r}) \leq 0$ is bounded, hence $\dot{V}_F(\overline{r}) \leq 0 \to 0$ by the Barbalat lemma [17]. By the LaSalle invariance principle [17], $\overline{r}$ globally converges to the largest set that satisfies both $\dot{V}_F(\overline{r}) = 0$ and 4.3. Since $\Gamma(\overline{r})$ is positive definite $\dot{V}_F(\overline{r}) = 0$ implies that $\frac{\partial V_F}{\partial \overline{r}} = \overline{0}$. In 4.3 this requires that $\dot{\overline{r}} = S(\overline{r})$. Observe that the function $S(\overline{r})$ cannot be zero on the attractor C since this would result in zero asymptotic vehicle velocity. Since $\frac{\partial V_F}{\partial \overline{r}} \to 0$ implies that $V_F(\overline{r}) \to 0$, we have shown that integral curves of the vector field converge to the desired

attractor, i.e. $\overline{r} \to C$.

The first term in the vector field 4.3 is a contraction which produces a vector field component that is directed opposite to the gradient of the potential function $V_F(\overline{r})$. When Γ is isotropic (a scaled identity matrix), this term is exactly opposite to the gradient of $V_F(\overline{r})$. A non-isotropic Γ allows a limited variation in this gradient-opposing direction, so that $V_F(\overline{r})$ remains monotone decreasing over time. The second term in 4.3 is a circulation term, which is always normal to the gradient of $V_F(\overline{r})$, hence does not contribute to the change in $V_F(\overline{r})$ over time.

For UAV tracking control, it is desirable that $\Gamma(\overline{r})$ and $S(\overline{r})$ be chosen so that the vector field 4.3 is normalized to provide a desired vehicle speed v at any point $\overline{r}$, i.e:

$$|h(\overline{r},\theta)| = \left| -\left[\frac{\partial V_F}{\partial \overline{r}}\Gamma(\overline{r})\right]^T + S(\overline{r})\right| = \nu \tag{4.6}$$

Note that ν can be any non-negative value. When ν is a function of time which is bounded away from zero, this makes the system non-autonomous, and the proof of stability must be modified to use the Barbalat lemma [17] instead of the LaSalle invariance principle. This is not developed here, however.

An example of functions $V_F(\overline{r})$, $\Gamma(\overline{r})$, and $S(\overline{r})$ that satisfy these assumptions, and produce a simple set C are as follows, which is similar to that originally provided by [19]. Later work ([16] [11], [26], [9]) has also utilized similar vector fields. Let the coordinates of $\overline{r}$ be given by the difference between the vehicle location (x, y, z) and the center of a desired loiter circle attractor C at (x_0, y_0, z_0).

Let the loiter circle lie in a plane normal to the unit vector $\hat{n}$, and let the desired in-plane radius of C be ρ. Define the normal component of $\overline{r}$ by $\overline{r} = \left(\overline{r}^T\hat{n}\right)\hat{n}$ and the tangential (in-plane) component by $\overline{r}_t = \left(I - \hat{n}\hat{n}^T\right)\overline{r}$. Then define

$$V_F(\overline{r}) = \frac{\left(\overline{r}_n^T\hat{n}\right)^2}{2} - \frac{\left(\overline{r}_t^T\hat{r}_t - \rho\right)^2}{2} \tag{4.7}$$

so that $r_n = \overline{r}^T \hat{n}$ and $r_t = |\overline{r}_t|$ so that $\hat{r}_t = \frac{\overline{r}_t}{r_t}$ it results

$$\frac{\partial V_F}{\partial \overline{r}} = r_n \hat{n}^T + (\hat{r}_t - \rho)\, \overline{r}_t^T \tag{4.8}$$

Also define

$$\Gamma(\overline{r}) = \frac{I}{\alpha(\overline{r})} \tag{4.9}$$

and

$$S(\overline{r}) = \frac{\gamma \hat{n} \overline{r}_t}{\alpha(\overline{r})} \tag{4.10}$$

where $\gamma > 0$ and the normalization $\alpha(\overline{r})$ is given by

$$\alpha(\overline{r}) = \sqrt{r_n^2 + (r_t - \rho)^2 + \rho^2 \gamma^2 \nu} \tag{4.11}$$

Note that $V_F(\overline{r})$ is zero only when the vehicle position $\overline{r}$ lies on the desired loiter circle C, so that $r_n = 0$ and $r_t = \rho$. If $\hat{n}$ is oriented vertically, the loiter circle is horizontal. Since 4.7 holds, the vector field velocity is everywhere given by ν. Also, on C there is the vector field contraction term $\frac{\partial V_F}{\partial \overline{r}} \Gamma(\overline{r}) = 0$ and from 4.7, the vector field circulation term $S(\overline{r}) = \nu$, providing the desired velocity on the loiter circle. The sign of $\gamma\ S(\overline{r})$ determines the direction of circulation on C. When $\overline{r}$ becomes large, the circulation term $S(\overline{r}) \to 0$ and the contraction term $\left|\frac{\partial V_F}{\partial \overline{r}} \Gamma(\overline{r}) \to 0\right|$. From 4.8, the vector field points toward the center of the loiter circle when far away, and smoothly veers into a circular loiter as the radial distance converges to ρ. The magnitude of γ controls the relative strength of the circulation and contraction terms, which modifies the abruptness of the transition from domination by contraction to domination by circulation.

Likewise, a non-isotropic $\Gamma(\overline{r})$ could be used to vary the strength of contraction normal to the circle relative to the contraction in the plane of the circle. Observe that $\frac{\partial V_F}{\partial \overline{r}} \Gamma(\overline{r}) \to 0$ implies $\frac{\partial V_F}{\partial \overline{r}} \to 0$, and $\frac{\partial V_F}{\partial \overline{r}} \to 0$ implies $V_F(\overline{r}) \to 0$, hence we have asymptotic convergence of $\overline{r}$ to the loiter circle C beginning at any initial conditions.

Figure 4.2 shows this vector field for $(x_0, y_0, z_0) = (0, 0, 10)$ [m], $\rho = 100$

[m], $\gamma = 0.2$, and $\nu = 10$ [m/s], as well as some integrated trajectories beginning at various initial conditions.

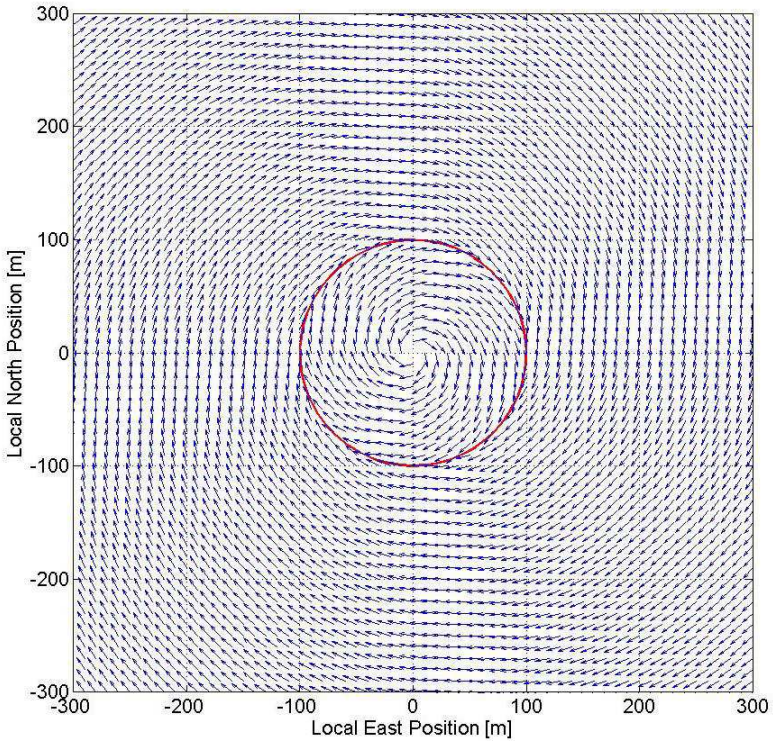

Figure 4.2: Example Vector Field satisfying the assumption for a globally attractive limit cycle

Note that this overall behavior is easy to understand: any initial state results in circular loitering flight centered at (x_0, y_0, z_0) with radius ρ and velocity ν. It provides the UAV with autonomous control which is simple to implement in an on-board microprocessor autopilot This globally attractive loiter circle behavior is specified through only 6 scalar parameters $\theta = (x_0, y_0, z_0, \rho, \gamma, \nu)$ and the normal vector $\hat{n}$, which can be modified at low communication rates to provide a variety of useful capabilities.

For example, the loiter circle approach can be used to construct robust waypoint navigation schemes, where the next waypoint is given as the loiter circle center., or as a point on the loiter circle so the vehicle flies directly over the way point. This is robust to waypoint generation timing: if the next waypoint is not available as the existing waypoint is approached, the

vehicle will simply orbit the existing waypoint until the next one is available. No complex decision logic is needed to initiate turns. Also, the next waypoint vector field can be enabled based on proximity to the current target loiter circle, providing automatic sequencing timing of waypoints to produce smooth transitions between waypoints.

Extending this idea further, switching circular loiter vector fields can be used to follow arbitrary way point sequences, e.g. that are produced by higher level task planning algorithms [13] and [2] This enables more complex flight patterns, without the need for pre-processed route information.

Another application that utilizes loiter circles is in-situ atmospheric sensing with large numbers of small UAVs [29]. There, each vehicle is guided by its own loiter circle vector field, but data sensed in this process is used to autonomously modify the loiter circle location, e.g. to cause vehicles to cluster in regions where high quality data is located. Here, a tilted loiter circle enables gradients of the atmospheric data to be estimated on each circuit, and this can be used to modify loiter circle location and diameter for desired clustering control. The robust, globally stable vector field behavior enables inter-vehicle coordination to be accomplished at higher levels in the control hierarchy, and at lower rates of intercommunication.

The loiter circle approach has also been used for stand-off tracking of ground targets [11] and [9], where range to the target optimizes the trade-off between sensor accuracy and field of view, or where close approach to a hostile target is undesirable for stealth or safety reasons. Both this application and the atmospheric sensing application have time variation in the loiter circle parameter vector, i.e. center location, that can cause mistracking of the desired path, with errors proportional to the speed of parameter motion. In some cases, e.g. [11], knowledge of the time variation can be used to recover asymptotic convergence, provided the parameter motion speed is smaller than the vehicle speed. This section is taken from [20].

4.3 The Lemniscate Vector Field

The Lyapunov vector field guidance law structure is shown in figure 4.3.

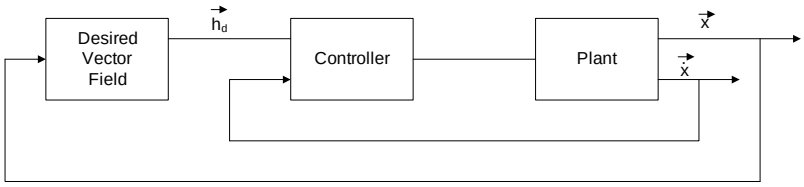

Figure 4.3: Vector Field Control Scheme

The desired asymptotic behaviour of the UAV is produced by a particular geometric curve, famous as Bernoulli Lemniscate where x and y are the components of the 2D position vector of the UAV in a local reference system, c and a are parameters of the Lemniscate.

$$\left(x^2+y^2\right)^2 = 4a^2\left(cy^2 - x^2\left(1-c\right)\right) \tag{4.12}$$

Figure 4.4 shows the flexibility of this equation. The different geometric figures are simply constructed tuning the coefficients c and a. This is an intersecting curve and consequently provides a continuous pass over the target. The Lyapunov Function that ensures the Lemniscate is the desired circuit attractor is the following:

$$F_{LF}\left(x,y\right) = \left[\left(x^2+y^2\right)^2 - 4a^2\left(cy^2 - x^2\left(1-c\right)\right)\right]^2 \tag{4.13}$$

Figure 4.5 demonstrates that the function is radially unbounded.

Figure 4.6 represents the Lyapunov vector Field associated to the Lemniscate. Its shape can be seen as an attractive loiter for an UAV. Far away from the path the vector field is directed perpendicular while, close to the Lemniscate, it becomes tangent.

Another assumption requested by the classical Lyapunov vector field theory is that $\frac{\partial F_{LF}}{\partial x}, \frac{\partial F_{LF}}{\partial y} \to 0$ implies $F_{LF}\left(x,y\right) \to 0$.

It is evident that the two derivatives just cited become zero also in the origin of the axis. This is a discontinuity point in the sense of Lipschitz definition. However this problem is considered negligible in the development of this discussion because of the inertia of the vehicle that mainly annuls its effect.

The desired vector field $\mathbf{h_d}$ is created according to the same formulation

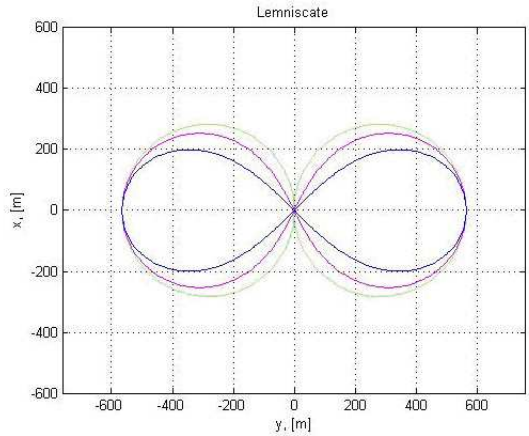

Figure 4.4: Lemniscate

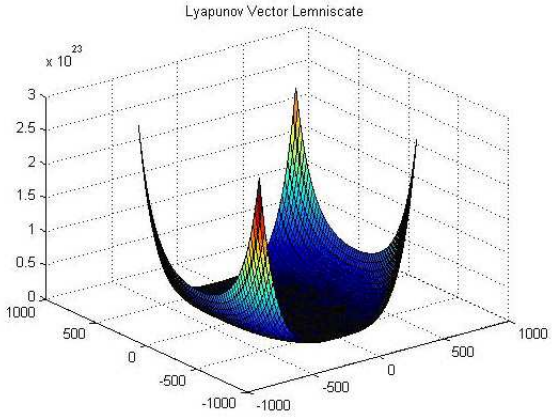

Figure 4.5: Lyapunov Function of Lemniscate

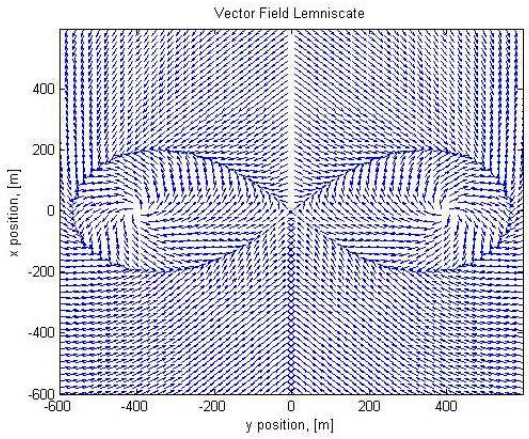

Figure 4.6: Lemniscate Vector Field

proposed by [20]. By defining $\mathbf{x} = [x, y]^T$, it becomes:

$$\mathbf{h}_d(\mathbf{x}) = -\left[\frac{\partial F_{LF}}{\partial \mathbf{x}}\Gamma(\mathbf{x})\right]^T + \gamma(\mathbf{x})\, S(\mathbf{x}) \tag{4.14}$$

where

$$\begin{cases} \Gamma(\mathbf{x}) = \dfrac{\arctan\left(\left|\left(x^2+y^2\right)^2 - 4a^2\left(cy^2 - x^2(1-c)\right)\right|\right)}{C} \\ \gamma(\mathbf{x}) = sign(y) \end{cases} \tag{4.15}$$

are position-dependent scalar functions chosen in a suitable way such to behave as position-dependent gains. Moreover, $\frac{\partial F_{LF}}{\partial \mathbf{x}}$, and $S(\mathbf{x})$, when evaluated along the Lemniscate, are orthogonal and tangent vectors, respectively. As a consequence, vector $S(\mathbf{x})$ is chosen in order to satisfy the orthogonality condition expressed by the following inner product equality:

$$\frac{\partial F_{LF}}{\partial \mathbf{x}}\mathbf{S} = 0 \tag{4.16}$$

From 4.16 the scalar components of $S(\mathbf{x}) = [S_x, S_y]^T$ results:

$$\begin{cases} S_x = y\left(x^2 + y^2 - 2a^2c\right) \\ S_y = -x\left(x^2 + y^2 + 2a^2\left(1 - c\right)\right) \end{cases} \tag{4.17}$$

Equation 4.14 is composed by two terms. The joint action of these terms acts in the following way. The vector field points toward the Lemniscate when the UAV is far from it and directs along the Lemniscate path when the UAV is over it. At intermediate distance there is a mix of these two movements that is modulated by the two position dependent gains defined in 4.15.

In particular, $\frac{\partial F_{LF}}{\partial \mathbf{x}}\Gamma\left(\mathbf{x}\right) \rightarrow 0$ when $\frac{\partial F_{LF}}{\partial \mathbf{x}} \rightarrow 0$ (this happens near the Lemniscate). $\frac{\partial F_{LF}}{\partial \mathbf{x}}$ is the contraction term cited in the last section. The term $\gamma\left(\mathbf{x}\right)S\left(\mathbf{x}\right)$ is the circulation term and ensures that when we are on the trajectory there is still a component of the desired vector field that drives the movement on the Lemniscates. Constant C in 4.15 acts as a sort of normalization of for function G. It has to be tuned according to the required performances for the UAV in terms of velocity of response of the guidance law accordingly to the dynamical constraints of the plane.

4.4 Guidance Law

The system dynamics in this particular section is described by the following kinematic model as exoressed to a fixed reference frame:

$$\begin{cases} \dot{x}_R = V\cos(\chi) + W_x \\ \dot{y}_R = V\sin(\chi) + W_y \\ \dot{\chi} = \frac{a_n}{V} \end{cases} \tag{4.18}$$

In order to allow the UAV to follow the desired trajectory in the velocity vector field, it can be assumed that the UAV has a heading autopilot. The autopilot controls the UAV for tracking the desired course angle χ_d.

The desired vector field and the desired course angle χ_d are related by the following equations:

$$\begin{cases} h_{dx} = V\cos(\chi_d) \\ h_{dy} = V\sin(\chi_d) \end{cases} \tag{4.19}$$

where $\mathbf{h} = [h_d x, h_d y]^T$.

Consequently, the guidance law has to provide the UAV an acceleration a_n able to steer the actual UAV course angle, χ, to its reference value expressed by χ_d. This is to be performed by a feedback control. Hence, the proposed guidance law has the following expression:

$$a_n = K(\psi - \chi_d) + V\dot{\chi}_d \tag{4.20}$$

that, when substituted into the third equation of 4.18, assures $\dot{\chi} = \dot{\chi}_d$ when $\chi = \chi_d$.

K is a suitable scalar gain: it is not the aim of this article to discuss the tuning of this gain in the proposed guidance law. It has to be chosen in order to provide a lateral acceleration whose maximum value does not exceed the UAV dynamic structural bounds.

It is possible to demonstrate that:

$$\dot{\chi}_d = \frac{\mathbf{h}_d \times \dot{\mathbf{h}}_d \cdot \mathbf{k}}{V^2} \tag{4.21}$$

and, in case of absence of wind,

$$\tan(\chi - \chi_d) = \frac{\dot{\mathbf{x}} \times \mathbf{h}_d \cdot \mathbf{k}}{\dot{\mathbf{x}} \times \mathbf{h}_d} \tag{4.22}$$

where bfK is the z-axis unit vector orthogonal to plane x-y in a clockwise reference system, while $\times$ and $\cdot$ are the usual symbols denoting cross and inner products, respectively.

Hence the guidance law becomes:

$$a_n = K\arctan\left(\frac{\dot{\mathbf{x}} \times \mathbf{h}_d \cdot \mathbf{k}}{\dot{\mathbf{x}} \times \mathbf{h}_d}\right) + \frac{\mathbf{h}_d \times \dot{\mathbf{h}}_d \cdot \mathbf{k}}{V} \tag{4.23}$$

Equation 4.23 is quite useful because it allows for expressing the guidance law in terms of the desired vector field and its time-derivative. In particular,

$\mathbf{h}_d$ and $\dot{\mathbf{h}}_d$ can be calculated from 4.14 and, of course, their expression is related to the selected Lyapunov function.

The closed loop stability of system 4.18 together with guidance law 4.23 has not been demonstrated here. While simulations show that stability is always reached, nevertheless an analytic demonstration is still under development.

A preliminary analysis of 4.23 has been carried on here in order to assess the behaviour of a_n. Note that the guidance law consists of two terms: the first one is bounded, due to the limitedness of function arctan ().

The second term can be shown is bounded too. The complete demonstration is not reported here because the length of algebraic calculations involved. Nevertheless the initial steps are given. The starting point is to express 4.18 as the sum of two perpendicular vectors:

$$\mathbf{h}_d(\mathbf{x}) = f_n\mathbf{n} + f_s\mathbf{s} \tag{4.24}$$

with f_n, f_s bounded scalar functions, $\mathbf{n}$ is a unit-vector pointing along $\frac{\partial F_L F}{\partial \mathbf{x}}$ direction, $\mathbf{s}$ is a unit-vector pointing along $S(\mathbf{x})$ direction (see 4.17). Of course it holds $\mathbf{ns} = 0$. After that, it is necessary to express the time-derivative of the desired vector field:

$$\dot{\mathbf{h}}_d(\mathbf{x}) = \dot{f}_n\mathbf{n} + f_n\dot{\mathbf{n}} + \dot{f}_s\mathbf{s} + f_s\dot{\mathbf{s}} = g_n\mathbf{n} + g_s\mathbf{s} \tag{4.25}$$

with g_n, g_s scalar functions. The course of the demonstration states the boundness of g_n, g_s. As a consequence, also the proposed guidance law has a bound.

4.5 Simulation Results

In this paragraph we want to show the different behaviour of the proposed guidance law in two different cases. The first one is a simulation without any disturbances while the second one is with the presence of a constant disturbance. In this way we tried to simulate the effect of the wind.

In particular, the two different case studies presented here are carried on in the following numerical simulations:

- Not wind effect, initial position of the UAV at (300,0), heading south;
- Presence of a constant wind, east direction, initial position of the UAV at (300,0), heading south.

Both the simulations last 600 s and the airspeed of the UAV is 10 m/s. In the second case the speed of the wind is 3 m/s.

As mentioned, this work is not focused on the tuning of the gain K. In both these simulations the values of K = 5 has been chosen in order to obtain a good behaviour. Under this choice the maximum lateral acceleration is always supported by the UAV.

The parameters defining the Lemniscate are the following:

a=400, C=0.5

The two different simulations show the similar behaviour that is reported in figure 4.7 and figure 4.8. In both simulations the tracking of the Lemniscate is performed. The main difference among the two simulations is that the presence of the wind, in the second case, obviously enforces the UAV to turn towards east. The preliminary design of the parameter of the guidance law allows for tracking the Lemniscate in a very good way.

The initial movement towards west in 4.7 is determined by the $\gamma(\mathbf{x})$ function.

4.6 Conclusion

A new guidance law, suitable for UAV missions, in order to loiter around a target by following a Lemniscate-type trajectory, has been proposed. The Lyapunov Vector Field methodology has been applied and described to solve this problem. Even though some mathematical singularities due to the unsingleness of the derivatives of the Lemniscate centre point, preliminary theoretical analysis together with simulation results have given very good results

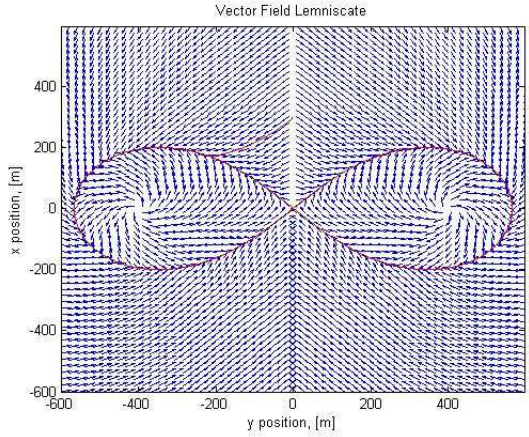

Figure 4.7: Behaviour of the Guidance Law without Wind

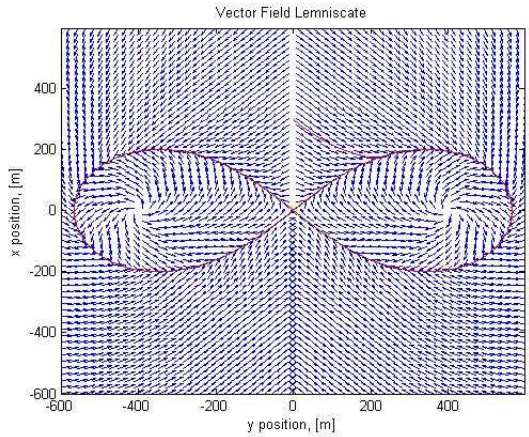

Figure 4.8: Tracking Law with Constant Wind

in terms of general behaviour of the feedback guidance and control system. While simulations has given good performances also in presence of wind, further theoretical investigation and tests will be needed in order to assure global stability and a globally stable functioning in presence of different types of disturbances.

Chapter 5

Oscillatory Control

5.1 Introduction

A pursuer UAV tracking and loitering around a target is the problem analyzed in this chapter. The UAV is always assumed to be a fixed-wing vehicle and constant airspeed together with bounded lateral accelerations are the main constraints of the problem. The pursuer motion control law proposed in this chapter is based on the definition of an oscillatory motion created by a center of oscillation: it allows the pursuer UAV for the fulfillment of the requirements of target tracking under the stated constraints. In particular, the center of oscillation tracks the real motion of the target and the UAV tracks the center of oscillation by means of a suitable guidance law.

One of the main problems in Unmanned Airplane Vehicle (UAV) research involves the determination of suitable autonomous guidance strategies that achieve specific tasks. For example, the ability to perform UAV surveillance operations or to track a specific target or to follow particular trajectories has demonstrated its importance in military context [36]. Similar types of surveillance and tracking activities are also important in civil and commercial operations, such as maritime and rural search and rescue. In these applications the ability of an UAV to track a pre-planned trajectory with high precision can be fundamental.

Different approaches have been proposed in literature for UAV trajectory

tracking applications; the two most significant main streams are path following and virtual waypoint techniques. One of the most innovative path following technique is the Lyapunov vector field guidance in which a field of vectors describes the heading angles required to guide the UAV onto the desired path [20], [31]. Alternatively, in a virtual point technique ([35], [12]), the UAV pursuer tracks the motion of a virtual point that is created and moves along the target trajectory. At the moment many research activities are focused on different techniques to construct trajectories for virtual points ([25], [23]).

In this chapter, the derivation of a Lyapunov based guidance law is proposed in order to track a reference trajectory created by means of the definition of a center of oscillation. A center of oscillation is a virtual point that moves along a sinusoidal oscillatory path created around the actual trajectory of the target (see also [18]). The great advantage of this method consists in creating a path with the same constant cruise speed of the UAV. Besides, if the target is fixed, a Lemniscate-like trajectory is gone by the UAV. This kind of guidance law seems to be suitable for convoy protection or continuous live sensing of a predefined target.

This chapter is structured as follows. In section 5.3 the mathematical model of the UAV and the center of oscillation idea is presented. Section 5.4 presents the technique of the oscillator motion. In section 5.5 shows different simulation results. The last section 5.6 provides some conclusion remarks of the proposed method.

5.2 Averaging: Theory and Definition

A large class of perturbed problems can (after a transformation) be posed in the standard form:

$$\frac{dx}{dt} = \epsilon F\left(x, \theta; \epsilon\right) \quad x \in \mathbb{R}^n \tag{5.1}$$

$$\frac{d\theta}{dt} = \omega(\theta)\,\epsilon G(x,\theta;\epsilon) \quad \theta \in \mathbb{R}^m \tag{5.2}$$

where $\epsilon \ll 1$, and both F and G are 2π-periodic in θ_i, $\theta = (\theta_1, \ldots, \theta_m)$. Some authors also pose standard form as

$$\frac{dx}{dt} = \epsilon F(x,t;\epsilon) \quad x \in \mathbb{R}^n \quad x(0) = x_0 \tag{5.3}$$

where F is 2π-periodic in t. The connection between the two standard forms can be seen if one rewrites 5.3 as the system

$$\frac{dx}{dt} = \epsilon F(x,t;\epsilon) \tag{5.4}$$

$$\frac{d\theta}{dt} = 1 \tag{5.5}$$

For 5.3 define the average

$$\overline{F}(x,\epsilon) \equiv \frac{1}{2\pi}\int_0^{2\pi} F(x,t,\epsilon)\,dt \tag{5.6}$$

Let y satisfy the initial value problem

$$\frac{dy}{dt} = \epsilon\overline{F}(y,\epsilon) \quad y(0) = x_0 \tag{5.7}$$

Then there are averaging theorems which prove, under certain conditions

$$\|x(t) - y(t)\| = O(\epsilon) \tag{5.8}$$

for $t = O\left(\frac{1}{t}\right)$.The method of averaging thus involves

1. A transformation to standard form

2. Solving the averaged equations

Transformation to Standard Form: Introductory example

Consider the problem

$$\ddot{x} + x = \epsilon f\left(x, dotx\right) \quad \dot{()} = \frac{d}{dt}() \tag{5.9}$$

The solution of the unperturbed problem ($\epsilon = 0$) is

$$x_0\left(t\right) = A_0 \cos\left(t + \phi_0\right) \tag{5.10}$$

where A_0 and ϕ_0 are constants. It can be found an exact solution of the perturbed problem using variation of parameters based on the amplitude-phase form of the solution $x_0(t)$:

$$x_0\left(t\right) = A\left(t\right) \cos\left(t + \phi\left(t\right)\right) \equiv A\cos\zeta \tag{5.11}$$

The assumption that x solves the sole equation 5.9 imposes one condition relating the two functions A, ϕ. Thus, we get to impose a second condition on A; ϕ. The second condition we impose on A and is one which guarantees

$$\dot{x}\left(t\right) = -A\left(t\right) \sin\left(t + \phi\left(t\right)\right) = -A\sin\zeta \tag{5.12}$$

that is, a condition which makes differentiation of x appear as if A and ϕ were constant.

Explicitly, we are therefore imposing the condition

$$\frac{d}{dt} A\cos\zeta = -A\sin\zeta \tag{5.13}$$

Using 5.11-5.12 in 5.9, it is readily seen that

$$-\dot{A}\sin\zeta - A\dot{\phi}\cos\zeta = \epsilon f\left(A\cos\zeta, -A\sin\zeta\right) \tag{5.14}$$

Expanding out the second condition 5.13 one gets

$$\dot{A}\cos\zeta - \dot{\phi}A\sin\zeta = 0 \tag{5.15}$$

Solving 5.14 - 5.15 for $\dot{A}$ and $\dot{\phi}$ yields

$$\dot{A} = \epsilon F_1 (A, \phi, t) \equiv -\epsilon \sin\zeta f (A\cos\zeta, -A\sin\zeta) \tag{5.16}$$

$$\dot{\phi} = \epsilon F_2 (A, \phi, t) \equiv -\epsilon \frac{1}{A} \cos\zeta f (A\cos\zeta, -A\sin\zeta) \tag{5.17}$$

Clearly, F_k is 2π-periodic in t, thus 5.16-5.17 is in standard form.

Transformation of weakly nonlinear problems

Let

$$\dot{x} = A(t)\, x + \epsilon g (x, t) \quad x(0) = x_0 \in \mathbb{R}^n \tag{5.18}$$

where $A(t) \in \mathbb{R}^{n\times n}$. This problem is said to be weakly nonlinear because the unperturbed problem

$$\dot{z} = A(t)\, z \tag{5.19}$$

is linear. The unperturbed problem has n linearly independent solutions $z_i(t), i = 1, \ldots, n$ from which a fundamental solution matrix

$$Z(t) = [z_1, \ldots, z_n] \tag{5.20}$$

can be formed. Furthermore, Z is invertible since the columns are independent. If we define y via

$$x = Z(t)\, y \tag{5.21}$$

and substitute 5.21 into 5.18 we get

$$\dot{x} = \dot{Z}y + Z\dot{y} = AZy + \epsilon g (Zy, t) \tag{5.22}$$

But, since $\dot{Z} = AZ$ and Z is invertible,

$$\dot{y} = \epsilon Z^{-1}(t)\, g (Zy, t) \tag{5.23}$$

If all z_i and g are T-periodic in t, the latter system is in standard form.

Transformation of strongly nonlinear problems

Let

$$\dot{x} = f(x,t) + \epsilon g(x,t,\epsilon) \quad x(0) = x_0 \in \mathbb{R}^n \tag{5.24}$$

We say this is strongly nonlinear because the unperturbed problem is nonlinear. Assume the unperturbed problem

$$\dot{y} = f(y,t) \quad y(0) = E \tag{5.25}$$

has a (explicitly) known solution

$$y = Y(t,E) \tag{5.26}$$

We then seek a solution of the perturbed problem of the form

$$x = Y(t, e(t)) \tag{5.27}$$

where $e(t) = (e_1(t), \ldots, e_n(t))$ is some vector valued function. Substitution of this expression into 5.24 yields

$$\frac{\partial y}{\partial t} + \frac{\partial y}{\partial e}\frac{\partial e}{\partial t} = f(y,t) + \epsilon g(y,t,\epsilon) \tag{5.28}$$

where

$$\frac{\partial y}{\partial z} = \left[\frac{\partial Y_i}{\partial E_j}\right]_{ij} \tag{5.29}$$

Since

$$\frac{\partial y}{\partial t} = f(y,t) \tag{5.30}$$

this simplifies to

$$\frac{\partial y}{\partial e}\frac{\partial e}{\partial t} = \epsilon g(y,t,\epsilon) \tag{5.31}$$

If $\frac{\partial y}{\partial e}$ is nonsingular, then

$$\frac{\partial e}{\partial t} = \epsilon \left(\frac{\partial y}{\partial e} \right)^{-1} g\left(y, t, \epsilon\right) \tag{5.32}$$

5.3 Description of the Problem

5.3.1 Mathematical Model of the UAV

In this paper the airspeed, i.e. the speed of the UAV with respect to air flow, is assumed to be constant. Constant speed assumption, also made in others papers ([26], [30] and [28]), is consistent with typical tracking requirements because fixed-wing aircraft velocity changes are generally considered undesirable, in order to avoid altitude variations due to changes in lift. Therefore, according to the scopes and objectives of most guidance problems, it is possible to describe the translation motion of the air vehicle as a mass-point moving in a two dimensional plane. An orthogonal Cartesian frame description of UAV dynamical motion is as follows (see also Figure 5.1):

$$\begin{aligned} \dot{x} &= V\cos(\chi) \\ \dot{y} &= V\sin(\chi) \\ \dot{\chi} &= \tfrac{a_n}{V} \end{aligned} \tag{5.33}$$

where $\mathbf{x} = [x,\ y,\ \chi]^T$ is the state vector of the UAV model. The angle χ is positive in an anti-clockwise sense and it represents the angle between the x axis and the direction of the UAV airspeed vector $\mathbf{V}$; $\mathbf{V}$ is supposed to lie along the aircraft longitudinal axis. V is the modulus of $\mathbf{V}$; a_n is the single input signal of the model and represents the value of lateral acceleration. No longitudinal acceleration respect to the air flow is considered because V is assumed constant. Figure 5.1 shows the direction of the lateral acceleration; its effect is to cause a change in the rate of turn while leaving the airspeed unchanged.

In this paper it is assumed that the position of the target is known by the pursuer guidance system. In [39] and [3] a description of typical sensors useful for this aim are given. The derivative of airspeed velocity vector respect with time is

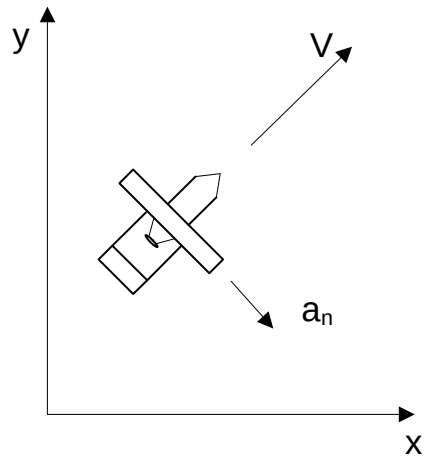

Figure 5.1: Control input, ground and air velocity

$$\dot{\mathbf{V}} = V\dot{\chi}\hat{\mathbf{n}} = a_n\hat{\mathbf{n}} \tag{5.34}$$

where $\hat{\mathbf{n}}$ is the unit vector along the direction orthogonal to the velocity vector.

The movement of the target is modeled by the same mathematical model described by 5.33. In the next section the variable χ_T represents the heading angle of the target and $\dot{\chi}_T$ its angular rate. Target speed is represented by the variable V_T.

5.3.2 Oscillatory idea for tracking a target

The aim of this work is to develop a guidance law for tracking a ground based target and/or loitering around it. It can be assumed that a car or a convoy which is moving in an urban context or military area, represents the target. Usually such a target has a speed slower than the UAV and, besides, it can stop its movement for a period. Consequently, the UAV must be able to stay around the target during all situations. In section 5.3 a fixed altitude UAV with a restricted flight envelope is considered. During the tracking of the target, constant height is desirable and hence constant airspeed is necessary.

The main idea is to define a center of oscillation, i.e. a virtual point that

moves along an oscillatory path that must be gone with the same speed of the UAV. This kind of trajectory must be flexible with respect to the position and the speed of the target. Besides, when the target is fixed, a stable trajectory must be created by the center of oscillation. Once the trajectory is created, a suitable guidance law will track it instead of directly tracking the real target. The control architecture is shown in figure 5.2.

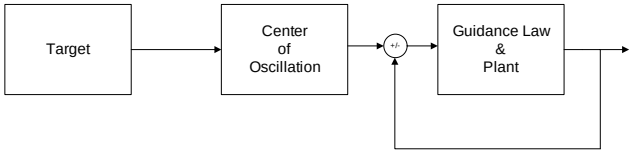

Figure 5.2: Control Architecture

5.4 Analysis of Oscillatory Motion

The proposed mathematical model that describes the motion of the center of oscillation (CO) is:

$$\begin{aligned} \dot{x}_{CO} &= V\cos(\chi_{CO}) \\ \dot{y}_{CO} &= V\sin(\chi_{CO}) \\ \dot{\chi}_{CO} &= \eta\omega_0\cos(\phi) + \dot{\chi}_T \end{aligned} \tag{5.35}$$

where η and ω are scalar parameters, ϕ is an input signal that acts as oscillation phase. In order to analyze the mathematical model of the center of oscillation, the dynamics of the target is considered to be with constant velocity along a straight line ($\dot{\chi}_T = 0$). With this assumption it can be seen that, when η is constant, a sinusoidal trajectory is created while when $\eta = 0$ the center of oscillation goes a straight-line at the same speed of the UAV. The value of η will be defined later in this section.

In order to control the phase and frequency of the oscillation, the phase rate $\dot{\phi}$ is forced to follow the subsequent law by means of a simple closed loop control:

$$\dot{\phi} = \omega_0 - \phi + \omega_0 t + \phi_0 \tag{5.36}$$

where ω_0 is the trim frequency (in this case equal to 1) and $\phi(0) = \phi_0 = 0$ is the commanded initial reference phase. The long term solution is $\phi(t) = \omega_0 t + \phi_0 = t$.

This statement allows to derive (by using the third equation of 5.35 and the stated assumptions):

$$\chi_{CO}(t) = \int_0^t \eta\omega_0 \cos\phi(\tau)d\tau + \chi_{0_{C0}} \tag{5.37}$$

By performing the integration, it results in the following periodic function:

$$\chi_{CO} = \eta \sin t + \chi_{0_{CO}} \tag{5.38}$$

The variable $\chi_{0_{CO}}$ represents the initial heading value of the center of oscillation. The period T is 2π [s].

In order to define the variable η, equation 5.38 is substituted into equation 5.35. In this way it is possible to calculate the mean components of the vector $\mathbf{V}$ in a period T:

$$\begin{aligned} \overline{\dot{x}}_{CO} &= \tfrac{1}{T}\int_0^T V\cos\left(\eta\sin t + \chi_{0_{CO}}\right)dt \\ \overline{\dot{y}}_{CO} &= \tfrac{1}{T}\int_0^T V\sin\left(\eta\sin t + \chi_{0_{CO}}\right)dt \end{aligned} \tag{5.39}$$

With the variable change $\theta = \frac{2\pi t}{T} - \pi = t - \pi$ the integrals in (5.39) become:

$$\begin{aligned} \overline{\dot{x}}_{CO} &= \tfrac{V}{2\pi}\int_{-\pi}^{\pi}\cos\left(\eta\sin\left(\theta+\pi\right) + \chi_{0_{CO}}\right)d\theta \\ \overline{\dot{y}}_{CO} &= \tfrac{V}{2\pi}\int_{-\pi}^{\pi}\sin\left(\eta\sin\left(\theta+\pi\right) + \chi_{0_{CO}}\right)d\theta \end{aligned} \tag{5.40}$$

Now, considering that the functions $\sin(\eta\sin\theta)$ and $-\sin(\eta\sin\theta)$ are odd, their integrals between the interval $[-\pi, \pi]$ are obviously zero. Therefore (5.40) becomes:

$$\begin{aligned} \overline{\dot{x}}_{CO} &= \frac{V\cos\chi_{0_{CO}}}{2\pi}\int_{-\pi}^{\pi}\cos\left(\eta\sin\theta\right)d\theta \\ \overline{\dot{y}}_{CO} &= \frac{V\sin\chi_{0_{CO}}}{2\pi}\int_{-\pi}^{\pi}\cos\left(\eta\sin\theta\right)d\theta \end{aligned} \tag{5.41}$$

The equation

$$\nu = \frac{1}{2\pi}\int_{-\pi}^{\pi}\cos\left(\eta\sin\theta\right)d\theta = J_0\left(\eta\right) \tag{5.42}$$

represents a order zero Bessel function of the first kind. In order to find the variable η, the airspeed of the center of oscillation can be equated to the speed of the target. As a consequence, it results:

$$\dot{\overline{x}}_{CO}^2 + \dot{\overline{y}}_{CO}^2 = \dot{x}_T^2 + \dot{y}_T^2 \rightarrow J_0(\eta) = \frac{V_T}{V} \tag{5.43}$$

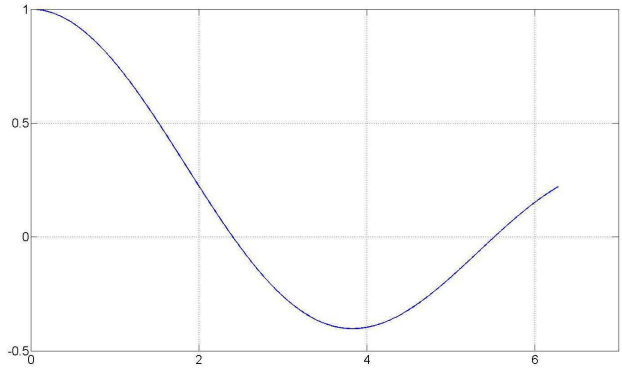

Figure 5.3: Bessel Function

The value of η will be calculated at every period T and it will be used in model equations 5.35 in order to define the trajectory of the center of oscillation. In this paper the assumption of $V_T \leq V$ is made. The domain of the Bessel function $J_0(\eta)$ can be restricted to $[0, 2.48]$. Once the magnitude of the speed of the target is known, the Bessel function can be inverted to find the value of η.

It is important to underline that when the target is fixed ($V_T = 0$) the value of η will be 2.48. The center of oscillation will create a Lemniscate-like trajectory centered nearby the fixed target position. Further investigations

have to be made to exactly overlap the center of the Lemniscate on the target position.

It is desirable that the trajectory of the center of oscillation has its average position centered around the position of the target. For this purpose it is important to define the maximum amplitude of the oscillation. Now, it is assumed a reference frame with its first axis along the target initial velocity vector, and the second axis orthogonal to the first. The initial heading and the initial value of the first coordinate of center of oscillation have to be chosen equal to the target ones (see figure 5.4).

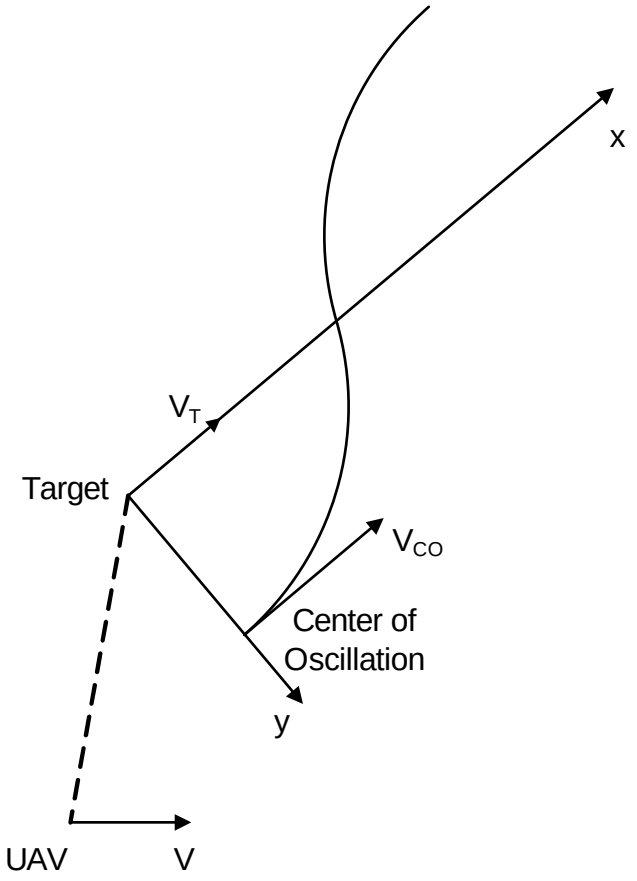

Figure 5.4: Initial Scheme

On the contrary, the second coordinate initial value will be half of the maximum oscillation below the initial second coordinate of the target. By

assuming x_{CO} and y_{CO} as the first and second position coordinates, respectively, it holds:

$$\int_0^{\pi} \dot{y}_{CO} dt = V \int_0^{\pi} \sin(\eta \sin t)\, dt \tag{5.44}$$

The second coordinate at the half of the period can be also written as:

$$\frac{y_{CO}(\pi)}{\pi} = \frac{V}{\pi} \int_0^{\pi} \sin(\eta \sin t)\, dt \tag{5.45}$$

By subtracting to both members the integrals
$-\frac{V}{\pi} \int_0^{\pi} 2\exp(-\eta \sinh(t))dt$
(5.45) becomes:

$$y_{CO}(\pi) = VY_0(\eta)\pi + 2V \int_0^{\pi} \exp(-\eta \sinh t)dt \tag{5.46}$$

where $Y_0(\eta)$ is the Bessel function of the second kind. Once the variable η is computed, the maximum amplitude of the oscillation is described by (5.46).

Hence, here the initial position of the center of oscillation is assumed to be:

$$\begin{aligned} x_{CO}(0) &= x_T(0) \\ y_{CO}(0) &= -\tfrac{1}{2}\left(VY_0(\eta)\pi + 2V \textstyle\int_0^{\pi} \exp(-\eta \sinh t)dt\right) \end{aligned} \tag{5.47}$$

Now, considering the cartesian coordinates (x_L, y_L) of the Lemniscate of Bernoulli can be represented by the subsequent equations:

$$\begin{aligned} x_L &= \tfrac{a\cos(\phi)}{1+\sin^2(\phi)} \\ y_L &= \tfrac{a\cos(\phi)\sin(\phi)}{1+\sin^2(\phi)} \end{aligned} \tag{5.48}$$

where a is a parameter and ϕ is a curvilinear coordinate.

The rate of the tangent vector to the Lemniscate can be represented by:

$$\dot{\chi}_L = \frac{\ddot{y}_L \dot{x}_L - \ddot{x}_L \dot{y}_L}{\dot{x}_L^2 + \dot{x}_L^2} \tag{5.49}$$

where

$$\begin{aligned} \dot{x}_L &= -\frac{\dot{\phi} a \sin(\phi)(3-\sin^2(\phi))}{(1+\sin^2(\phi))^2} \\ \dot{y}_L &= \frac{\dot{\phi} a \sin(\phi)(1-3\sin^2(\phi))}{(1+\sin^2(\phi))^2} \end{aligned} \tag{5.50}$$

and

$$\begin{aligned} \ddot{x}_L &= -\frac{\dot{\phi}^2 a \cos(\phi)(\sin^6(\phi)-11\sin^4(\phi)-9\sin^2(\phi)+3)}{(1+\sin^2(\phi))^4} \\ \ddot{y}_L &= \frac{\dot{\phi}^2 a \cos(\phi)(6\sin^5(\phi)-4\sin^3(\phi)-10\sin(\phi)}{(1+\sin^2(\phi))^4} \end{aligned} \tag{5.51}$$

By substituting equation 5.51 and 5.50 into equation 5.49 it results:

$$\dot{\chi}_L = \frac{3\cos(\phi)\dot{\phi}}{\sin^2(\phi)+1} \tag{5.52}$$

By keeping in mind that $\dot{\phi} = \omega_0$, a comparison between equation 5.52 and the third equation of 5.35 can be made. χ_T can be considered zero because the Lemniscate is created when the target is fixed.

Considering $f(x) = \frac{3\cos(\phi)}{1+\sin^2(\phi)}$, its Fourier terms are:

$$\begin{aligned} a_0 &= \tfrac{1}{\pi}\textstyle\int_{-\pi}^{\pi} f(x)dx = 0 \\ a_1 &= \tfrac{1}{\pi}\textstyle\int_{-\pi}^{\pi} f(x)\cos(x)dx = 2.48 \\ b_1 &= \tfrac{1}{\pi}\textstyle\int_{-\pi}^{\pi} f(x)\cos(x)dx = 0 \end{aligned} \tag{5.53}$$

As cited in at the beginning of this section section the value of η when the target is fixed is 2.48 which is the same value found by analyzing the Lemniscate of Bernoulli.

5.5 Simulation Results

In this section different simulations are presented in order to demonstrate the effectiveness of the proposed guidance law and the center of oscillation motion. The guidance law used for these simulations is the same descripted in section 2.3.2. The position and the lateral acceleration of the target are supposed to be known by an external sensor. The value of η is sampled every 2π s and its value is found with a numerical solution which inverts the Bessel function $J_0(\eta)$. In all the simulations the velocity of the target

is supposed to be lower than the UAV speed and not constant. Besides, different trajectories are performed by the target. All the simulations are shown with the comparison between the classical Proportional Navigation Guidance (**PNG**) law and the proposed guidance law.

As a reminder, the PNG is described by $\dot{\chi} = C\dot{\sigma}$ where C is the navigation gain. In all the simulations the value of C is 4.

The initial position of the target is assumed at $(0, 0)$, the origin of the reference system, while the initial position of the UAV is in $(-50, 0)$. The speed is $V = 35\ m/s$. The values of the gains K_1, K_2 and K_3 are chosen respectively equal to 1, 1 and 0.1.

Case 1

In this simulation the target is supposed to go along a straight trajectory with a different velocity profile. The simulation lasts 90 s. Figure 5.5 shows the velocity profile chosen for the ground target. A constant acceleration, after a constant speed, then a deceleration and finally a zero speed phase are simulated. The target trajectory is supposed to be a straight line.

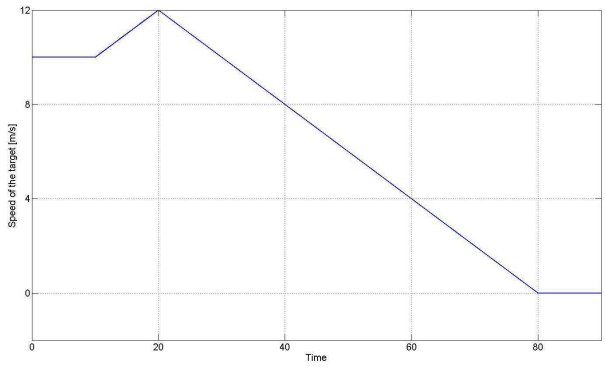

Figure 5.5: Target Speed Profile

Figure 5.6 shows the behavior of the UAV and how it is able to track the center of oscillation trajectory. Although the PNG seems to have a good performance too, it is important to remember that when the distance between the UAV and the center of oscillation becomes small a high acceleration command results. A real UAV cannot achieve that kind of normal acceleration requested. With the proposed guidance law the vehicle approaches the cen-

ter of oscillation trajectory with a smoother profile and acceptable normal accelerations.

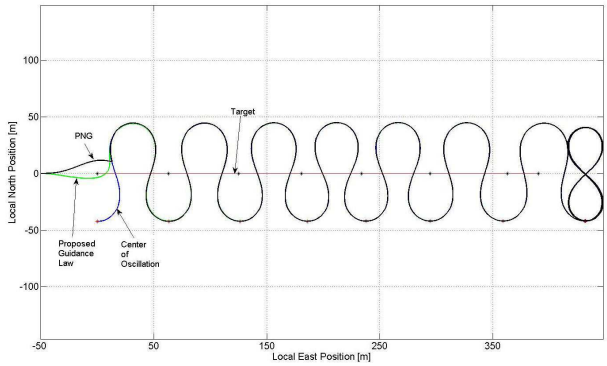

Figure 5.6: UAV trajectories

Case 2

In this second case a more complex target trajectory is used. The first part is the same as in Case 1 but after 60 s the target performs a left turn at a constant velocity and afterwards it continues to go straight. The entire simulation lasts 150 $[s]$. Figure 5.7 shows the velocity profile of the target in this case.

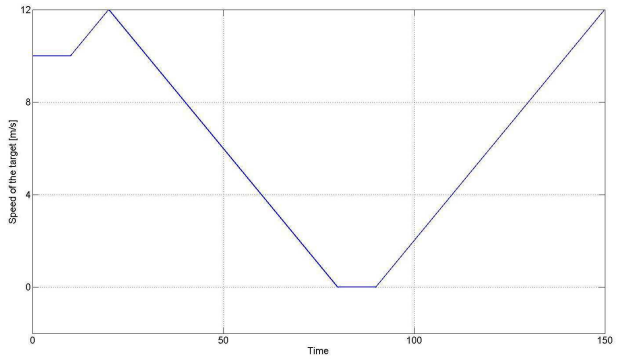

Figure 5.7: Target Speed Profile (Case 2)

Figure 5.8 shows that, after loitering around the stopped target in the first half of the simulation with a Lemniscate-like trajectory, the center of oscillation starts again in order to construct a new oscillating trajectory

tracking the restarted target. Also in this simulation a comparison with the PNG guidance law is done. Obviously the same considerations made in Case 1 can be repeated here. Once the PNG intercepts the center of oscillation, the trajectories overlap.

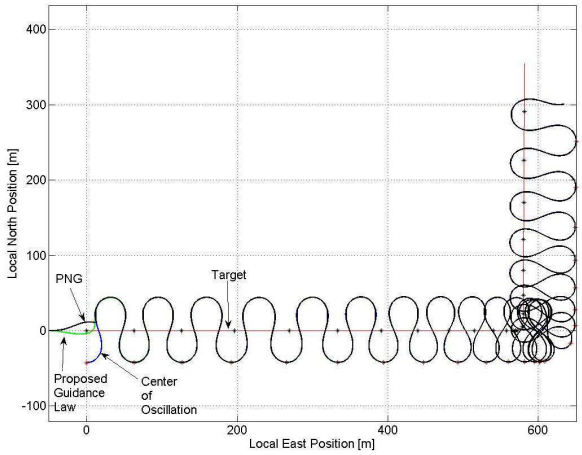

Figure 5.8: UAV trajectories (Case 2)

Case 3

In the third case a circling trajectory is created for the target. It travels at a constant velocity of 10 m/s with a constant lateral acceleration of 0.2 $\frac{m}{s^2}$.

As figure 5.9 shows, the center of oscillation creates a trajectory that both PNG and the proposed guidance law are able to track. The simulation lasts 30 s.

5.6 Conclusion

In this paper a method for creating and tracking an oscillatory trajectory based on the position of the target is presented. The value of the parameter η is sampled every 2π s. Once the measurement of the speed of the target is obtained, through equation 5.43, the value of η is numerically calculated. The path created by the center of oscillation is particularly suitable for aerial vehicle with constant speed constrains and generates smooth turns that are

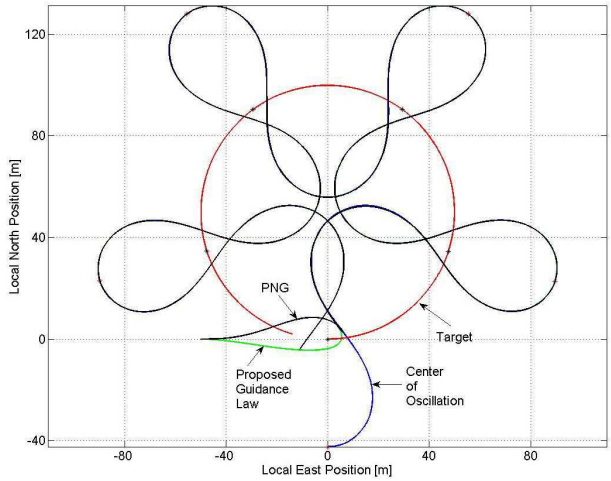

Figure 5.9: UAV trajectories (Case 3)

easily navigable by the UAV. However, the trim frequency ω_0 can be chosen small enough that the trajectory created by the center of oscillation results with an acceptable lateral acceleration.

Besides, the new guidance law presented in chapter 3 is used for tracking this type of trajectory.

Simulation results where a comparison of the performances between the proposed law and the classical PNG have given: they show promising results especially in the lateral (normal) required acceleration. A stability proof of the guidance is given and consequently it guarantees that the UAV will fly directly on the center of oscillation trajectory.

Chapter 6

Pioneer UAV

6.1 BackGround History

In June 1982, Israeli forces very successfully used UAVs as a key element in their attack on Syria. Scout and Mastiff UAVs were used to locate and classify SAM and AAA weaponry and to act as decoys for other aircraft. This action resulted in heavy Syrian losses and minimal Israeli losses. A year and a half later, the U.S. Navy launched strikes against Syrian forces in the same area with losses much higher for the Navy than those of the Israelis.

The Commandant of the Marine Corps, General P. X. Kelly, recognized the effectiveness of the Israeli UAVs. Secretary of the Navy John Lehman then initiated development of a UAV program for the U.S. Anxious to get UAVs to the fleet, Secretary Lehman stipulated that UAV technology would be off-the-shelf. After the contract award to AAI Corporation of Baltimore, Maryland for the Pioneer UAV, developmental and operational testing took place concurrently.

This approach resulted in quick integration of the Pioneer into the fleet. Unfortunately, such quick integration into the fleet can result in problerm identified during operational use which had not been fully explored in the test and evaluation process. The UAV Office a. the Pacific Missile Test Center (PMTC, now the Naval Air Warfare Center, NAWC, Weapons Division, Pt. Mugu) was tasked with Developmental Test and Evaluation of the

Pioneer. Testing revealed the following concerns which warranted further investigation:

1. discrepancies in predicted with flight-tested rate of climb, time to climb,and fuel flow at altitude;
2. apparent autopilot-related pitch instability;
3. tall boom structural failure;
4. severely limited lateral control;
5. slow pitch response causing degraded maneuverability at high gross weights;
6. insufficient testing to determine the effects of the icew wing on flight endurance.

The Target Simulation Laboratory at Pt. Mugu was tasked to develop a computer simulation of the Pioneer in order to provide cost-effective training for pilots. Aerodynamic data were needed to provide the stability and control derivatives necessary for the simulation as well as to answer questions concerning basic flying qualities of the Pioneer. In order to provide support to the research being done at Pt. Mugu and to provide for future UAV project support, a research program was begun at the Naval Postgraduate School (NPS). An instrumented half-scale radio-controlled model of the Pioneer was used 6 for the research at NPS.

Research performed included wind tunnel tests, flight tests, and numerical modeling. Initial NPS research on the Pioneer, performed by Capt. Daniel Lyons, involved a computer analysis of the Pioneer in its original configuration and with a proposed larger tail. A low order panel method (PMARC) was used for the aerodynamic analysis. Static longitudinal and directional stability derivatives, the neutral point, and crosswind limitations were calculated. Drag polars were constructed using the component buildup method for profile drag, and drag reduction measures were considered. In conjunction with Capt. Lyons work, Lt. James Tanner conducted wind tunnel' tests to

Figure 6.1: Pioneer RQ2 on a Platform Laucher during Desert Shield Military Operation

determine propeller efficiencies and thrust coefficients for drag studies. Lt. Tanner also conducted flight tests to determine power required curves and drag polars.

Capt. Robert Bray later conducted wind tunnel tests of a 0.4-scale model at Wichita State University to determine static stability and control derivatives. Aerodynamic data obtained by Capt. Lyons and Bray have been supplied to PMTC to be used for simulation. Lt. Jim Salmons performed initial flying qualities flight testing using an onboard data recording system in order to determine static stability parameters. Unfortunately, vibration problems with the onboard recorder rendered much of the data unusable [Ref 10]. Following up on Lt. Salmons' work, Lt. Kent Aitcheson installed the CHOW-IG telemetry system, designed by Lt. Kevin Wilhelm, in an attempt to alleviate the vibration 7 probiem experienced by Lt. Salmons. The new flight test configuration was used to test static longitudinal and lateral-directional stability characteristics of the Pioneer.

The vibration problem experienced by Lt. Salmons was overcome, though not enough data were acquired for a complete and thorough analysis of the

Pioneeres characteristics. Much insight was gained, however, concerning instrumentation. Resolution needed to be improved for flight control position indication. Lt. Paul Koch conducted further flight tests of the Pioneer with the CHOW-IG telemetry system. Static longitudinal stability results from the flight tests correlated well with theoretical predictions and with simulations of a full-scale Pioneer. Electromagnetic interference with the flight control system at the test site resulted in loss of the half-scale model Pioneer before further data collection and analysis could be performed

6.2 Technical Charateristic

The Pioneer RQ2 was designed on the IAI Israelian Scouth Air vehicle and, similarly with this one, it has a twin-boom structure with a rectilinear wing.

The UAV propulsion is a bicilindrical engine Sachs & Fichtel SF2-350 of 19 kW and a rotary group UEL AR-741 of 28.3 kW.

The vehicle has a fixed landing gear. It is composed by metal and fiber glass in order to make it low observable by the radar.

The technical charateristic are summarized by tables 6.1 and 6.2.

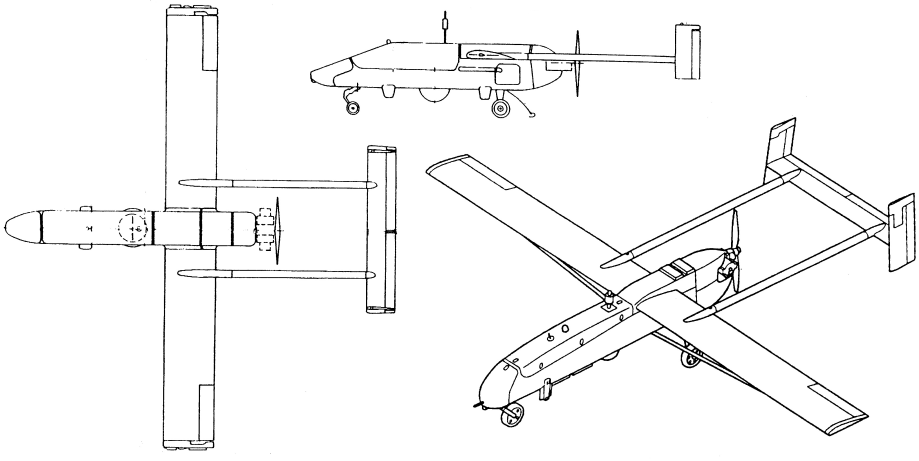

Figure 6.2: Geometric Pioneer RQ2

These information are taken from [5].

Wing	
Area	2.826 m^2
Span	5.151 m
A.R	9.36
Mean Aerodynamic Chord	0.549 m
Airfoil	NACA 4415
Incidence	0.035 rad
Airelon Deflection	$\pm$0.350 rad
Horizontal Stabilizer	
Area	0.564 m^2
Span	1.850 m
A.R	6.07
Mean Aerodynamic Chord	0.305 m
Airfoil	NACA 0012
Incidence	-0.052 rad
Elevetor Deflection	$\pm$0.350 rad
Vertical Stabilizer	
Area	0.202 m^2
Apertura alare	0.661 m
A.R	2.16
Mean Aerodynamic Chord	0.305
Airfoil	NACA 0012
Rudder Deflection	$\pm$0.350 rad
Geometric Charateristic	
Length	4.96 m
Height	1.02 m

Table 6.1: Pioneer Geometric Charateristic

Cruise Speed	89-130 km/h
Max Speed	185 km/h
Cruise Range	185 km
Endurance	8 h
Ceiling	4600 m
Maximum TakeOff	200 kg
Payload	40 kg

Table 6.2: Airvehicle Perfomance

6.3 Equation of Motion

This section and the subsequent are based on the work published by M. Cook [7].

The equation of motion for a 6Dof aircfraft are:

$$\begin{cases} m(\dot{U} - rV + qW) = X \\ m(\dot{V} - pW + rU) = Y \\ m(\dot{W} - qU + pV) = Z \end{cases} \tag{6.1}$$

$$\begin{cases} I_x\dot{p} - (I_y - I_z)qr - I_{xz}(pq + \dot{r}) = L \\ I_y\dot{q} + (I_x - I_z)pr + I_{xz}(p^2 - r^2) = M \\ I_z\dot{r} - (I_x - I_y)pq + I_{xz}(qr - \dot{p}) = N \end{cases} \tag{6.2}$$

where m is the mass of the vehicle, (U,V,W) and (X,Y,Z) are the velocity components respect to the body frame (o,x,y,z) (see figure 6.4). (p,q,r) and (L,M,N) represent the angular velocity and moment in the same frame.

Considering the effect of disturbances it results:

$$\begin{cases} m(\dot{U} - rV + qW) = X_a + X_g + X_c + X_p + X_d \\ m(\dot{V} - pW + rU) = Y_a + Y_g + Y_c + Y_p + Y_d \\ m(\dot{W} - qU + pV) = Z_a + Z_g + Z_c + Z_p + Z_d \\ I_x\dot{p} - (I_y - I_z)qr - I_{xz}(pq + \dot{r}) = L_a + L_g + L_c + L_p + L_d \\ I_y\dot{q} + (I_x - I_z)pr + I_{xz}(p^2 - r^2) = M_a + M_g + M_c + M_p + M_d \\ I_z\dot{r} - (I_x - I_y)pq + I_{xz}(qr - \dot{p}) = N_a + N_g + N_c + N_p + N_d \end{cases} \tag{6.3}$$

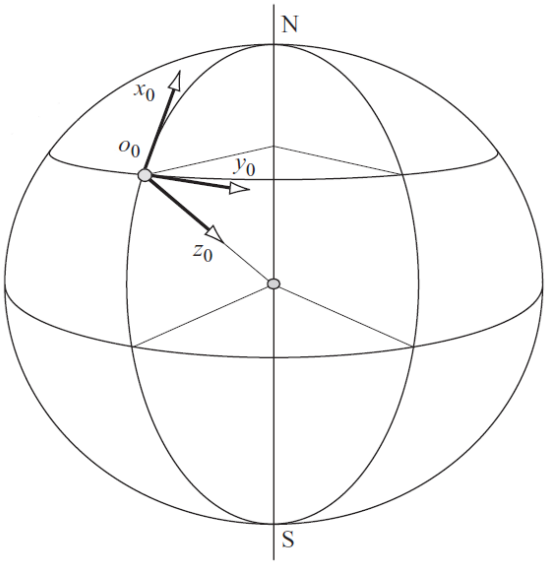

Figure 6.3: North Est Down Frame

The equation 6.3 are nonlinear and consequently a closed form solution is not obtainable. Besides, the term on the right side should be substituded with expression which are very difficult to express. Usually these equation of motion are linearized around a trim condition.

6.4 Linearized Equation of Motion

Initially the aeroplane is assumed to be flying in steady trimmed rectilinear flight with zero roll, sideslip and yaw angles. Thus, the plane of symmetry of the aeroplane oxz is vertical with respect to the earth reference frame. At this flight condition the velocity of the aeroplane is V_0, the components of linear velocity are (Ue,Ve,We) and the angular velocity components are all zero. Since there is no sideslip $V_e = 0$. A stable undisturbed atmosphere is also assumed such that

$$X_d = Y_d = Z_d = L_d = M_d = N_d = 0 \tag{6.4}$$

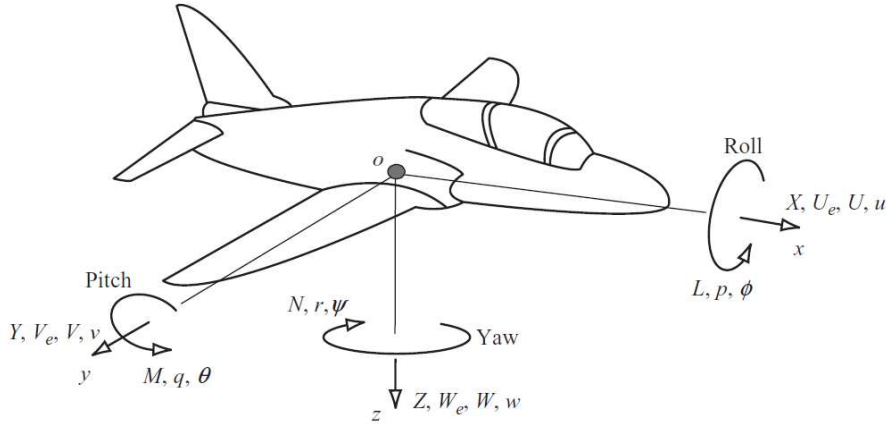

Figure 6.4: Body Frame

If now the aeroplane experiences a small perturbation about trim, the components of the linear disturbance velocities are (u, v,w) and the components of the angular disturbance velocities are (p, q, r) with respect to the undisturbed aeroplane axes (oxyz). Thus the total velocity components of the cg in the disturbed motion are given by

$$\begin{aligned} U &= U_e + u \\ V &= V_e + v = v \\ W &= W_e + w \end{aligned} \tag{6.5}$$

Now, by definition (u, v,w) and (p, q, r) are small quantities such that terms involving products and squares of these terms are insignificantly small and may be ignored. Thus, substituting equations 6.4 and 6.5 into equations 6.3, note that (U_e, V_e,W_e) are steady and hence constant, and eliminating the insignificantly small terms, the linearised equations of motion are obtained:

$$\begin{cases} m(\dot{u} + qW_e) = X_a + X_g + X_c + X_p \\ m(\dot{v} - pW_e + rU_e) = Y_a + Y_g + Y_c + Y_p \\ m(\dot{w} - qU_e) = Z_a + Z_g + Z_c + Z_p \\ I_x\dot{p} - I_{xz}\dot{r} = L_a + L_g + L_c + L_p \\ I_y\dot{q} = M_a + M_g + M_c + M_p \\ I_z\dot{r} - I_{xz}\dot{p} = N_a + N_g + N_c + N_p \end{cases} \tag{6.6}$$

The development of expressions to replace the terms on the right hand sides of equations 6.6 is now much simpler since it is only necessary to consider small disturbances about trim.

The gravitational terms can be espressed by:

$$\begin{cases} X_g = -mg\sin\theta_e - mg\theta\cos\theta_e \\ Y_g = mg\psi\sin\theta_e + mg\phi\cos\theta_e \\ Z_g = mg\cos\theta_e - mg\theta\sin\theta_e \\ L_g = 0 \\ M_g = 0 \\ N_g = 0 \end{cases} \tag{6.7}$$

The variables with the pedix e are reffered to the trim condition while the other are referred to the perturbation (see figure 6.5).

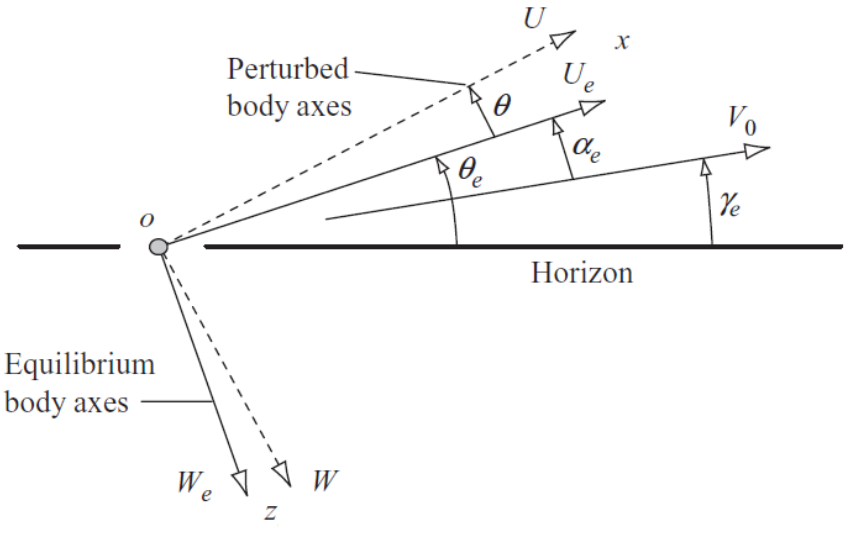

Figure 6.5: Body Axis with and without a perturbation

The aerodynamic terms can be expressed as:

$$\begin{cases} X_a = X_{a_e} + \overset{\circ}{X}_u\, u + \overset{\circ}{X}_v\, v + \overset{\circ}{X}_w\, w + \overset{\circ}{X}_p\, p + \overset{\circ}{X}_q\, q + \overset{\circ}{X}_r\, r + \overset{\circ}{X}_{\dot{w}}\, \dot{w} \\ Y_a = Y_{a_e} + \overset{\circ}{Y}_u\, u + \overset{\circ}{Y}_v\, v + \overset{\circ}{Y}_w\, w + \overset{\circ}{Y}_p\, p + \overset{\circ}{Y}_q\, q + \overset{\circ}{Y}_r\, r + \overset{\circ}{Y}_{\dot{w}}\, \dot{w} \\ Z_a = Z_{a_e} + \overset{\circ}{Z}_u\, u + \overset{\circ}{Z}_v\, v + \overset{\circ}{Z}_w\, w + \overset{\circ}{Z}_p\, p + \overset{\circ}{Z}_q\, q + \overset{\circ}{Z}_r\, r + \overset{\circ}{Z}_{\dot{w}}\, \dot{w} \\ L_a = X_{a_e} + \overset{\circ}{L}_u\, u + \overset{\circ}{L}_v\, v + \overset{\circ}{L}_w\, w + \overset{\circ}{L}_p\, p + \overset{\circ}{L}_q\, q + \overset{\circ}{L}_r\, r + \overset{\circ}{L}_{\dot{w}}\, \dot{w} \\ M_a = X_{a_e} + \overset{\circ}{M}_u\, u + \overset{\circ}{M}_v\, v + \overset{\circ}{M}_w\, w + \overset{\circ}{M}_p\, p + \overset{\circ}{M}_q\, q + \overset{\circ}{M}_r\, r + \overset{\circ}{M}_{\dot{w}}\, \dot{w} \\ N_a = X_{a_e} + \overset{\circ}{N}_u\, u + \overset{\circ}{N}_v\, v + \overset{\circ}{N}_w\, w + \overset{\circ}{N}_p\, p + \overset{\circ}{N}_q\, q + \overset{\circ}{N}_r\, r + \overset{\circ}{N}_{\dot{w}}\, \dot{w} \end{cases} \tag{6.8}$$

The coefficients $\overset{\circ}{X}_u$, $\overset{\circ}{X}_v$, $\overset{\circ}{X}_w$ etc. are called aerodynamic stability derivatives and the dressing $\circ$ denotes the derivatives to be dimensional.

The aerodynamic control terms are:

$$\begin{cases} X_c = \overset{\circ}{M}_\xi\, \xi + \overset{\circ}{X}_\eta\, \eta + \overset{\circ}{X}_\zeta\, \zeta \\ Y_c = \overset{\circ}{Y}_\xi\, \xi + \overset{\circ}{Y}_\eta\, \eta + \overset{\circ}{Y}_\zeta\, \zeta \\ Z_c = \overset{\circ}{Z}_\xi\, \xi + \overset{\circ}{Z}_\eta\, \eta + \overset{\circ}{Z}_\zeta\, \zeta \\ L_c = \overset{\circ}{L}_\xi\, \xi + \overset{\circ}{L}_\eta\, \eta + \overset{\circ}{L}_\zeta\, \zeta \\ M_c = \overset{\circ}{M}_\xi\, \xi + \overset{\circ}{M}_\eta\, \eta + \overset{\circ}{M}_\zeta\, \zeta \\ N_c = \overset{\circ}{N}_\xi\, \xi + \overset{\circ}{N}_\eta\, \eta + \overset{\circ}{N}_\zeta\, \zeta \end{cases} \tag{6.9}$$

Since equation 6.9 describes the effect of the aerodynamic controls with respect to the prevailing trim condition it is important to realise that the control angles, ξ, η and ζ are measured relative to the trim settings ξ_e, η_e and ζ_e respectively.

The power terms are described by the subsequent relations:

$$\begin{cases} X_p = \overset{\circ}{X}_\tau \tau \\ Y_p = \overset{\circ}{Y}_\tau \tau \\ Z_p = \overset{\circ}{Z}_\tau \tau \\ L_p = \overset{\circ}{L}_\tau \tau \\ M_p = \overset{\circ}{M}_\tau \tau \\ N_p = \overset{\circ}{N}_\tau \tau \end{cases} \tag{6.10}$$

As for the aerodynamic controls, power changes are measured with respect to the prevailing trim setting.

Now, substituting equations (6.7), (6.8), (6.9), (6.10) into (6.6) and simplyfing it results:

$$
\begin{cases}
m\dot{u} - \overset{\circ}{X}_u\, u - \overset{\circ}{X}_v\, v - \overset{\circ}{X}_{\dot{w}}\, \dot{w} - \overset{\circ}{X}_w\, w - \overset{\circ}{X}_p\, p - (\overset{\circ}{X}_q - mW_e)q - \overset{\circ}{X}_r\, r \\
+ mg\theta\cos\theta_e = \overset{\circ}{X}_\xi\, \xi + \overset{\circ}{X}_\eta\, \eta + \overset{\circ}{X}_\zeta\, \zeta + \overset{\circ}{X}_\tau\, \tau \\
\\
- \overset{\circ}{Y}_u\, u + m\dot{v} - \overset{\circ}{Y}_v\, v - \overset{\circ}{Y}_{\dot{w}}\, \dot{w} - \overset{\circ}{Y}_w\, w - (\overset{\circ}{Y}_p + mW_e)p - \overset{\circ}{Y}_q\, q - (\overset{\circ}{Y}_r - mU_e)r \\
- mg\phi\cos\theta_e - mg\psi\sin\theta_e = \overset{\circ}{Y}_\xi\, \xi + \overset{\circ}{Y}_\zeta\, \zeta + \overset{\circ}{Y}_\eta\, \eta + \overset{\circ}{Y}_\tau\, \tau \\
\\
- \overset{\circ}{Z}_u\, u - \overset{\circ}{Z}_v\, v + (m - \overset{\circ}{Z}_{\dot{w}})\dot{w} - \overset{\circ}{Z}_w\, w - \overset{\circ}{Z}_p\, p - (\overset{\circ}{Z}_q + mU_e)q - \overset{\circ}{Z}_r\, r \\
+ mg\sin\theta_e = \overset{\circ}{Z}_\xi\, \xi + \overset{\circ}{Z}_\eta\, \eta + \overset{\circ}{Z}_\zeta\, \zeta + \overset{\circ}{Z}_\tau\, \tau \\
\\
- \overset{\circ}{L}_u\, u - \overset{\circ}{L}_v\, v - \overset{\circ}{L}_{\dot{w}}\, \dot{w} - \overset{\circ}{L}_w\, w + I_x\dot{p} - \overset{\circ}{L}_p\, p - \overset{\circ}{L}_q\, q - I_{xy}\dot{r} - \overset{\circ}{L}_r\, r = \overset{\circ}{L}_\xi\, \xi \\
+ \overset{\circ}{L}_\eta\, \eta + \overset{\circ}{L}_\zeta\, \zeta + \overset{\circ}{L}_\tau\, \tau \\
\\
- \overset{\circ}{M}_u\, u - \overset{\circ}{M}_v\, v - \overset{\circ}{M}_{\dot{w}}\, \dot{w} - \overset{\circ}{M}_w\, w - \overset{\circ}{M}_p\, p + I_y\dot{q} - \overset{\circ}{M}_q\, q - \overset{\circ}{M}_r\, r = \overset{\circ}{M}_\xi\, \xi \\
+ \overset{\circ}{M}_\eta\, \eta + \overset{\circ}{M}_\zeta\, \zeta + \overset{\circ}{M}_\tau\, \tau \\
\\
- \overset{\circ}{N}_u\, u - \overset{\circ}{N}_v\, v - \overset{\circ}{N}_{\dot{w}}\, \dot{w} - \overset{\circ}{N}_w\, w - I_{xy}\dot{p} - \overset{\circ}{N}_p\, p - \overset{\circ}{N}_q\, q + I_z\dot{r} - \overset{\circ}{N}_r\, r = \overset{\circ}{N}_\xi\, \xi \\
+ \overset{\circ}{N}_\eta\, \eta + \overset{\circ}{N}_\zeta\, \zeta + \overset{\circ}{N}_\tau\, \tau
\end{cases}
\tag{6.11}
$$

Equations 6.11 are the small perturbation equations of motion, referred to body axes, which describe the transient response of an aeroplane about the trimmed flight condition following a small input disturbance. The equations comprise a set of six simultaneous linear differential equations written in the traditional manner with the forcing, or input, terms on the right hand side. As written, and subject to the assumptions made in their derivation, the equations of motion are perfectly general and describe motion in which longitudinal and lateral dynamics may be fully coupled.

However, for the vast majority of aeroplaneswhen small perturbation transient motion only is considered, as is the case here, longitudinallateral

coupling is usually negligible. Consequently it is convenient to simplify the equations by assuming that longitudinal and lateral motion is in fact fully decoupled.

6.5 Decoupled Equations of Motion

6.5.1 The longitudinal Equation of Motion

Decoupled longitudinal motion is motion in response to a disturbance which is constrained to the longitudinal plane of symmetry, the oxz plane, only. The motion is therefore described by the axial force X , the normal force Z and the pitching moment M equations only. Since no lateral motion is involved the lateral motion variables v, p and r and their derivatives are all zero. Also, decoupled longitudinallateral motion means that the aerodynamic coupling derivatives are negligibly small and may be taken as zero whence

$$\overset{\circ}{X}_v=\overset{\circ}{X}_p=\overset{\circ}{X}_r=\overset{\circ}{Z}_v=\overset{\circ}{Z}_p=\overset{\circ}{Z}_r=\overset{\circ}{M}_v=\overset{\circ}{M}_p=\overset{\circ}{M}_r= 0 \tag{6.12}$$

Similarly, since aileron or rudder deflections do not usually cause motion in the longitudinal plane of symmetry the coupling aerodynamic control derivatives may also be taken as zero thus

$$\overset{\circ}{X}_\xi=\overset{\circ}{X}_\zeta=\overset{\circ}{Z}_\xi=\overset{\circ}{Z}_\zeta=\overset{\circ}{M}_\xi=\overset{\circ}{M}_\zeta= 0 \tag{6.13}$$

The equations of longitudinal symmetric motion are therefore obtained by extracting the axial force, normal force and pitching moment equations from equations 6.11 and substituting equations 6.12 and 6.13 as appropriate. If it assumed that the aeroplane is in level flight and the reference axes are wind or stability axes then $\theta_e = W_e = 0$and the equations become:

$$\begin{cases} m\dot{u}- \overset{\circ}{X}_u\, u- \overset{\circ}{X}_{\dot{w}}\, \dot{w}- \overset{\circ}{X}_w\, w- \overset{\circ}{X}_q\, q + mg\theta =\overset{\circ}{X}_\eta\, \eta+ \overset{\circ}{X}_\tau\, \tau \\ - \overset{\circ}{Z}_u\, u + (m- \overset{\circ}{X}_{\dot{w}}\, \dot{w})- \overset{\circ}{Z}_w\, w - (\overset{\circ}{Z}_q\, +mU_e)q =\overset{\circ}{Z}_\eta\, \eta+ \overset{\circ}{Z}_\tau\, \tau \\ - \overset{\circ}{M}_u\, u- \overset{\circ}{M}_{\dot{w}}\, \dot{w}- \overset{\circ}{M}_w\, w + I_y\dot{q}- \overset{\circ}{M}_q\, q =\overset{\circ}{M}_\eta\, \eta+ \overset{\circ}{M}_\tau\, \tau \end{cases} \tag{6.14}$$

Equations 6.14 represent the simplest possible form of the decoupled longitudinal equations of motion.

6.5.2 The lateral-directional Equation of Motion

Decoupled lateral directional motion involves roll, yawand sideslip only. The motion is therefore described by the side force Y , the rolling moment L and the yawing moment N equations only. As no longitudinal motion is involved the longitudinal motion variables u, w and q and their derivatives are all zero. Also, decoupled longitudinallateral motion means that the aerodynamic coupling derivatives are negligibly small and may be taken as zero whence

$$\overset{\circ}{Y}_u=\overset{\circ}{Y}_{\dot{w}}=\overset{\circ}{Y}_w=\overset{\circ}{Y}_q=\overset{\circ}{L}_u=\overset{\circ}{L}_{\dot{w}}=\overset{\circ}{L}_w=\overset{\circ}{L}_q=\overset{\circ}{N}_u=\overset{\circ}{N}_{\dot{w}}=\overset{\circ}{N}_w=\overset{\circ}{N}_q= 0 \tag{6.15}$$

Similarly, since the airframe is symmetric, elevator deflection and thrust variation do not usually cause lateraldirectional motion and the coupling aerodynamic control derivatives may also be taken as zero thus

$$\overset{\circ}{Y}_\eta=\overset{\circ}{Y}_\tau=\overset{\circ}{L}_\eta=\overset{\circ}{L}_\tau=\overset{\circ}{N}_\eta=\overset{\circ}{N}_\tau= 0 \tag{6.16}$$

The equations of lateral asymmetric motion are therefore obtained by extracting the side force, rolling moment and yawing moment equations from equations 6.11 and substituting equations 6.15 and 6.16 as appropriate. If it is assumed that the aeroplane is in level flight and the reference axes are wind or stability axes then, as before,$\theta_e = W_e = 0$ and the equations becomes:

$$\begin{cases} m\dot{v}- \overset{\circ}{Y}_v\, v- \overset{\circ}{Y}_p\, p - (\overset{\circ}{Y}_r\, -mU_e)r - mg\phi =\overset{\circ}{Y}_\xi\, \xi+ \overset{\circ}{Y}_\zeta\, \zeta \\ - \overset{\circ}{L}_v\, v + I_x\dot{p}- \overset{\circ}{L}_p\, p - I_{xz}\dot{r}- \overset{\circ}{L}_r\, r =\overset{\circ}{L}_\xi\, \xi+ \overset{\circ}{L}_\zeta\, \zeta \\ - \overset{\circ}{N}_v\, v - I_{xz}\dot{p}- \overset{\circ}{N}_p\, p + I_z\dot{r}- \overset{\circ}{N}_r\, r =\overset{\circ}{N}_\xi\, \xi+ \overset{\circ}{N}_\zeta\, \zeta \end{cases} \tag{6.17}$$

Equations 6.17 represent the simplest possible form of the decoupled lat-

eraldirectional equations of motion.

6.6 Solution of Equation of Motion

The primary reason for solving the equations of motion is to obtain a mathematical, and hence graphical, description of the time histories of all the motion variables in response to a control input, or atmospheric disturbance, and to enable an assessment of stability to be made. It is also important that the chosen method of solution provides good insight into the way in which the physical properties of the airframe influence the nature of the responses. Since the evolution of the development of the equations of motion and their solution followed in the wake of observation of aeroplane behaviour, it was no accident that practical constraints were applied which resulted in the decoupled small perturbation equations. The longitudinal and lateral decoupled equations of motion are each represented by a set of three simultaneous linear differential equations which have traditionally been solved using classical mathematical analysis methods.

Although laborious to apply, the advantage of the traditional approach is that it is capable of providing excellent insight into the nature of aircraft stability and response. However, since the traditional methods of solution invariably involve the use of the dimensionless equations of motion considerable care in the interpretation of the numerical results is required if confusion is to be avoided.

Operational methods have also enjoyed some popularity as a means for solving the equations of motion. In particular, the Laplace transform method has been, and continues to be used extensively. By transforming the differential equations, they become algebraic equations expressed in terms of the Laplace operator s. Their manipulation to obtain a solution then becomes a relatively straightforward exercise in algebra. Thus the problem is transformed into one of solving a set of simultaneous linear algebraic equations, a process that is readily accomplished by computational methods. Further, the inputoutput response relationship or transfer characteristic is described by a simple algebraic transfer function in terms of the Laplace operator. The

time response then follows by finding the inverse Laplace transform of the transfer function for the input of interest.

Now the transfer function as a means for describing the characteristics of a linear dynamic system is the principal tool of the control systems engineer and a vast array of mathematical tools is available for analysing transfer functions.With relative ease, analysis of the transfer function of a system enables a complete picture of its dynamic behaviour to be drawn. In particular, stability, time response and frequency response information is readily obtained.

Furthermore, obtaining the system transfer function is usually the prelude to the design of a feedback control system and an additional array of mathematical tools is also available to support this task. Since most modern aeroplanes are dependent, to a greater or lesser extent, on feedback control for their continued proper operation, it would seem particularly advantageous to be able to describe the aeroplane in terms of transfer functions.

Fortunately this is easily accomplished. The Laplace transform of the linearised small perturbation equations of motion is readily obtained and by the subsequent application of the appropriate mathematical tools the response transfer functions may be derived. An analysis of the dynamic properties of the aeroplane may then be made using control engineering tools as an alternative to the traditional methods of the aerodynamicist.

Thus the process of solution requires that the equations of motion are assembled in the appropriate format, numerical values for the derivatives and other parameters are substituted and then the whole model is input to a suitable computer program. The output, which is usually obtained instantaneously, is most conveniently arranged in terms of response transfer functions.

The remainder of this sectioin is therefore concerned with a discussion of the use of the Laplace transform for solving the small perturbation equations of motion to obtain the response transfer functions. This is followed by a description of the computational process involving matrix methods which is normally undertaken with the aid of a suitable computer software package.

6.7 The Longitudinal Response Transfer Function

The solution of the longitudinal equations of motion by, for example, the methods described in this section enables the response transfer functions to be obtained. These completely describe the linear dynamic response to a control input in the plane of symmetry. Implicit in the response are the dynamic properties determined by the stability characteristics of the aeroplane. The transfer functions and the response variables described by them are linear since the entire modelling process is based on the assumption that the motion is constrained to small disturbances about an equilibrium trim state. However, it is common practice to assume that the response to controls is valid when the magnitude of the response can hardly be described as a small perturbation.

The longitudinal transfer function are:

$$\frac{u(s)}{\eta(s)} \equiv \frac{N_\eta^s(s)}{\Delta(s)} = \frac{k_u(s+1/T_u)(s^2+2\zeta_u\omega_{n_u}s+{\omega_{n_u}}^2)}{(s^2+2\zeta_p\omega_{n_p}s+{\omega_{n_p}}^2)(s^2+2\zeta_s\omega_{n_s}s+{\omega_{n_s}}^2)} \tag{6.18}$$

$$\frac{w(s)}{\eta(s)} \equiv \frac{N_\eta^w(s)}{\Delta(s)} = \frac{k_w(s+1/T_\alpha)(s^2+2\zeta_\alpha\omega_{n_\alpha}s+{\omega_{n_\alpha}}^2)}{(s^2+2\zeta_p\omega_{n_p}s+{\omega_{n_p}}^2)(s^2+2\zeta_s\omega_{n_s}s+{\omega_{n_s}}^2)} \tag{6.19}$$

$$\frac{q(s)}{\eta(s)} \equiv \frac{N_\eta^q(s)}{\Delta(s)} = \frac{k_q s(s+1/T_{\theta_1})(s+1/T_{\theta_2})}{(s^2+2\zeta_p\omega_{n_p}s+{\omega_{n_p}}^2)(s^2+2\zeta_s\omega_{n_s}s+{\omega_{n_s}}^2)} \tag{6.20}$$

$$\frac{\theta(s)}{\eta(s)} \equiv \frac{N_\eta^\theta(s)}{\Delta(s)} = \frac{k_\theta(s+1/T_{\theta_1})(s+1/T_{\theta_2})}{(s^2+2\zeta_p\omega_{n_p}s+{\omega_{n_p}}^2)(s^2+2\zeta_s\omega_{n_s}s+{\omega_{n_s}}^2)} \tag{6.21}$$

As has already been indicated, the common denominator of the transfer functions describes the characteristic polynomial which, in turn, describes the

stability characteristics of the aeroplane. Thus the response of all variables to an elevator input is dominated by the denominator parameters namely, damping ratios and natural frequencies. The differences between the individual responses is entirely determined by their respective numerators. It is therefore important to fully appreciate the role of the numerator in determining response dynamics.

6.7.1 Short Period Mode

The short period mode is typically a damped oscillation in pitch about the oy axis. Whenever an aircraft is disturbed from its pitch equilibrium state the mode is excited and manifests itself as a classical second order oscillation in which the principal variables are incidence $\alpha(w)$, pitch rate q and pitch attitude θ.

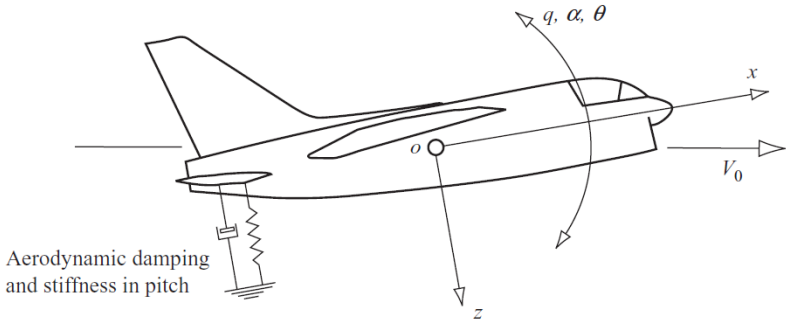

Figure 6.6: Mass Spring Damper

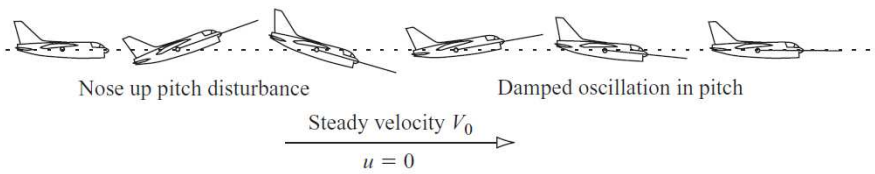

Figure 6.7: Short Period Mode

6.7.2 Phugoid Period Mode

The phugoid mode is most commonly a lightly damped low frequency oscillation in speed u which couples into pitch attitude and height h. A significant feature of this mode is that the incidence $\alpha(w)$ remains substantially constant during a disturbance.

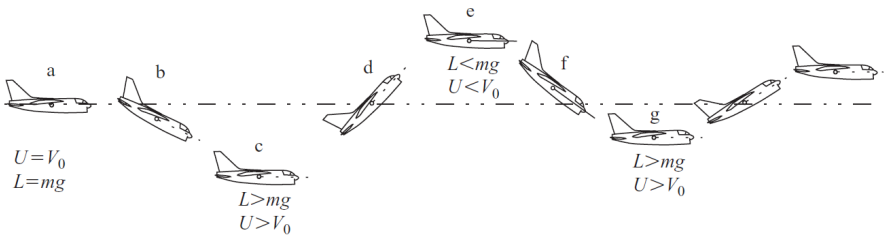

Figure 6.8: Velivolo soggetto a modo fugoide stabile

6.8 Lateral Directional Dynamics

The procedures for investigating and interpreting the lateraldirectional dynamics of an aeroplane are much the same as those used to deal with the longitudinal dynamics and are not repeated at the same level of detail in this section.

As for the longitudinal response transfer functions, it is convenient to adopt a shorthand style of writing the transfer functions. The transfer functions describing response to aileron are conveniently written

$$\frac{v(s)}{\xi(s)} \equiv \frac{N_\xi^v(s)}{\Delta(s)} = \frac{k_v(s+1/T_{\beta 1})(s+1/T_{\beta 2})}{(s+1/T_s)(s+1/T_r)(s^2+2\zeta_d\omega_{n_d}s+{\omega_{n_d}}^2)} \tag{6.22}$$

$$\frac{p(s)}{\xi(s)} \equiv \frac{N_\xi^p(s)}{\Delta(s)} = \frac{k_{ps}(s^2+2\zeta_\phi\omega_{n_\phi}s+{\omega_{n_\phi}}^2)}{(s+1/T_s)(s+1/T_r)(s^2+2\zeta_d\omega_{n_d}s+{\omega_{n_d}}^2)} \tag{6.23}$$

$$\frac{r(s)}{\xi(s)} \equiv \frac{N_\xi^r(s)}{\Delta(s)} = \frac{k_r(s+1/T_\psi)(s^2+2\zeta_\psi\omega_{n_\psi}s+{\omega_{n_\psi}}^2)}{(s+1/T_s)(s+1/T_r)(s^2+2\zeta_d\omega_{n_d}s+{\omega_{n_d}}^2)} \tag{6.24}$$

$$\frac{\phi(s)}{\xi(s)} \equiv \frac{N_\xi^\phi(s)}{\Delta(s)} = \frac{k_\phi(s^2+2\zeta_\phi\omega_{n_\phi}s+{\omega_{n_\phi}}^2)}{(s+1/T_s)(s+1/T_r)(s^2+2\zeta_d\omega_{n_d}s+{\omega_{n_d}}^2)} \tag{6.25}$$

$$\frac{v(s)}{\zeta(s)} \equiv \frac{N_\zeta^v(s)}{\Delta(s)} = \frac{k_v(s+1/T_{\beta1})(s+1/T_{\beta2})(s+1/T_{\beta3})}{(s+1/T_s)(s+1/T_r)(s^2+2\zeta_d\omega_{n_d}s+{\omega_{n_d}}^2)} \tag{6.26}$$

$$\frac{p(s)}{\zeta(s)} \equiv \frac{N_\zeta^p(s)}{\Delta(s)} = \frac{k_p s(s+1/T_{\phi1})(s+1/T_{\phi2})}{(s+1/T_s)(s+1/T_r)(s^2+2\zeta_d\omega_{n_d}s+{\omega_{n_d}}^2)} \tag{6.27}$$

$$\frac{r(s)}{\zeta(s)} \equiv \frac{N_\zeta^r(s)}{\Delta(s)} = \frac{k_r(s+1/T_\psi)(s^2+2\zeta_\psi\omega_{n_\psi}s+{\omega_{n_\psi}}^2)}{(s+1/T_s)(s+1/T_r)(s^2+2\zeta_d\omega_{n_d}s+{\omega_{n_d}}^2)} \tag{6.28}$$

$$\frac{\phi(s)}{\zeta(s)} \equiv \frac{N_\zeta^\phi(s)}{\Delta(s)} = \frac{k_\phi(s+1/T_{\phi1})(s+1/T_{\phi2})}{(s+1/T_s)(s+1/T_r)(s^2+2\zeta_d\omega_{n_d}s+{\omega_{n_d}}^2)} \tag{6.29}$$

As before, the denominator of the transfer functions describes the characteristic polynomial which, in turn, describes the lateral directional stability characteristics of the aeroplane. The transfer function denominator is therefore common to all response transfer functions. Thus the response of all variables to an aileron or to a rudder input is dominated by the denominator parameters namely, time constants, damping ratio and natural frequency. The differences between the individual responses are entirely determined by their respective numerators and the response shapes of the individual variables are determined by the common denominator and coloured by their respective numerators.

6.8.1 The Roll Subsidence Mode

The roll subsidence mode, or simply the roll mode, is a non-oscillatory lateral characteristic which is usually substantially decoupled from the spiral and dutch roll modes. Since it is non-oscillatory it is described by a single real root of the characteristic polynomial, and it manifests itself as an exponential lag characteristic in rolling motion.

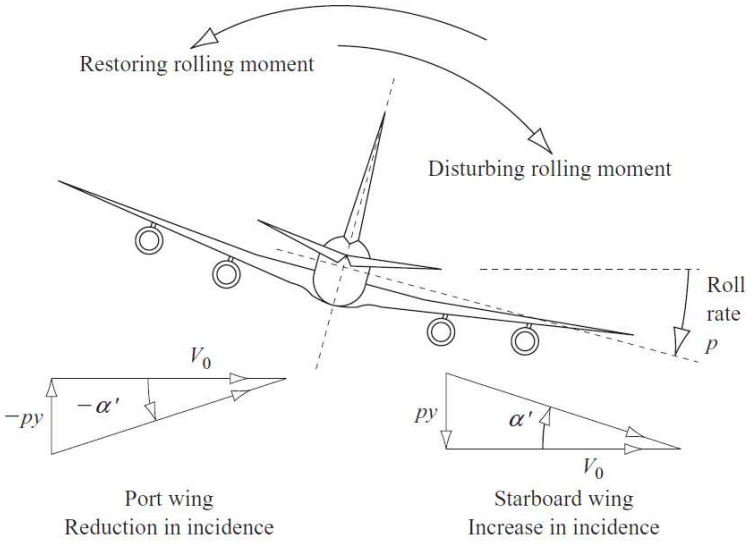

Figure 6.9: Description of the Roll Mode

6.8.2 Spiral Mode

The spiral mode is also non-oscillatory and is determined by the other real root in the characteristic polynomial. When excited, the mode dynamics are usually slow todevelop and involve complex coupled motion in roll, yaw and sideslip.

6.8.3 Dutch Roll Mode

The dutch roll mode is a classical damped oscillation in yaw, about the oz axis of the aircraft, which couples into roll and, to a lesser extent, into

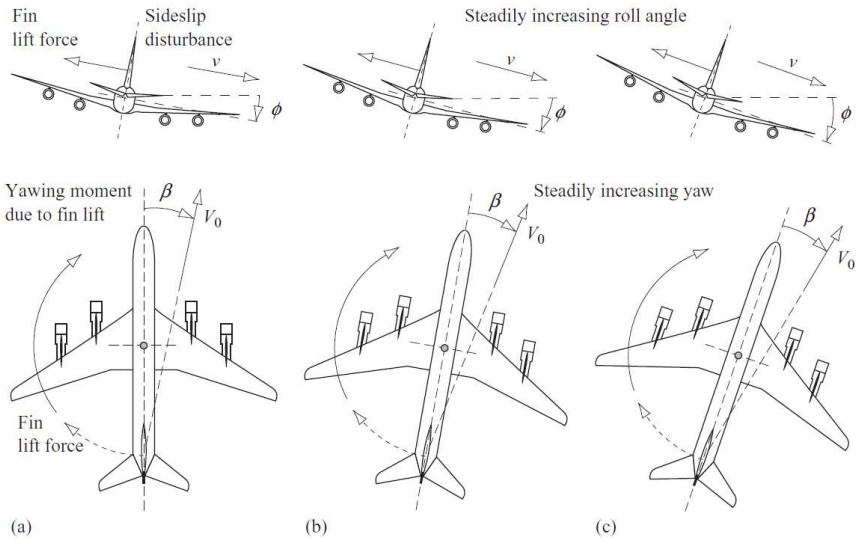

Figure 6.10: Description of the Spiral Mode

sideslip. The motion described by the dutch roll mode is therefore a complex interaction between all three lateraldirectional degrees of freedom. Its characteristics are described by the pair of complex roots in the characteristic polynomial. Fundamentally, the dutch roll mode is the lateraldirectional equivalent of the longitudinal short period mode.

6.9 Analysis of the Pioneer

6.9.1 Transfer Function of the Pioneer

The transfer function of the Pioneer are obtained in the trim condition showed by equation 6.30. This condition was chosen based on the work developed by Bray [5].

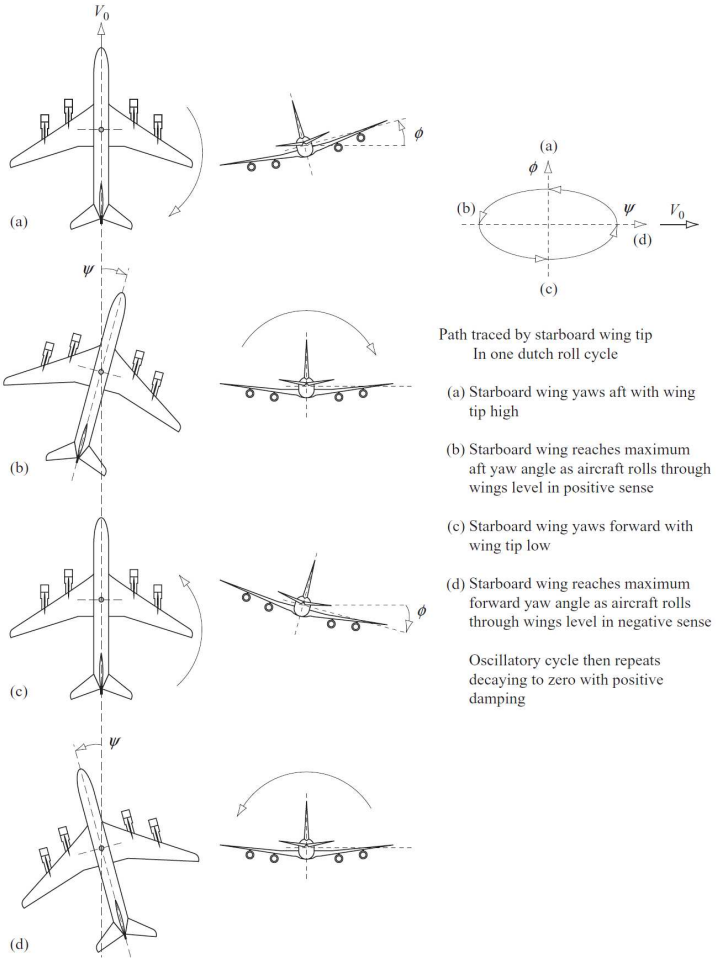

Figure 6.11: Description of the Dutch Roll Mode

$$\begin{cases} h_{trim} = 500\ m \\ V_{trim} = 35\ m/s \\ \alpha_{trim} = 0.0988\ rad \\ \beta_{trim} = -3.15 \cdot 10^{-8}\ rad \\ \theta_{trim} = 0.0988\ rad \\ \phi_{trim} = 1.427 \cdot 10^{-8}\ rad \\ \psi_{trim} = 0\ rad \\ \eta_{trim} = 0.0047\ rad \\ \tau_{trim} = 177.8486\ N \\ \xi_{trim} = 7.4103 \cdot 10^{-9}\ rad \\ \zeta_{trim} = -2.7280 \cdot 10^{-7}\ rad \end{cases} \tag{6.30}$$

Following the procedure explained in the precedent sections the longitudinal transfer function of the Pioneer are:

$$\frac{V(s)}{\eta(s)} = \frac{-0.14441(s+29.24)(s-22.66)(s+3.016)}{(s^2+0.04138s+0.1308)(s^2+4.998s+30.67)}\ \frac{m/s}{rad} \tag{6.31}$$

$$\frac{\alpha(s)}{\eta(s)} = \frac{-0.12446(s+176.6)(s^2+0.05184s+0.1546)}{(s^2+0.04138s+0.1308)(s^2+4.998s+30.67)}\ \frac{rad}{rad} \tag{6.32}$$

$$\frac{q(s)}{\eta(s)} = \frac{-21.9706s(s+1.271)(s+0.1247)}{(s^2+0.04138s+0.1308)(s^2+4.998s+30.67)}\ \frac{rad/s}{rad} \tag{6.33}$$

$$\frac{\theta(s)}{\eta(s)} = \frac{-21.9706(s+1.271)(s+0.1247)}{(s^2+0.04138s+0.1308)(s^2+4.998s+30.67)}\ \frac{rad}{rad} \tag{6.34}$$

$$\frac{h(s)}{\eta(s)} = \frac{4.3563(s+15.48)(s-15.32)(s+0.002931)}{s(s^2+0.04138s+0.1308)(s^2+4.998s+30.67)}\ \frac{m}{rad} \tag{6.35}$$

$$\frac{V(s)}{\tau(s)} = \frac{0.0052234(s - 0.02338)(s^2 + 4.995s + 30.72)}{(s^2 + 0.04138s + 0.1308)(s^2 + 4.998s + 30.67)} \frac{m/s}{N} \tag{6.36}$$

$$\frac{\alpha(s)}{\tau(s)} = \frac{-1.4788 \cdot 10^{-5}(s + 5.639)(s + 3.496)(s + 2.032 \cdot 10^{-7})}{(s^2 + 0.04138s + 0.1308)(s^2 + 4.998s + 30.67)} \frac{rad}{N} \tag{6.37}$$

$$\frac{q(s)}{\tau(s)} = \frac{0.00038371s(s + 5.639)}{(s^2 + 0.04138s + 0.1308)(s^2 + 4.998s + 30.67)} \frac{rad/s}{N} \tag{6.38}$$

$$\frac{\theta(s)}{\tau(s)} = \frac{0.00038371(s + 5.639)}{(s^2 + 0.04138s + 0.1308)(s^2 + 4.998s + 30.67)} \frac{rad}{N} \tag{6.39}$$

$$\frac{h(s)}{\tau(s)} = \frac{0.00051759(s + 5.639)(s^2 + 3.496s + 25.95)}{s(s^2 + 0.04138s + 0.1308)(s^2 + 4.998s + 30.67)} \frac{m}{N} \tag{6.40}$$

The lateral directional dynamics are:

$$\frac{\beta(s)}{\xi(s)} = \frac{6.4212(s + 8.161)(s + 0.2477)}{(s + 7.139)(s - 0.1297)(s^2 + 2.153s + 16.59)} \frac{rad}{rad} \tag{6.41}$$

$$\frac{p(s)}{\xi(s)} = \frac{39.7152(s - 0.02712)(s^2 + 1.495s + 14.21)}{(s + 7.139)(s - 0.1297)(s^2 + 2.153s + 16.59)} \frac{rad/s}{rad} \tag{6.42}$$

$$\frac{r(s)}{\xi(s)} = \frac{-2.5172(s + 16.3)(s - 2.454)(s + 1.533)}{(s + 7.139)(s - 0.1297)(s^2 + 2.153s + 16.59)} \frac{rad/s}{rad} \tag{6.43}$$

$$\frac{\phi(s)}{\xi(s)} = \frac{39.4658(s^2 + 1.38s + 14.38)}{(s + 7.139)(s - 0.1297)(s^2 + 2.153s + 16.59)} \frac{rad}{rad} \tag{6.44}$$

$$\frac{\psi(s)}{\xi(s)} = \frac{-2.5172(s + 16.3)(s - 2.454)(s + 1.533)}{s(s + 7.139)(s - 0.1297)(s^2 + 2.153s + 16.59)} \frac{rad}{rad} \tag{6.45}$$

$$\frac{\beta(s)}{\zeta(s)} = \frac{0.040515(s + 270.2)(s + 7.24)(s - 0.1615)}{(s + 7.139)(s - 0.1297)(s^2 + 2.153s + 16.59)} \frac{rad}{rad} \tag{6.46}$$

$$\frac{p(s)}{\zeta(s)} = \frac{3.4117(s - 12.62)(s + 1.553)(s - 0.02493)}{(s + 7.139)(s - 0.1297)(s^2 + 2.153s + 16.59)} \frac{rad/s}{rad} \tag{6.47}$$

$$\frac{r(s)}{\zeta(s)} = \frac{-10.5877(s + 7.548)(s^2 + 0.1869s + 0.2105))}{(s + 7.139)(s - 0.1297)(s^2 + 2.153s + 16.59)} \frac{rad/s}{rad} \tag{6.48}$$

$$\frac{\phi(s)}{\zeta(s)} = \frac{2.3626(s - 20.83)(s + 1.375)}{(s + 7.139)(s - 0.1297)(s^2 + 2.153s + 16.59)} \frac{rad}{rad} \tag{6.49}$$

$$\frac{\psi(s)}{\zeta(s)} = \frac{-10.6395(s + 7.548)(s^2 + 0.1869s + 0.2105)}{s(s + 7.139)(s - 0.1297)(s^2 + 2.153s + 16.59)} \frac{rad}{rad} \tag{6.50}$$

6.9.2 Longitudinal Mode

The charateristacal polyniomial of the longitudinal transfer function of the Pioneer in the trim condition expressed before is:

$$(s^2 + 0.04138s + 0.1308)(s^2 + 4.998s + 30.67) \tag{6.51}$$

The phugod mode is descripted by the subsequent natural frequency and

damping ratio

$$\begin{cases} 2\zeta_1\omega_{n_1} = 0.04138 \\ {\omega_{n_1}}^2 = 0.1308 \end{cases} \rightarrow \begin{cases} \omega_{n_1} \approx 0.362\ rad/s \\ \zeta_1 \approx 0.0572 \end{cases}$$

while the short period presents

$$\begin{cases} 2\zeta_2\omega_{n_2} = 4.998 \\ {\omega_{n_2}}^2 = 30.67 \end{cases} \rightarrow \begin{cases} \omega_{n_2} \approx 5.54\ rad/s \\ \zeta_2 \approx 0.451 \end{cases}$$

The figure 6.12 shows the poles in the phase plain.

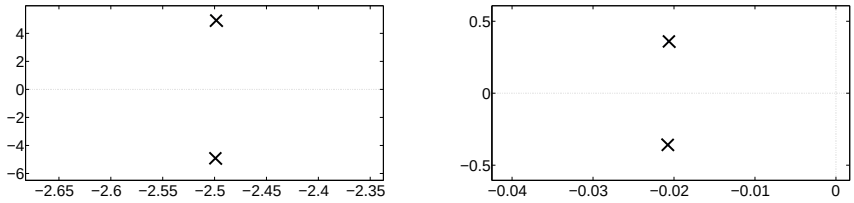

(a) Short Period Poles (b) Phugoid Poles

Figure 6.12: Poles of the Longitudinal Transfer Functions

In the time domain it results:

$$\begin{cases} \omega_p \approx 0.361\ rad/s \\ T_p \approx 17.4\ s \\ T_{a_p} \approx 145\ s \end{cases} \tag{6.52}$$

$$\begin{cases} \omega_s \approx 4.94\ rad/s \\ T_s \approx 1.27\ s \\ T_{a_s} \approx 1.20\ s \end{cases} \tag{6.53}$$

6.9.3 Lateral Directional Mode

As in the precedent section, the charateristacal polyniomial of the lateral transfer function of the Pioneer in the trim condition expressed before is:

$$(s + 7.139)(s - 0.1297)(s^2 + 2.153s + 16.59) \tag{6.54}$$

The first value indicated in 6.55 the roll mode while the second represents the spiral:

$$\begin{cases} \tau_1 = \frac{1}{7.139} \approx 0.140\ s \\ \tau_2 = \frac{1}{-0.1297} \approx -7.71\ s \end{cases} \tag{6.55}$$

For the dutch roll model it results:

$$\begin{cases} 2\zeta_d\omega_{n_d} = 2.153 \\ {\omega_{n_1}}^2 = 16.59 \end{cases} \rightarrow \begin{cases} \omega_{n_d} \approx 4.07\ rad/s \\ \zeta_d \approx 0.264 \end{cases}$$

In the next figure it can be seen the position of the poles in the phase plane:

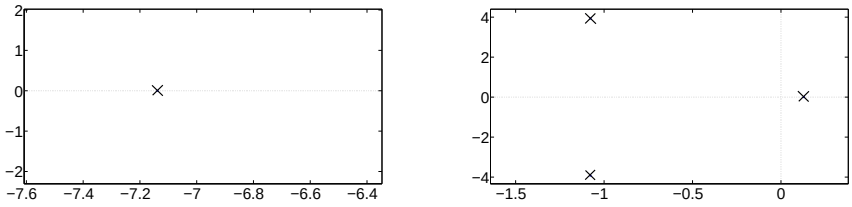

(a) Roll Mode Pole (b) Dutch-Roll and Spiral Poles

Figure 6.13: Poles in the phase plane

In the time domain it results:

$$\begin{cases} \omega_d \approx 3.93\ rad/s \\ T_d \approx 1.60\ s \\ T_{a_d} \approx 2.79\ s \end{cases} \tag{6.56}$$

6.9.4 Static Stability of the Pioneer

The static stability of an aircraft is commonly interpreted to describe its tendency to converge on the initial equilibrium condition following a small

disturbance from trim. Dynamic stability, on the other hand, describes the transient motion involved in the process of recovering equilibrium following the disturbance. Figure 6.14 includes two illustrations showing the effects of static stability and static instability in an otherwise dynamically stable aircraft. Following an initial disturbance displacement, for example in pitch, at time $t = 0$ the subsequent response time history is shown and is clearly dependent on the stability of the aircraft.

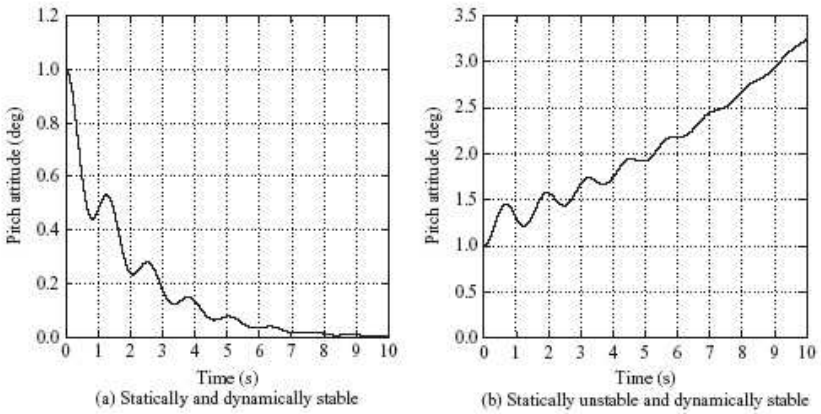

Figure 6.14: Statically Stable and Unstable examples

It should be noted that the damping of the dynamic oscillatory component of the responses shownwas deliberately chosen to be low in order to best illustrate the static and dynamic stability characteristics. In establishing trim equilibrium the pilot adjusts the elevator angle and thrust to obtain a lift force sufficient to support the weight and thrust sufficient to balance the drag at the desired speed and flight path angle. Since the airframe is symmetric the equilibrium side force is of course zero. Provided that the speed is above the minimum drag speed then the force balance will remain

stable with speed. Therefore, the static stability of the aircraft reduces to a consideration of the effects of angular disturbances about the three axes. Following such a disturbance the aerodynamic forces and moments will no longer be in equilibrium, and in a statically stable aircraft the resultant moments will cause the aircraft to converge on its initial condition. The condition for an aircraft to be statically stable is therefore easily deduced.

Consider a positive pitch, or incidence, disturbance from equilibrium. This is in the nose up sense and results in an increase in incidence α and hence in lift coefficient C_L. In a stable aircraft the resulting pitching moment must be restoring, that is, in the negative or nose down sense. And of course the converse must be true following a nose down disturbance. Thus the condition for longitudinal static stability may be determined by plotting pitching moment M, or pitching moment coefficient C_m, for variation in incidence α about the trim value α_e as shown in figure 6.15. The nose up disturbance increases α and takes the aircraft to the out-of-trim point p where the pitching moment coefficient becomes negative and is therefore restoring. Clearly, a nose down disturbance leads to the same conclusion. As indicated, the aircraft is stable when the slope of this plot is negative. Thus, the condition for stable trim at incidence α_e may be expressed:

$$C_{m\alpha} = \frac{dC_m}{d\alpha} < 0 \tag{6.57}$$

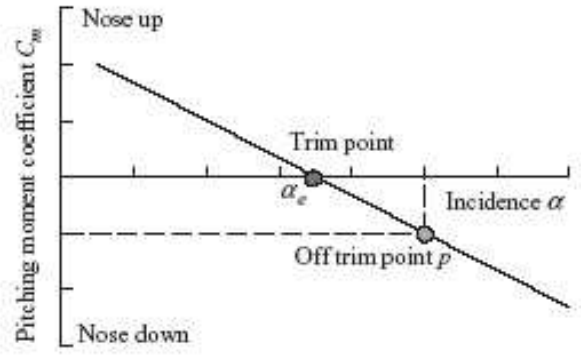

Figure 6.15: Pitching Moment Variation with Incidence for a Stable Aircfraft

In a similar way the conditions for lateraldirectional static stability may

be deduced as

$$\begin{cases} C_{n\beta} = \frac{dC_n}{d\beta} < 0 \\ C_{l\beta} = \frac{dC_l}{d\beta} < 0 \end{cases} \tag{6.58}$$

where C_l and C_n are rolling moment and yawing moment coefficients respectively and ϕ and β are roll angle and sideslip angle respectively.

The stability derivatives of the Pioneer are obtained in the same linearized condition descripted in the precedent subsection and result:

Pitching Stiffness	C_{m_α}	-2.12
Yaw Stiffness	$C_{n\beta}$	0.153
Diedral Effect	$C_{l\beta}$	-0.0230

Table 6.3: Stability Derivatives

The Pioneer is yaw unstable.

This page is intentionally left blank.

Chapter 7

Stability Augmentation System

Stability augmentation systems makes the aircraft more stable. There are SASs for both the dynamic stability (whether the eigenmotions don not diverge) and the static stability (whether the equilibrium position itself is stable). This work has been inspired by the work of Roskam (see [33] and [32])

7.1 Yaw Damper

When an aircraft has a low speed at a high altitude, the Dutch roll properties of the aircraft deteriorate. To prevent this, a yaw damper is used. An overview of this system can be seen in figure 7.1 ($G_R(s)$ is the yaw damper gain and amplifier; $G_\zeta(s)$ is the rudder servo transfer function). The transfer function of the rate gyro $G_H(s)$ has been chosen equal to 1.

The yaw damper gets its input (feedback) from the yaw rate gyro. It then sends a signal to the rudder servo. The rudder is then moved in such a way that the Dutch roll is damped much more quickly than usual. As a designer, it is possible only to influence the yaw damper. However, it is necessary to know how the other systems work as well. For this reason, all the other systems are modelled. Usually it is assumed that the model of the aircraft is known in order to examine only the other systems.

Based on the equation 6.48 considering a $G_\zeta(s) = \frac{20}{20+s}$ as the transfer function of the servo, the gain of $G_R(s)$ has be chosen equal to -1.7.

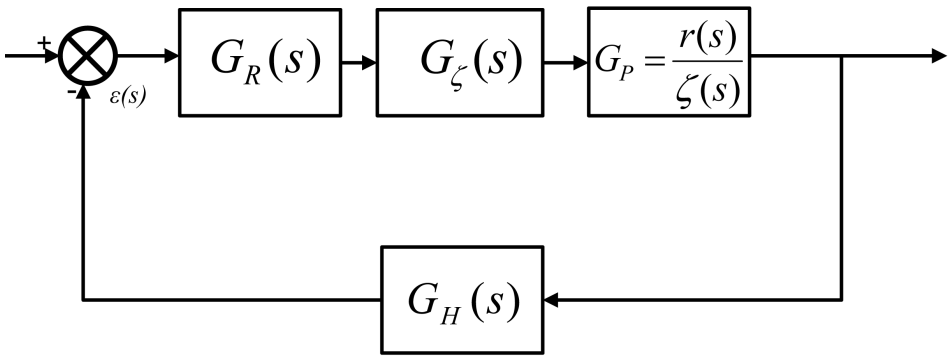

Figure 7.1: Block Diagram fo a Yaw Damper

7.2 Pitch Damper

When an aircraft flies at a low speed and a high altitude, the short period eigenmotion has a low damping. To compensate for this, a pitch damper is used. The pitch damper is in many ways similar to the yaw damper. Also the set-up is similar. Only this time, the elevators and a pitch rate gyro are used, instead of the rudder and a yaw rate gyro.

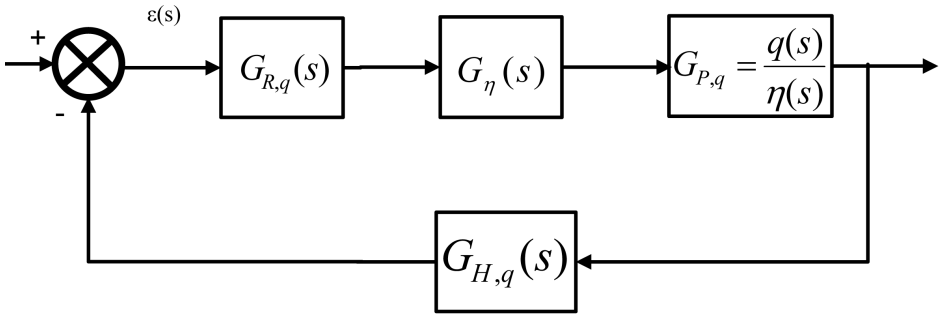

Figure 7.2: Block Diagram fo a Pitch Damper

Observing figure 7.2, the transfer function $G_{P,q}$ is defined in equation 6.33. The servo transfer function $G_\eta(s)$ is, as the yaw damper, equal to $\frac{20}{20+s}$ while the transfer function of the rate gyro $G_{H,q}$ has been considered equal to 1.

After a linear analysis and the well-known design procedure the gain $G_{R,q}$ has been chosen equal to -0.22.

7.3 Basic Longitudinal Autopilot System

7.3.1 Pitch Attitude Hold Mode

The pitch attitude hold mode prevents pilots from constantly having to control the pitch attitude. Especially in turbulent air, this can get tiring for the pilot. This system uses the data from the vertical gyroscope as input (feedback). It then controls the aircraft through the elevators. To be more precise, it sends a signal to the SAS, which then again uses this as a reference signal to control the servo. An overview of the system can be seen in figure 7.3. The transfer function of the servo is modelled as for the pitch damper. In this figure $G_{tot,q}(s)$ is the transfer function of the pitch damper while $G_{p,\gamma}$ can be easily derived from equation 6.34. The transfer equation of the pitch attitude gyro $G_{H,\gamma}(s)$ has been set equal to one.

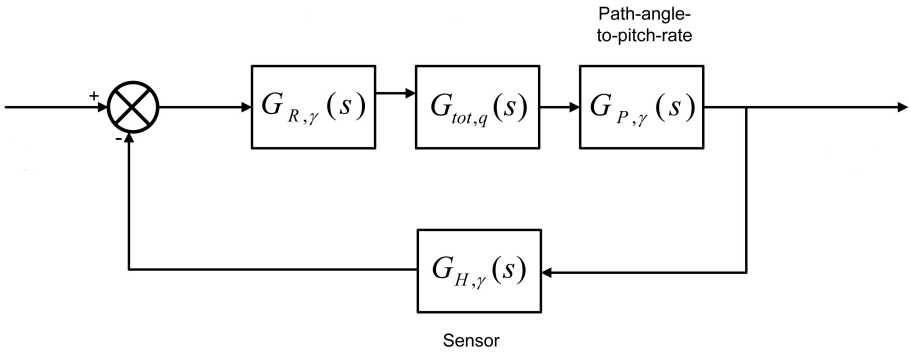

Figure 7.3: Block Diagram for the Pitch Attitude

There is also the reference pitch angle θ that needs to be set. This is done when the pitch attitude hold mode is activated. In fact, the hold mode usually tries to keep the current pitch angle. The reference pitch angle θ is thus the pitch angle that was present at the moment that the hold mode was activated. Finally, it is necessary to design the pitch controller block. It usually consists of a proportional, an integral and a derivative action: the right gains K_p, K_I and K_D must be chosen. It can happen that, with the new gains, the damping ratio of (for example) the short period motion has shifted a bit. If it falls outside of the requirements, the SAS of the aircraft

needs to be adjusted. This is not a problem in the case of an UAV.

The trasnfer function of the regularor $G_{R,\gamma}(s)$ is equal only to a gain $K_p = -3.5$.

7.3.2 Altitude Hold Mode

The altitude hold mode prevents pilots from constantly having to maintain their altitude. The input (feedback) comes from the altimeter. The system then uses the elevator to control the altitude. The way in which the altimeter is modelled depends on the type of altimeter. For a radar or GPS altimeter, it is used $H_{altimeter} \approx 1$. However, for a barometric altimeter, it is possible to include a lag. The servo trasnfer function is always considered as in the precedent cases.

The reference value of the height h is set in the mode control panel. To control h, we must have some expression for h in our aircraft model. But h is not one of the parameters in the basic state space model of the aircraft. So, we need to derive an expression for it. This is done, using $\dot{h} = V \sin\gamma \approx V\gamma$. The altitude hold mode also consists of a proportional, an integral and a derivative action. However, often it turns out that an integral action is not necessary. And since generally it is necessary to keep controllers as simple as possible, it can be simply a P_D controller.

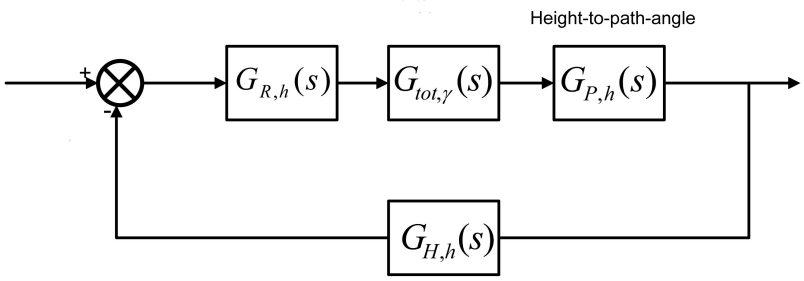

Figure 7.4: Block Diagram for the Altitude Hold Mode

In figure 7.4 the transfer function $G_{tot,\gamma}(s)$ represents the pitch attitude autopilot designed while $G_{p,h}$ is the transfer function 6.35. As in the prece-

dent cases the transfer function of the sensor $G_{H,h}(s)$ is not considered. In this case the regulator $G_{R,h}(s)$ is equal to a proportional gain $K_p = 0.005$.

A clearly scheme which includes all the longitudinal basic autopilots is depicted in figure 7.5.

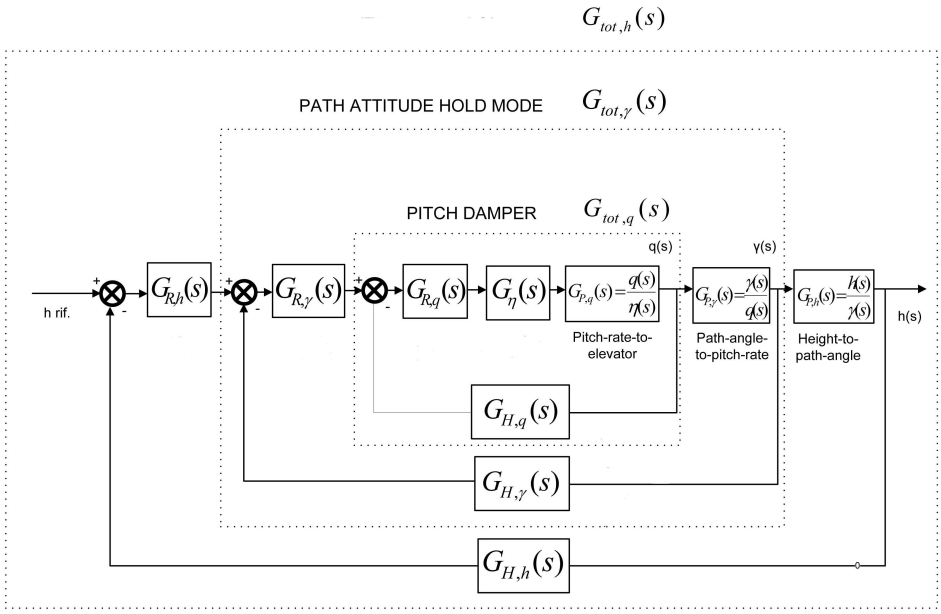

Figure 7.5: Block Diagram for the Complete Autopilot System

7.3.3 Speed Hold Mode

The airspeed hold mode holds a certain airspeed. It uses the airspeed sensor as input and it controls the throttle. Of course, the airspeed sensor should be modelled. For GPS airspeed calculations, it is possible to use $H_{V-sensor}(s) \approx 1$. However it is supposed to be equal to one. The engine servo has been modelled with a lag of $\tau = 20$ while the engine with a $\tau = 1$ (due to lack of experimental data). Taking the engine model into account might seem complicated. Luckily, there is an alternative. It is possible to include the engine effects in the state space model and consequently it is possible to add a term $K_{th}\delta_T$ to the equation for $\dot{u}$. This term then represents the thrust, due to the throttle setting. In this way it is necessary to model only the servo. The reference value of the velocity V is often set at the mode control panel.

Alternatively, it can be derived from the actions of the pilot. For example, if the pilot manually pushes the throttle forward, the computer increases the desired (reference) velocity V. The $G_P(s)$ transfer function is described by equation 6.36.

The diagram block is showed in figure 7.6

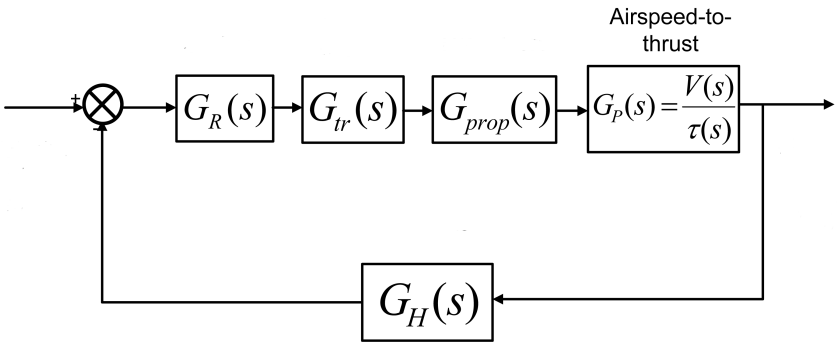

Figure 7.6: Block Diagram for the Speed Hold Mode

For this control the proportional gain $K_p = 100$.

7.4 Basic Lateral Autopilot System

7.4.1 The roll angle hold mode

The roll angle hold mode prevents the pilot from constantly having to adjust/control the roll angle during a turn. It uses the roll angle gyro as sensor and it effects the ailerons. The roll angle gyro and the aileron servo are again modelled as $H_{gyro}(s) \approx 1$ and $H_{servo}(s) = \frac{20}{s+20}$.The roll angle that is used as reference angle is defined on the mode control panel. When modelling the aircraft, it is often assumed that rolling is the only degree of freedom. This reduced model significantly simplifies matters. In fact, the transfer function between $\phi(s)$ and $\delta_a(s)$ is descripted in equation 6.44.

Nevertheless, it is often worth while to check whether the behaviour of the full model (without the simplifications) is much different from that of the reduced model. It can, for instance, occur that the Dutch roll becomes

unstable in the full model, whereas the reduced model does not indicate this. The block diagram presented in figure 7.7 explains this loop.

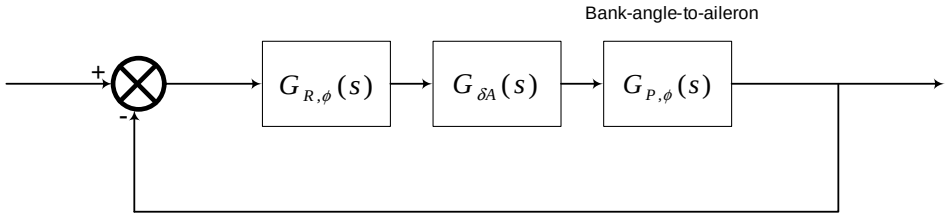

Figure 7.7: Block Diagram for the Roll Angle Hold Mode

The regulator of the roll angle has been set $K_p = 0.25$.

7.4.2 Heading Angle Control Mode

The heading angle control mode controls the heading. It does this by giving the aircraft a roll angle. In fact, it sends a signal to the (coordinated) roll angle hold mode, telling it which roll angle the aircraft should have. This roll angle is maintained until the desired heading is achieved. As sensor, this system uses the directional gyro, modelled as $H_{gyro}(s) \approx 1$. Its output effects the ailerons. (The latter is evident, since the system controls the roll angle hold mode).

The reference angle ψ is defined by the pilot, through the mode control panel. There is, however, a problem. In the aircraft model, it is not always possible to have ψ as one of the state parameters. To find it, it is possible to use the equation: $\dot{\psi} = q\frac{\sin\phi}{\cos\theta} + r\frac{\cos\phi}{\cos\theta}$.

This can be simplified assuming $q = 0$ and $\theta = cost.$ Besides, ϕ is considered a small angle and it results: $\dot{\psi} = \frac{r}{\cos\theta}$ or $\psi = \frac{r}{s\cos\theta}$.

The transfer function is 6.45. The block diagram presented in figure 7.8 all the scheme of the lateral autopilot.

The gain K_p of this loop has been set equal to 0.8.

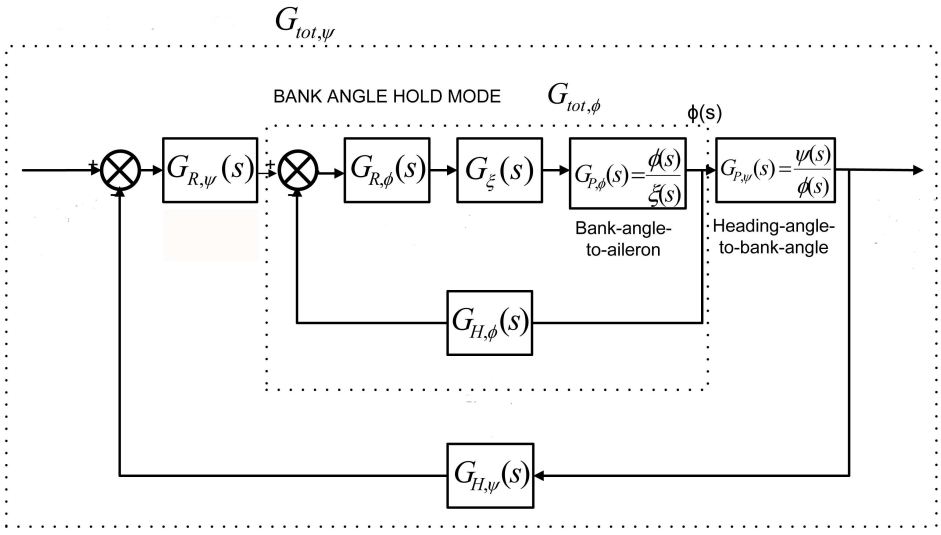

Figure 7.8: Block Diagram for the Heading Angle Hold Mode

7.5 Simulation on the 6DoF Software Simulator

The guidance laws presented in chapter 3 and 5 are simulated on a software simulator of the Pioneer.

The guidance law created with the Lyapunov vector field technique is not presented because, as it will be shown later, the guidance law created through the oscillatory control is able to create a Lemniscate when the target is fixed. Considering that this thesis is focused on different approaches to follow a ground moving target, it is more convenient to present the results of the oscillatory control than the Lyapunov vector field.

However it must be considered that, only through the application of the vector field to the Lemniscate, it has been possible to derive the oscillation control solution. Besides, if the position of the target is sampled every T period, a Lemniscate vector field could be created (this solution is still under research).

The equation of motion described at the beginnig of this section are easily implemented on the Matlab Simulink software. One of the most important thing is that all the aerodynamic coefficents derived from [5] are reproduced

inside the simulator through the use of different look-up tables (see figures 7.9 and 7.10).

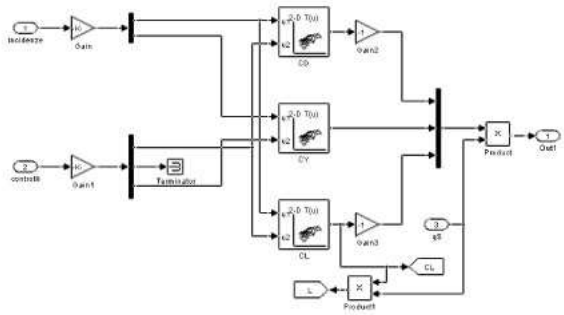

Figure 7.9: Look-up table for the forces

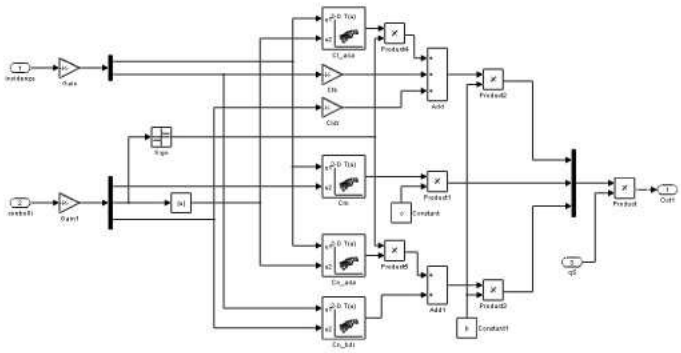

Figure 7.10: Look-up table for the moment

The UAV is supposed to be equipped with a standard autopilot performing typical autopilots mode: altitude hold, heading angle hold, yaw damping and speed hold mode. These autopilots have been descripted in the precedent section.The cruise speed of the Pioneer is $35[m/s]$ at an altitude of $500[m]$.

A comparison between the nonlinear guidance law and the oscillatory approach is made in order to appreciate the different trajectories.

In this section two different paths are supposed for the target:

1. Target along a straigh line with a different velocity profile (see figure 7.11)

2. Target with a constant velocity along a slightly bend

Case 1

The target velocity profile chosen for both the guidance laws is depicted in figure 7.11 where it can be also derived that the simulation lasts 2000[s].

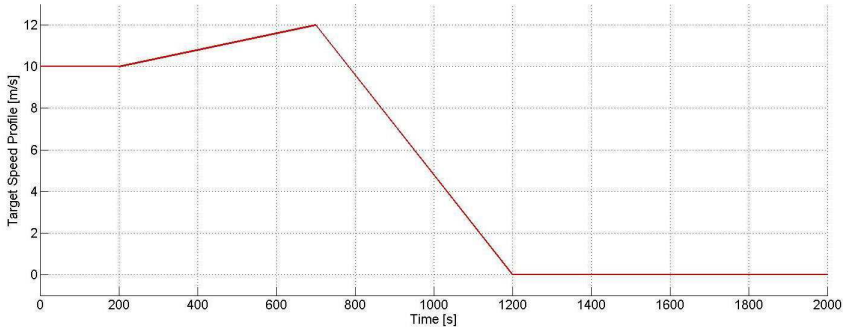

Figure 7.11: Target velocity profile Case 1

Nonlinear Guidance Law

In figure 7.12 the trajectory created by the nonlinear guidance law is depicted: the distance remains around the fixed value of 500[m]. Even if the error on the radious desired $e = R - R_D$ is not equal to zero, the UAV remains around the target. In particular, when the target stops its movement, the UAV starts a circle loitering circuit ensuring a continuos live sensing. Figure 7.13 shows that, through the altitude hold autopilot designed, the UAV is able to mantain the desired altitude. The oscillations around the desired value are due to the continuos turns given by the guidance laws. However figure 7.14, shows that the roll angle and the pitch angle are limited and acceptable for an UAV.

Oscillatory Control

The results of the oscillatory control (with the gain $K_1 = 40$) are represented in the subsequent figures (7.15, 7.16 and 7.17). The trim frequency ω_0 is set to 0.01. This choice influences the amplitude of the oscillation around

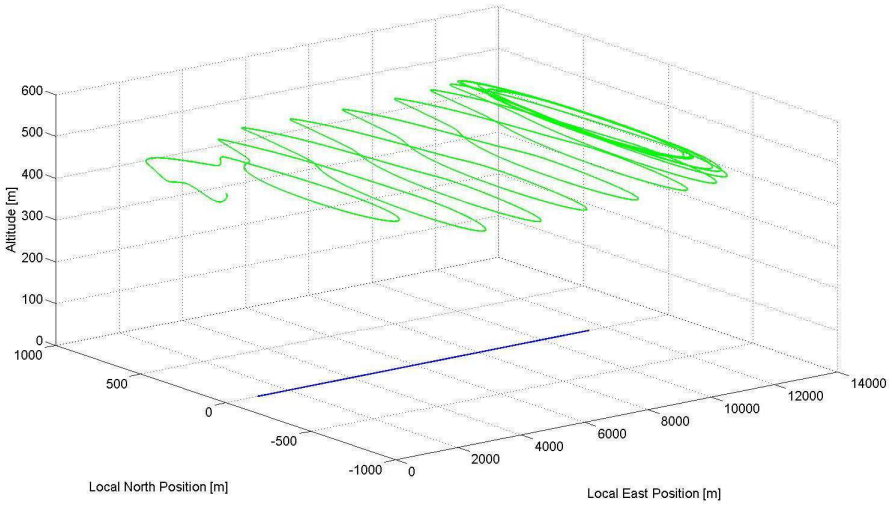

Figure 7.12: 3D positions with Oscillatory Control

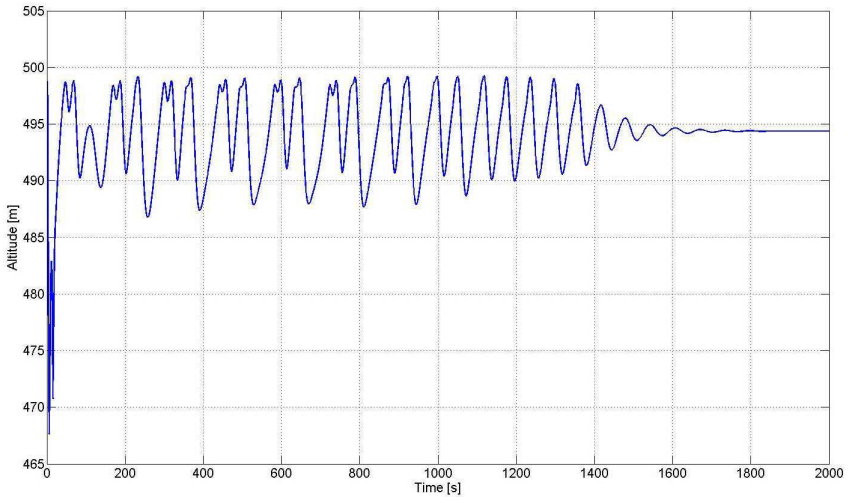

Figure 7.13: Altitude with Oscillatory Control

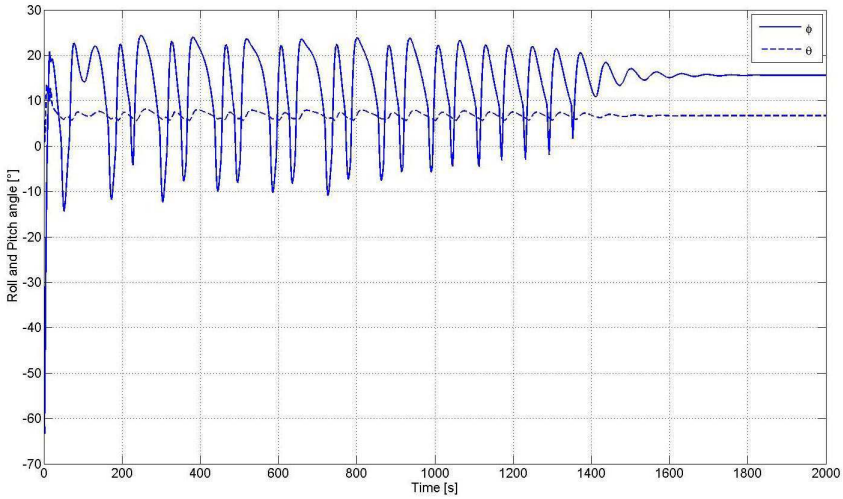

Figure 7.14: Attitude with Oscillatory Control Case 1

the target.As it can be seen the roll angle ϕ and the pitch angle θ have respectively: the former a maximum value around 20$[deg]$, the latter remains constant for almost all the simulation (figure 7.17).

The altitude plot (see figure 7.16) shows a small oscillation around the fixed trim value of 500 [m]. This is simply due to the turns that the UAV performs during the tracking: in fact the speed hold mode maintains the prescribed value of 35$[m/s]$ but this value is the trim value for a steady flight. During a turn the lift force decreases and an increment of thrust should be applied for holding a constant height value.

Case 2

The target velocity profile is considered at a constant value of 10$[m/s]$. The simulation lasts 2000$[s]$ as in the precedent case.

Nonlinear Guidance Law

All the considerations written for the Case 1 can be repeated here, where the target performs a curve path (see figures: 7.18, 7.19 and 7.20).

Oscillatory Control

The oscillatory control, as it can be seen in figure 7.21, shows an os-

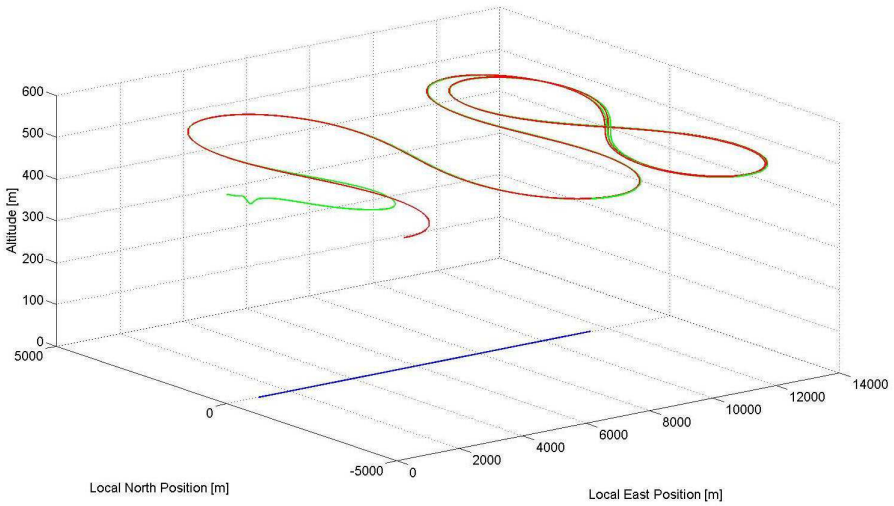

Figure 7.15: 3D positions with Oscillatory Control

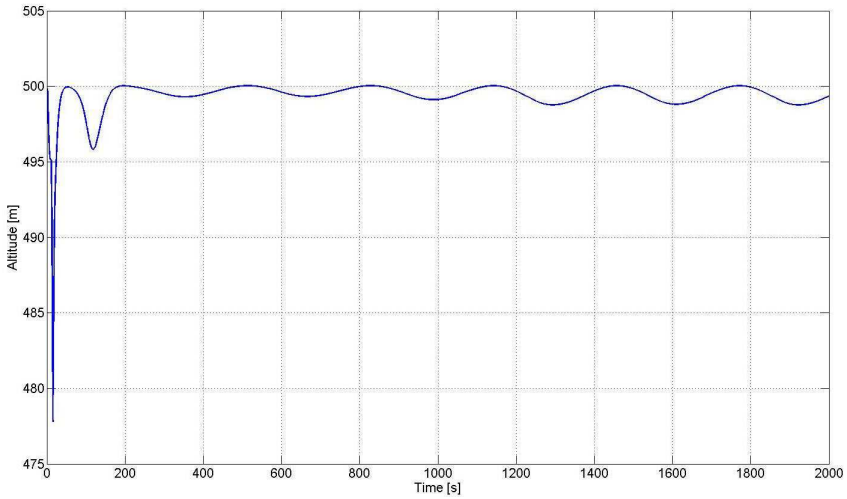

Figure 7.16: Altitude with Oscillatory Control

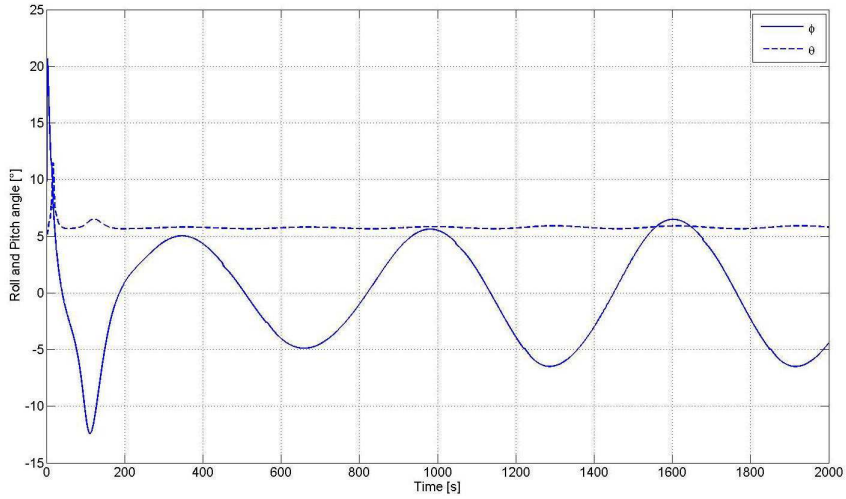

Figure 7.17: Attitude with Oscillatory Control Case 1

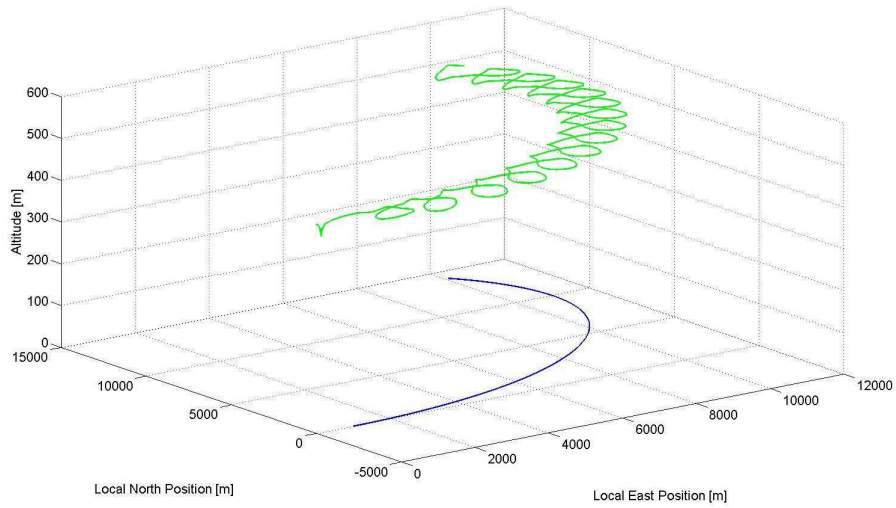

Figure 7.18: 3D positions with Oscillatory Control Case 2

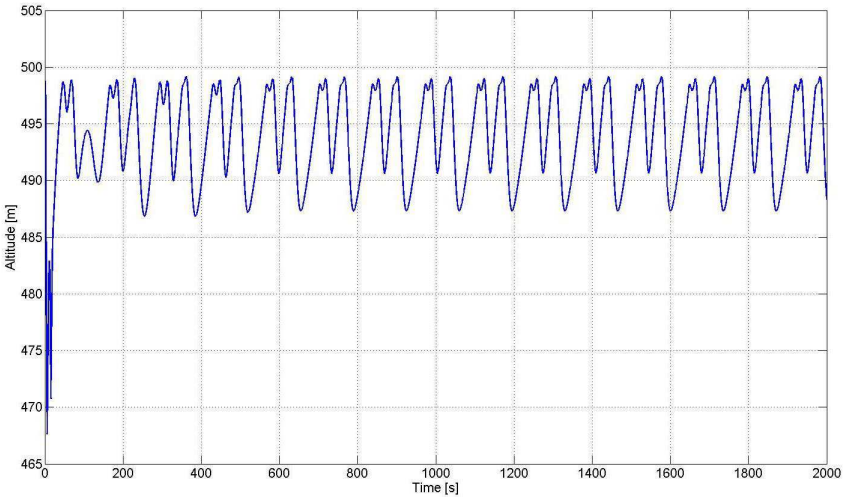

Figure 7.19: Altitude with Oscillatory Control Case 2

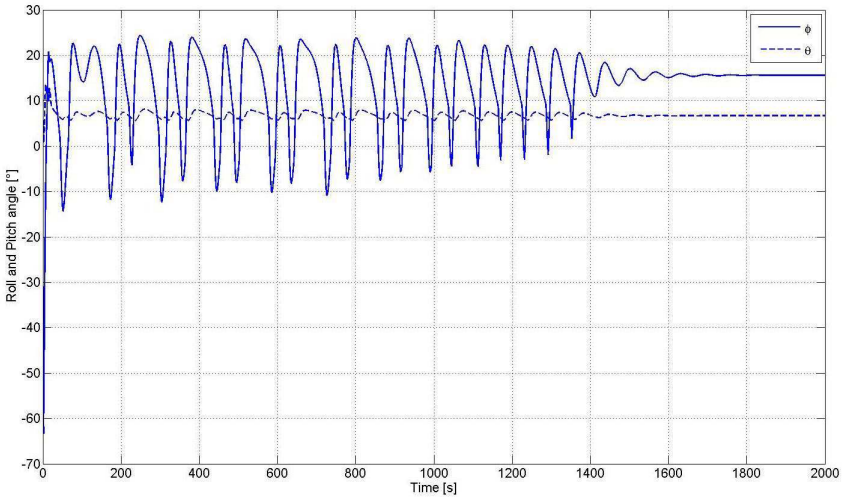

Figure 7.20: Attitude with Oscillatory Control Case 2

cillation trajectory around the positions of the target and the Lemniscate trajectory once the target stops. All the considerations on the attitude angle and altitude can be repeated as in the precedent case.

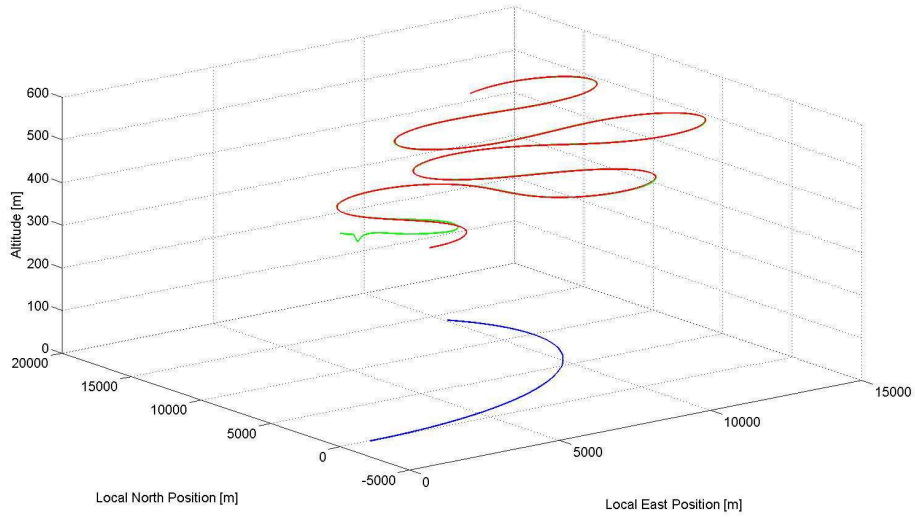

Figure 7.21: 3D positions with Oscillatory Control Case 2

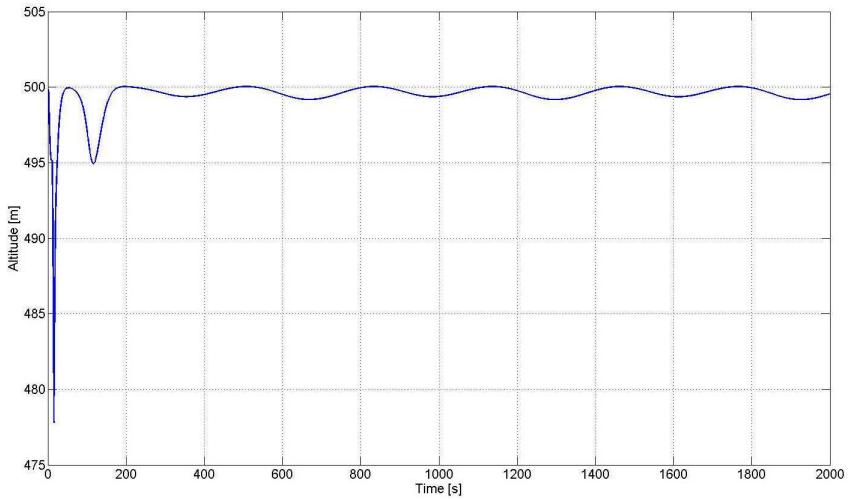

Figure 7.22: Altitude with Oscillatory Control Case 2

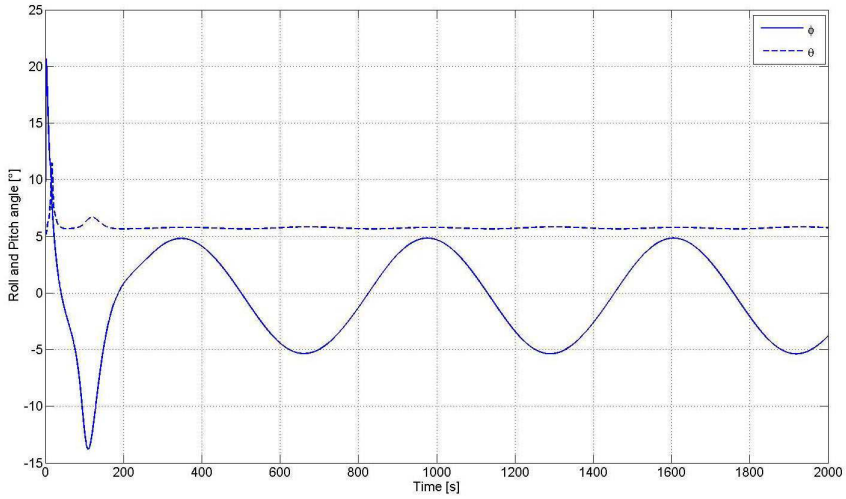

Figure 7.23: Attitude with Oscillatory Control Case 2

This page is intentionally left blank.

Chapter 8

Conclusion

The problem of tracking a moving or fixed ground target with an UAV has different solutions. In particular, the constraints of a fixed airspeed and minimum normal accelleration avoid different nonlinear technique used in robotics application. Besides, the effect of the wind makes some other guidance laws adopted for the unicycle, useless.

In this thesis, different novel approaches are proposed not only for following a ground moving target but also for monitoring it when the target stops. In chapter 3, a wind robust guidance law able to guide the UAV towards the target and, once reached, to ensure a circular loiter path around the follower is preseted. Further investigations must be carried out in order to make the final error between the circle reached and the desired one equal to zero.

In chapter 4 a novel application of the known Lyapunov vector field technique is proposed. The chance to overfly the target more than one time, as it is with the nonlinear guidance law of chapter 3, could be very useful. Besides, the lemniscate figure ensures a maximum visibility of the target which is considered in the middle of the figure. The vector fields presents a fail safe towards wind effect.

The impossibility to use the guidance law proposed with the Lyapunov vector fields when the target is moving, has created the oscillator control approach presented in chapter 5. The use of a center of oscillation moving around the positions of the target, together with a particular guidance law presented in section 2.3 ensures a particular pursuit of the target. It is

important to underline that, with this method a Lemniscate figure is ensured when the target is fixed. Further investigations must be done, in order to make the creation of the oscillatory trajectory stable for all the possible target trajectories.

In chapter 6 a static and dynamic analysis of a particular UAV model is made and in chapter 7 classical autopilots are designed in order to try the proposed guidance on a 6DoF software simulator.

Bibliography

[1] M. Aicardi, G. Cannata, G. Casalino, and G. Indiveri. On the stabilization of unicycle model projecting a holomonic solution. In *Proceedings of World Automation Congress*, Maui, HW, US, 2000. IEEE.

[2] R. Beard, D. Kingston, M. Quigley, D. Snyder, R. Christiansen, W. Johnson, T. McLein, and M. Goodrich. Autonomous vehicle technologies for small fixed-wing uavs. *Journal of Aerospace Compution*, 2, 2005.

[3] L.F. Bertuccelli and J.P. How. Search for dynamic targets with uncertain probability maps. In *Proceedings of American Control Conference*, Minneapolis, MI, US, 2006. IEEE.

[4] F. Blanchini. Set invariance control: a survey. *Automatica*, 35(11), 2007.

[5] R. M. Bray. A wind tunnel study of the pioneer remotely piloted vehicle. Ad-a247 028, Naval Postgraduate School, Monterey California, June 1991.

[6] N. Ceccarelli, J. Heinright, E. Frazzoli, S. Rasmussen, and C. Schumacher. Microuav path planning for reconissance in wind. In *Proceedings of American Control Conference*, New York, NY, US, 2007.

[7] M. V. Cook. *Flight Dynamics Principles*. Arnold, 1997.

[8] L.E. Dubins. On curves with minimal length with constraint on average curvature and with prescribed initial and terminal poasition. *American Journal of Mathematics*, 79(3), 1957.

[9] E. Frew. Cooperative stand-off tracking of uncertain moving targets using active robotics networks. In *Proceedings of International Conference on Robotics and Automation*, Rome, Italy, 2007. IEEE.

[10] E. Frew, D. A. Lawrence, and S. Morris. Coordinated standoff tracking of moving targets using lyapunov guidance vector fields. *Journal of guidance, control and dynamics*, 31(2), 2008.

[11] E. Frew and D.A. Lawrence. Cooperative stand off tracking of moving targets by a team of autonomous aircraft. In *Proceedings of Guidance Navigation and Control Conference*, San Francisco, CA, US, 2005. AIAA.

[12] D. Gates. Nonlinear path following method. *Journal of Guidance, Control and Dynamics*, 33(2), 2010.

[13] D. Grundel and D. Jeffcoat. Formulation and solution of the target visitation problem. In *Proceedings of 1st International System Technology Conference*, Chicago, IL,US, 2004. AIAA.

[14] J. Guckenheimer and P. Holmes. *Nonlinear Oscillation, Dynamical System, and bifurcation of Vector Fields*. Springler-Verlag, 1983.

[15] M. Jankovic, R. Sepulchre, and P. Kototovic. Constructive lyapunov stabilization of nonlinear cascade sytem. *IEEE Trasaction of Automatic and Control*, 41(12), 1996.

[16] E.W Justin and P.S Krishnaprasad. Steering laws and continuum models for planar formations. In *Proceedings of the 42nd Conference on Cecision and Control*, 2003.

[17] H.K. Khalil. *Nonlinear System*. Prentice Hall, 2002.

[18] E. Lalish, K. Morgansen, and T. Tsukamaki. Oscillatory control for constant-speed unicycle-type vehicles. In *Proceedings of 46th IEEE Conference on Decision and Control*, pages 5246 – 5251, New Orleans, LA, US, 2007. IEEE.

[19] D. Lawreance. Lyapunov vector fields for uav flock coordination. In *Proceedings of 2nd Unmanned Unlimited System, Technologies and Operation Conference*, Minneapolis, MN, US, 2006. AIAA.

[20] D. Lawreance, E. Frew, and W. Pisano. Lyapunov vector field for autonomous uav flight control. In *Proceedings of Guidance and Navigation Control Conference*, pages 6317 – 6339, Hilton Head, SC, US, 2007. AIAA.

[21] C.F. Lin. *Modern Navigation Guidance and Control Processing Vol.2*. Prentice Hall,Upper Saddle River (NJ), 1991.

[22] Maksimov and Gorgonov. *Electronic Homing System*. Artech House, 1999.

[23] M. Mattei and L. Blasi. Smooth flight trajectory planning in the presence of no-fly zones and obstacles. *Journal of Guidance, Control and Dynamics*, 33(2), 2010.

[24] T. McGee, S. Spry, and K. Hedrick. Optimal path planning in a constant wind with a bounding turning rate. In *Proceedings of Guidance Navigation and Control Conference*, KeyStone, CO, US, 2006. AIAA.

[25] R. McNeely, R.Iyer, and P. Chandler. Tour plannig for an unmanned air vehicle under wind conditions. *Journal of Guidance, Control and Dynamics*, 30(5), 2007.

[26] D. Nelson, B. Barber, T. McLain, and W. Beard. Vector field path following for miniature airvehicle. *IEEE Transaction on Robotics*, 23(3), 2007.

[27] S. Park, J. Deyst, and J.P. How. A new nonlinear guidance logic for trajectory tracking. In *Proceedings of Guidance and Navigation and Control Conference*, Providence, Rhode Island, 2004. AIAA.

[28] S. Park, J. Deyst, and J.P. How. Performance and lyapunov stability of a nonlinear path-following guidance method. *Journal of Guidance,Control and Dynamics*, 30(6), 2007.

[29] VW. Pisano and D. Lawreance. Concentration gradient and information energy decentralized uav control. In *Proceedings of Guidance Navigation and Control Conference*, Keystone, CO, US, 2006. AIAA.

[30] N. Regina and M. Zanzi. 2d tracking and overflight of a target by means of nonlinear guidance law for uav. In *Proceedings of Aerospace Conference*, Big Sky, MT, US, 2009. AIAA/IEEE.

[31] N. Regina and M. Zanzi. Uav guidance law for target tracking along a constrained bow-shaped trajectory based on lyapunov vector field. In *Proceedings of Symposioum on Aerospace Control Automation*, Nara, Japan, 2010. IFAC.

[32] J. Roskam. *Airplane Flight Dynamics and Automatic Flight Controls, Part I.* Darcorporation, 2003.

[33] J. Roskam. *Airplane Flight Dynamics and Automatic Flight Controls, Part II.* Darcorporation, 2003.

[34] S. Sastry. *Nonlinear System.* Springer, 1999.

[35] D. Soetano, L. Lapierre, and A. Pascoal. Adaptive, non-singular path following control of dynamic wheeled robots. In *Proceedings of 42nd IEEE Conference on Decision and Control*, pages 1765 – 1770 Vol.2, Maui, HW, US, 2003. IEEE.

[36] J.L. Vian and J.R. Moore. Trajectory optimization with risk minimization for military aircraft. *Journal of Guidance, Control and Dynamics*, 12(3), 1989.

[37] J.H. Vriends. *Missile Guidance and Control.* Pergamon Press, 1987.

[38] J.T. Wen. A unified perspective on robot control: the energy lyapunov function approach. In *Proceedings of the 29th Conference on Cecision and Control*, 1990.

[39] K. ZuWhan and R.Sengupta. Target detection and position likelihood using an aerial image sensor. In *Proceedings of International Conference on Robotics and Automation*, Pasadena, CA, US, 2008. ICRA/IEEE.